CRYSTALLOGRAPHIC EFFECTS IN PEARLITE

A Dissertation

Presented to

the faculty of the School of Engineering and Applied Science

University of Virginia

In Partial Fulfillment

of the requirements for the Degree

Doctor of Philosophy

by

Stephen Andrew Hackney

May, 1985

APPROVAL SHEET

This dissertation is submitted in partial fulfillment of the

requirements for the degree of

Doctor of Philosophy

AUTHOR

This dissertation has been read and approved by the examining Committee:

Dissertation Adviser

Accepted for the School of Engineering and Applied Science:

Dean, School of Engineering and
Applied Science

May, 1985

'Whence arises all that order and beauty we see in the world?'

Isaac Newton

Table of Contents

Page

ABSTRACT

An experimental re-evaluation of the Smith/Hillert and Hull/Mehl models of the pearlite transformation has been made by application of transmission electron microscopy techniques to suitable alloy systems. The observed behavior of the ferrite:cementite lamellar interface shows the strict crystallographic adherence predicted by the Hull/Mehl model. However, the presence of "direction steps" at this boundary allows the necessary geometric freedom for pearlite to develop by the Hillert branching mechanism, which, until now, has been associated with unimportant ferrite:cementite crystallography. It is found that the crystallography at the pearlite:austenite interface plays a much expanded role in determining the mechanism of growth and morphological development of the pearlite colony. Based on these observations, a new model with extensive deference to the ferrite:cementite:austenite crystallographic relationship is proposed for the pearlite transformation.

Acknowledgments

I would like to acknowledge Dr. G.J. Shiflet who was the first to recognize the expanded role crystallography must play in the pearlite transformation. Dr. Shiflet not only provided the creative impetus for this project, but he also provided the guidance, patience, and understanding necessary during the experimentally difficult portions of this study. I would be remiss if I did not acknowledge Dr. R.F. Mehl and Dr. M. Hillert for their careful experimental work which formed the basis for this dissertation.

Acknowledgments are also in order for Mr. Greg Bartlett, who I worked with on the ferrite:cementite interface and who is responsible for Figure 4.5c, Mr. William Cassada, who was of invaluable assistance on the computer work, and my wife, Paige, who not only supported me in spirit, but also typed the entire manuscript with a smile.

The National Science Foundation is acknowledged for support under grant number DMR-83-00888.

List of Tables

List of Figures

I. INTRODUCTION

Since the work of Sorby (1) there have been many investigations of pearlite both in ferrous and non-ferrous alloy systems. On the basis of these studies, two major theories of pearlite have evolved. The theory of Hull and Mehl (2) was the first to be consistent with all of the experimental information available at the time it was written. It was nearly universally accepted until Hillert re-examined both the old and more recent data and also performed some important new critical experiments (3). His theory soon gained wide-spread acceptance. The differences between the two theories are fundamental in nature. Where the Hull-Mehl theory depends heavily on crystallographic effects upon the nucleation and growth kinetics of both ferrite and carbide phases, Hillert considers these effects as secondary and "fairly unimportant" (4) and relies instead upon the gradual evolution of structure-insensitive, cooperative diffusional growth of the two phases in the formulation of his theory.

In the twenty years which have elapsed since the publication of Hillert's theory of pearlite formation, substantial advances have been made in fundamental understanding of the mechanisms of both diffusional nucleation and diffusional growth. In particular, it is becoming increasingly apparent that viable kinetics of solid-solid nucleation require orientation relationships capable of yielding low energy interphase boundaries on critical nuclei (5-7). These relationships, in turn, result in the development of partially coherent interphase boundaries during growth; when the crystal structures of matrix and precipitate are sufficiently different,

such boundaries can migrate only by means of the ledge mechanism (8,9). Hence, despite the impressive evidence compiled by Hillert in support of his view that the crystallography which requires the presence of such a growth mechanism, with all of its implications for the boundary orientation-dependence of growth kinetics (10), is not present, it now seems appropriate to reconsider the Hull-Mehl approach to pearlite formation through detailed observation and characterization of all interphase boundary structures involved in the formation of pearlite. Although there has been considerable work done centered on the orientation relationships between ferrite and cementite in pearlite (11-18) and pearlitic ferrite and cementite with austenite (18), the more crucial studies of interfacial structure have not been accomplished. As shown in other studies of this type (19-21), it is necessary that the atomic habit planes be identified with high-resolution transmission electron microscopy and computer analysis, as these can be quite different from apparent habit planes determined from trace analysis of lower resolution TEM micrographs. That these studies have not been done is due in part, of course, to the circumstance that the resolution and stability of image prerequisite for high resolution TEM have been generally available for only a few years.

In this investigation, the application of TEM techniques to suitable alloy systems has allowed the re-evaluation of both the Hull-Mehl and the Hillert theories. Efforts to establish the relative importance of crystallography to the growth and development of the lamellar pearlite morphology has led to the proposal of a new model for the pearlite transformation.

II. BACKGROUND

1. Interphase Interfaces in Solids

An interphase interface separates two different phases that can have different crystal structures and/or compositions. The majority of phase transformations in solids occur by the nucleation and growth of a new phase within the parent phase. The interphase boundary thus created plays an important role in determining the morphology and kinetics of phase transformations.

A. Origins of Interfacial Structure

The nearly ubiquitous occurrence of low energy interphase boundaries is a direct result of the importance of ΔG^*, the free energy of formation for the critical nucleus. From classical nucleation theory the nucleation rate is proportional to $\exp[\Delta G^*]$ and further ΔG^* is proportional to the interfacial energy, γ, cubed. That is:

$$\text{Nucleation Rate} \sim \exp[-\Delta G^*] \sim \exp[-\gamma^3]$$

It then follows that the critical nucleus morphology with the lowest ΔG^*, which means, those with low energy coherent interphase boundaries will predominate and hence survive into growth. These low energy interfacial structures formed during nucleation will remain in growth unless destroyed by a recrystallization reaction or some type of thermo-mechanical treatment. However, unless the matching is perfect, which is unlikely, the interphase boundary will be partially coherent during growth rather than coherent as is

likely during nucleation.

B. Classification of Interphase Boundaries

Currently, interphase interface boundaries are generally divided into three categories: coherent, partially coherent (or semi-coherent), and incoherent (or disordered).

a) The coherent interphase boundary is one in which the interfacial plane is part of the stacking sequence of both crystal structures (Figure B1). Only elastic distortions across the interphase boundaries are needed to accommodate any small mismatch between the two lattices. As might be expected, since this type of interface introduces minimum distortions in the lattice stacking sequence it is usually considered to have the lowest energy of the three types of boundaries.

b) Partially coherent interphase boundaries may be thought of as interfaces between crystals with different lattice parameters and/or crystal structures in which the misfit is sufficient so that it must be absorbed by periodically spaced misfit correcting dislocations (Figure B2). The regions in between misfit dislocations have been considered to be fully coherent without severe elastic distortions except in the vicinity of the misfit dislocations. In practice, misfit usually exists in two dimensions and in this case the coherency strain fields can be completely relieved if the interface contains two non-parallel sets of dislocations or if the structural ledge (to be discussed below) is introduced in combination with the misfit dislocation.

The semicoherent interface can be considerably more complex by

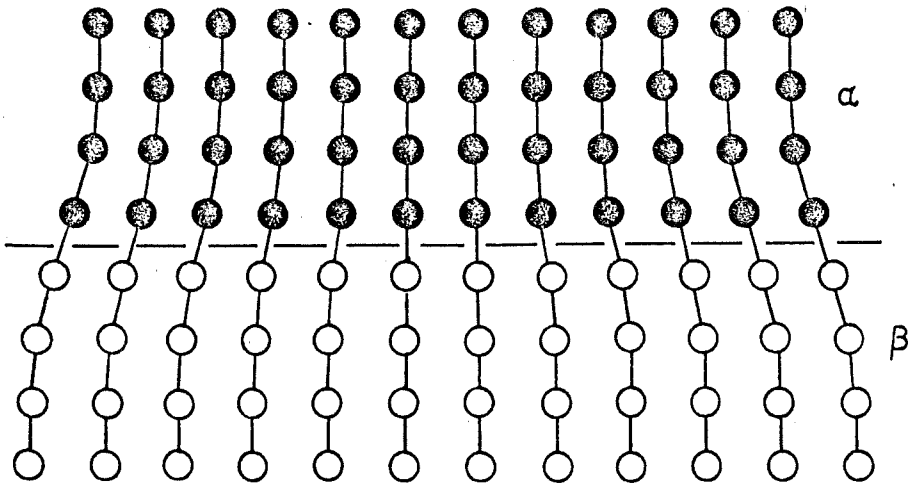

Figure B.1 A coherent interface with slight mismatch leads to coherency strains in the adjoining lattices (22).

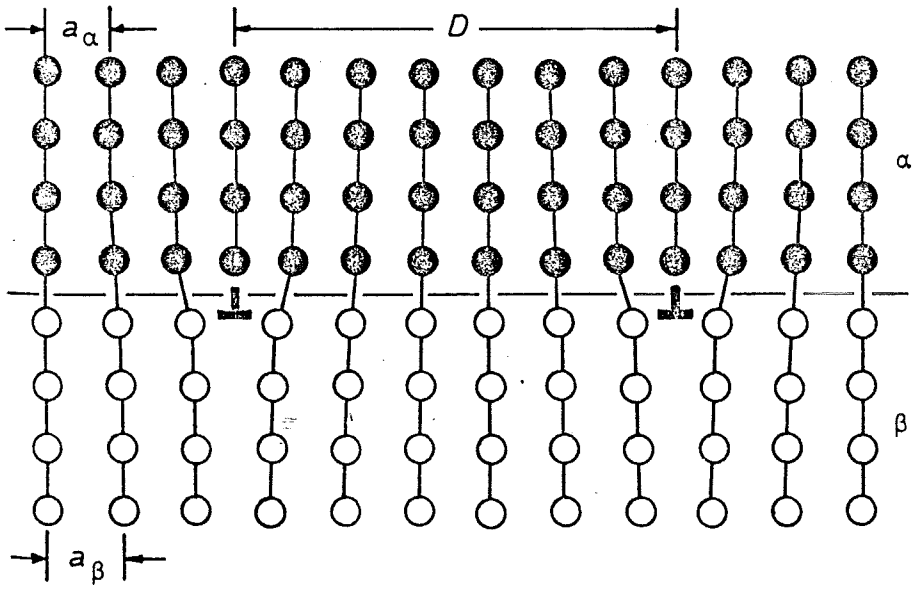

Figure B.2 A semicoherent interface. The misfit parallel to the interface is accommodated by a series of edge dislocations (22).

the introduction of the structural ledge (19). These ledges do not contribute to the growth process but are another way of increasing the level of coherency between two badly matching lattices. If we use the fcc:bcc crystal structures studied by Aaronson and coworkers (20, 21), Figure B3 shows the atomic matching resulting from the Nishiyama-Wasserman (N-W) and the Kurdjumov-Sachs (K-S) relationships. These drawings exhibit the following orientation relationships:

N-W (110)bcc//(111)fcc
[001]bcc//[101]fcc

and

K-S (110)bcc//(111)fcc
[111]bcc//[011]fcc

The only difference between the two is a rotation in the closest packed planes of 5.26 degrees. The region of good fit obtained in each case is outlined with heavy dashed lines. The K-S region of good fit contains about 30 atoms and the N-W region contains 9 atoms which is only 8% of the interfacial atoms.

Coherency can be greatly increased if a one atomic layer high step is introduced. This is illustrated in Figure B4 for the N-W relationship where the step added is at the tip of the diamond-shaped coherent patch. A second coherent patch immediately follows the step. This process is repeated throughout the interface increasing coherency to 25%. The remaining misfit is compensated for by an edge dislocation midway between coherent patches with the extra half plane in the fcc lattice. Such a structure would then provide the conventional barrier to the migration of dislocation

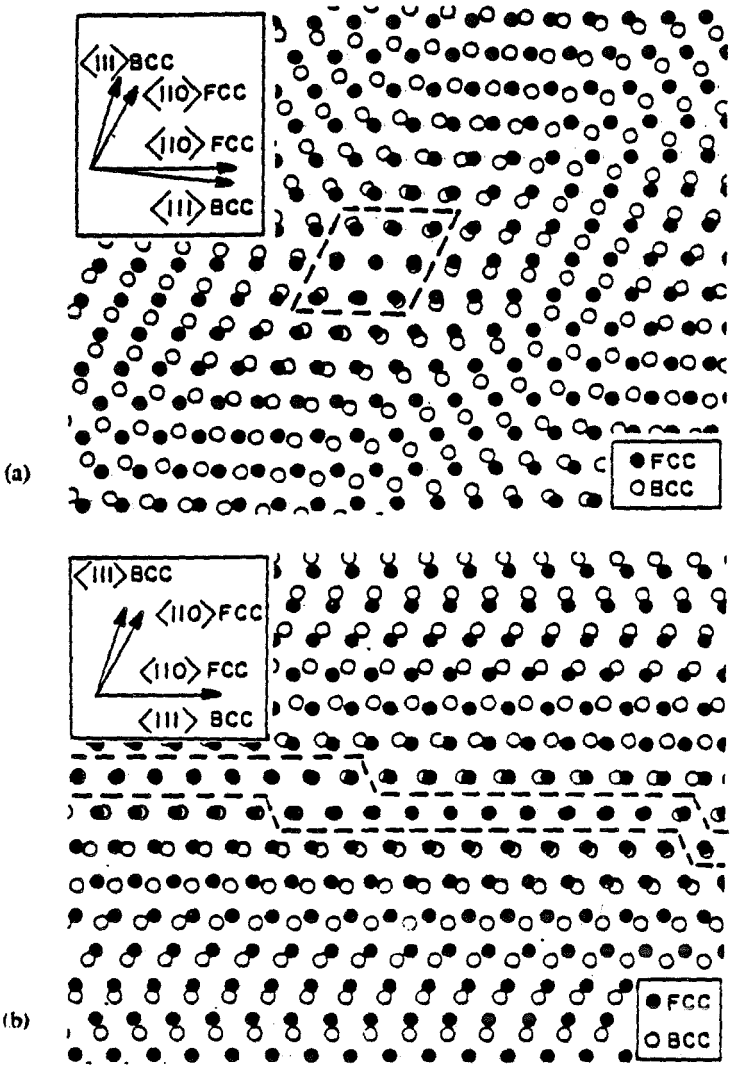

Figure B.3 Superposed plots of the atomic configurations in the {111} fcc and {110} bcc planes (19).

a. Nishiyama-Wasserman orientation relationships.

b. Kurdjumov-Sachs orientation relationship.

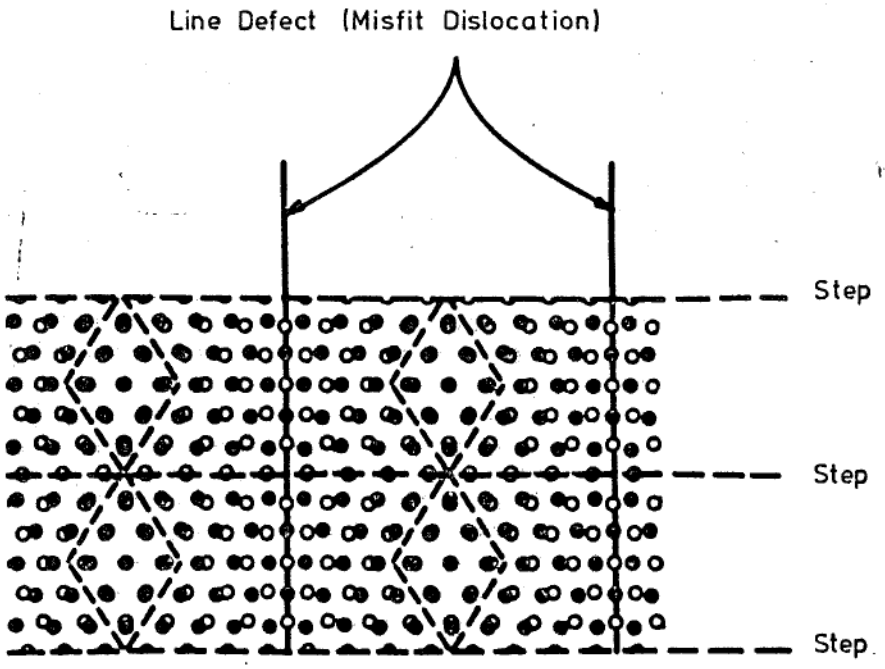

Figure B.4 Coherent patches separated by line defects.

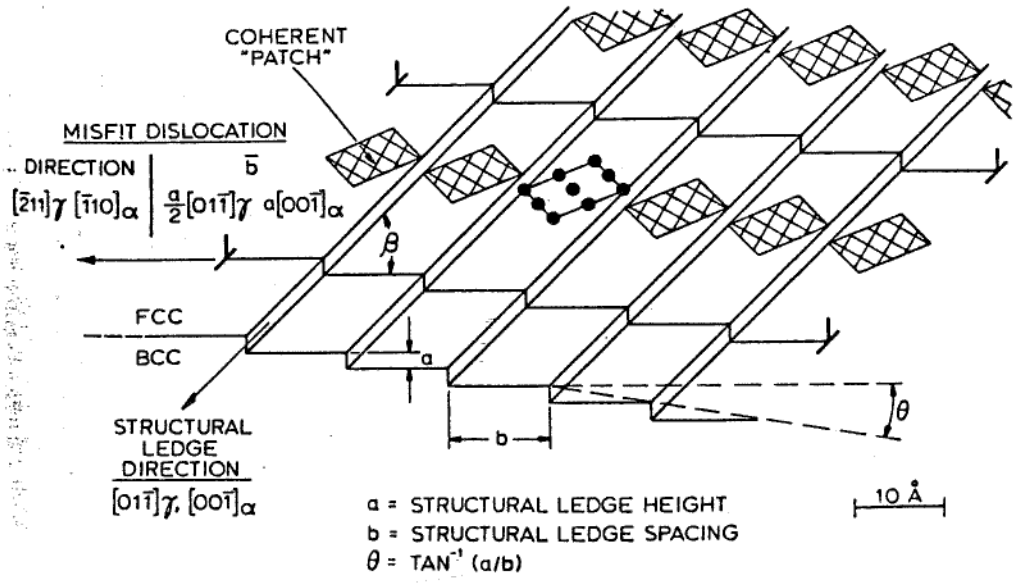

Figure B.5 Isometric drawing of partially coherent fcc:bcc interface (21).

interphase boundaries. An isometric sketch of this interface by Rigsbee and Aaronson (21) is shown in Figure B5. Since there is the added component of the misfit dislocation energy, partially coherent boundaries are considered to be of higher energy than fully coherent boundaries, but of lower energy than the third type of interface to be discussed.

c) Disordered or incoherent interphase boundaries occur when atomic matching between the two lattices is so poor that the atoms in the vicinity of the interface assume positions which are compromises between the demands of the two bulk crystal structures (Figure B6). Very little is known about the detailed atomic structure of incoherent interfaces. They do, however, have many features in common with high angle grain boundaries, such as, they are characterized by a high energy (~1000 mJ/m^2) which is relatively insensitive to the orientation of the interfacial plane.

The disordered interface, as the name implies, is thought to be void of interfacial structure. As noted by Aaronson, however, "by analogy to high-angle grain boundaries it is quite possible that the boundary structure may be resolved into a succession of polyhedra of a limited number of types, each containing but a few atoms." Figure B7 is taken from a paper by Pond et al. (23) which shows the five basic "random, close packed" polyhedra (plus related structures) discovered for hard sphere models of liquid structures along with the polyhedra occurring in computer simulated, two-dimensional representations of (110) tilt boundaries in FCC metals. On the basis of these results, and the fact that resolvable interfacial defects are seen on almost all grain boundaries (by TEM), the terms "disordered" and "incoherent" have fallen out of vogue in grain

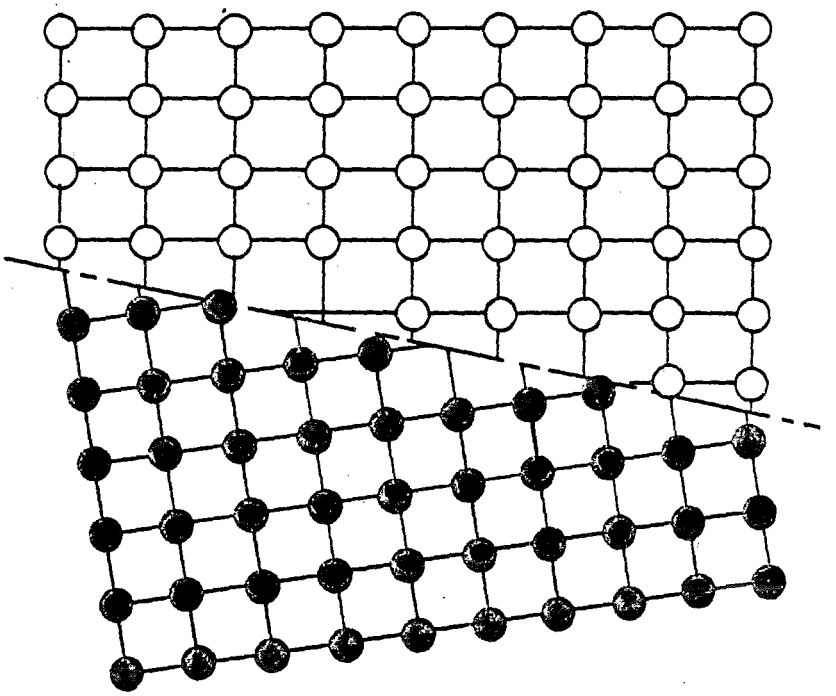

Figure B.6 An incoherent interface (22).

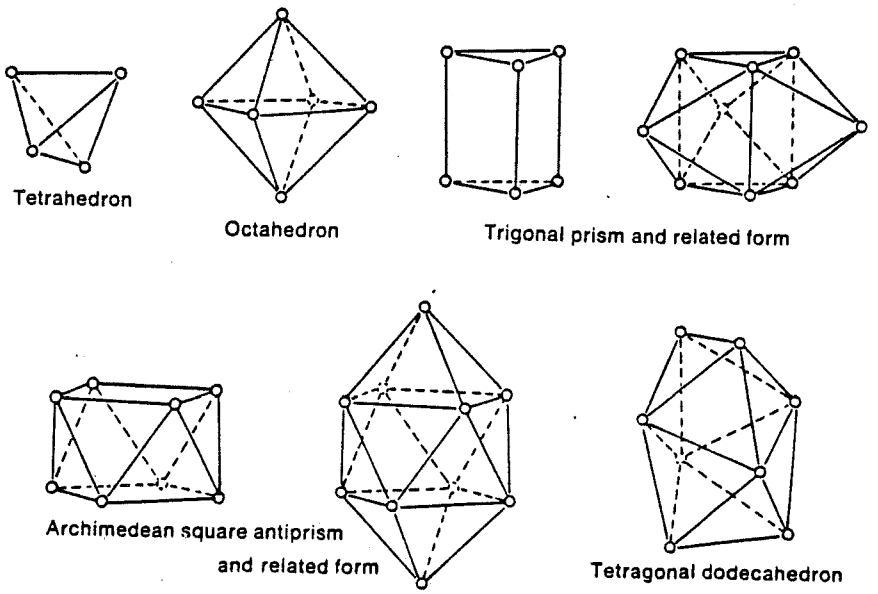

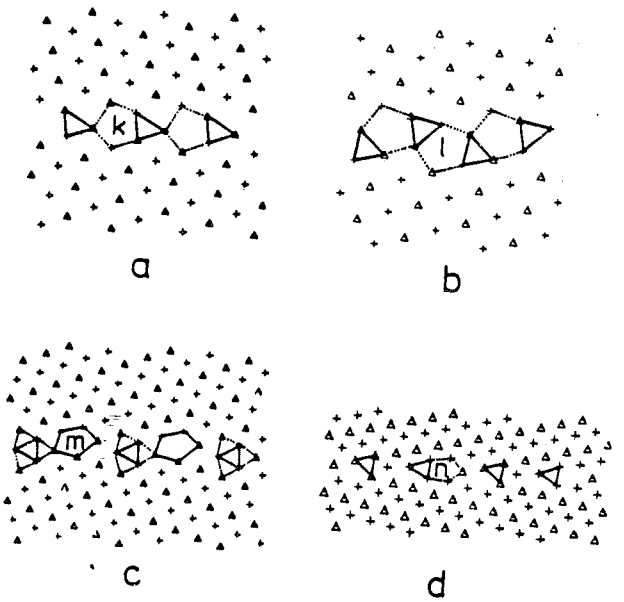

Figure B.7 Computer simulated high angle grain boundary structure (23).

boundary research. It remains to be seen whether or not interphase boundary research will lead to similar conclusions.

C. Mechanism of Boundary Displacement (Growth)

In the case of partially coherent interphase boundaries, it has been proposed that these boundaries are wholly immobile in the direction perpendicular to the boundary plane (10). The immobile nature of this interface is thought to arise from the presence of coherent regions. Consider that to displace these regions by essentially uncoordinated diffusional jumps, it is necessary for atoms to be situated in what are temporarily interstitial sites. According to Aaronson (24), "For more or less close packed crystal lattices, the energetics of this should be most unfavorable . . . these boundaries should be atomically flat." High resolution electron microscopy by Howe et al (25). has shown this to be true for γ' AlAg plates precipitated from fcc α in an Al-Ag alloy. The hypothesis was introduced in 1962 by Aaronson (8-10) that partially coherent interphase boundaries advance by the ledge mechanism, a concept originally proposed by Gibbs for the migration of close packed solid:liquid and solid:vapor interfaces. This is illustrated in Figure B8, where the migration of the alpha:beta interphase boundary occurs by the lateral movement of growth ledges, and the risers of the ledges are taken to have a disordered type structure.

The rate of migration or growth (G_t) of this boundary is dependent on the height of the ledges (h), the ledge velocity (V), and the ledge spacing (λ). These variables may be combined to give the expression:

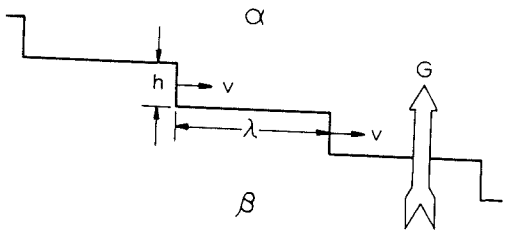

Figure B.8 Growth by the ledge mechanism (26).

$$G_t = hV/\lambda$$

As long as the ledges are sufficiently widely spaced, this mode of growth will give a growth rate less than that allowed by volume diffusion.

2. The Pearlite Transformation

The pearlite transformation is an eutectoid reaction product. It consists of alternate lamellar plates which grow synchronously into the matrix and is further characterized by a certain degree of cooperation between the two growing phases. Pearlite occurs in nearly all eutectoid transformations but is most widely associated with ferrous alloys and for the purposes of this discussion, the transformation will be referred to in terms applicable to the iron-carbon eutectoid reaction. On cooling a suitably alloyed Fe-C steel below the eutectoid temperature the transformation can be expressed as:

$$\underset{\text{(fcc)}}{\text{austenite}} \longrightarrow \underset{\text{(bcc)}}{\text{ferrite}} + \underset{\text{(complex orthorhombic)}}{\text{cementite}}$$

and is schematically illustrated in Figure B9. As is apparent from this figure, various interfaces between the ferrite, cementite, and austenite phases are present during the pearlite transformation. The relative importance of these interfaces during development and growth of pearlite has been keenly debated

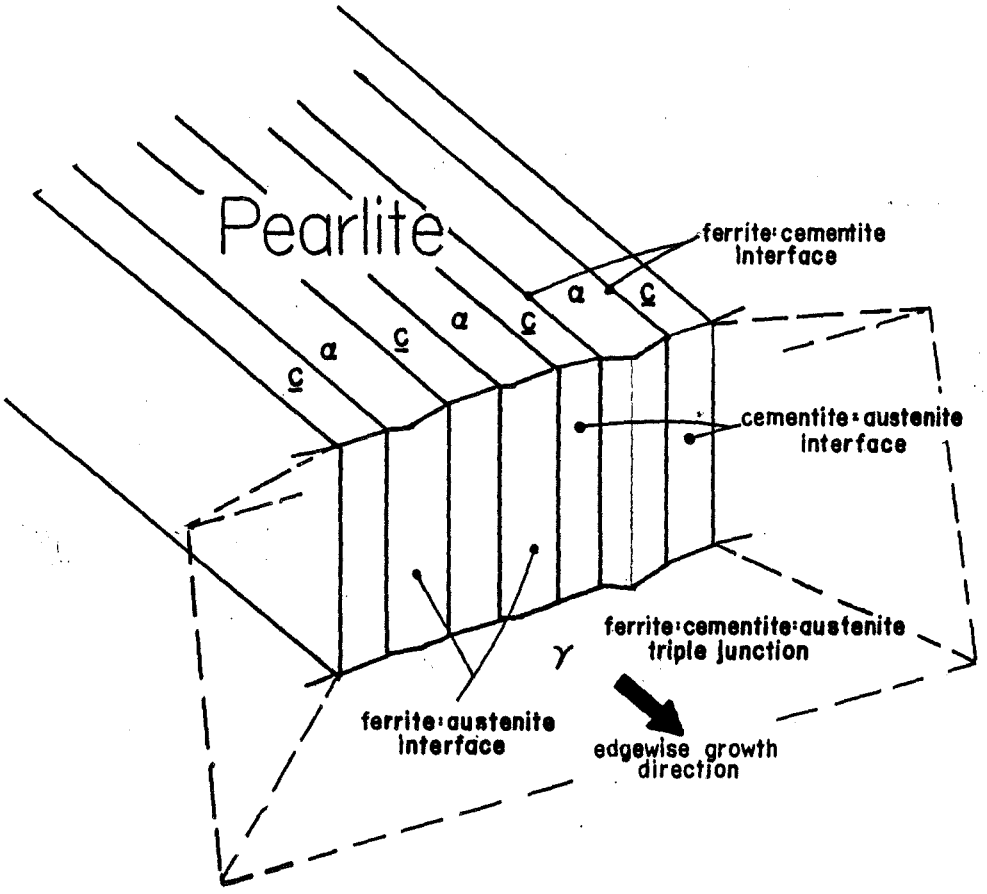

Figure B.9 Lamellar pearlite.

throughout the history of this transformation and is currently considered to be unimportant. It is the study of these interfaces that is the primary objective of this dissertation.

A. Brief History of Pearlite Models

a. Hull-Mehl Model

Hull and Mehl (2, 27) provided the first comprehensive answer to how a pearlite colony develops. According to their theory, which remains active in the current literature, the nucleation of a cementite plate at an austenite grain boundary initiates formation of a pearlite colony (Figure B10). This is followed by the nucleation of a ferrite plate on each side of the initial cementite plate. Sidewise growth is accomplished by continued alternate nucleation of ferrite and cementite plates. Edgewise growth is accounted for by synchronous growth of the edges of the ferrite and cementite plates into the interior of the austenite grain in which growth began. That the advancing edges of the ferrite and cementite plates (also called "lamellae") have a disordered structure is implicit in this mechanism. The plate morphology of the ferrite and cementite determines the lamellar nature of a pearlite colony. The presence of only one ferrite orientation and one cementite orientation within a given colony was proposed on indirect evidence including etching and parallel fracture markings.

That the "active nucleus", i.e., the first formed phase, is cementite was criticized (28-31) as being too restrictive. Evidence

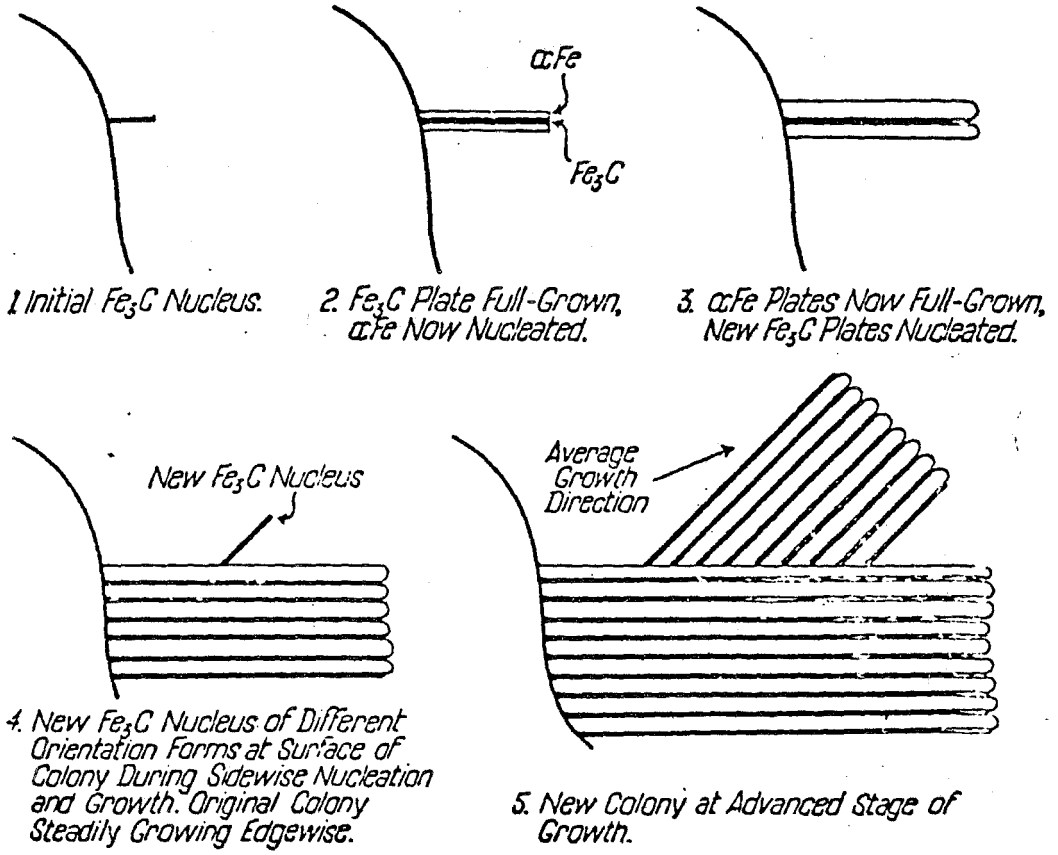

Figure B.10 The Hull-Mehl model.

was provided (29-32) that either ferrite or cementite could serve this function, as originally proposed by Benedicks (27).

b. Hillert Model

In 1962 Hillert (3) combined old and new evidence into an integrated picture of pearlite formation very different from that of Hull and Mehl (2, 33). Hillert proposed a model for growth of pearlite based on his own experimental work and Smith's (34) theory of cellular growth. Most investigators consider that the Smith/Hillert hypothesis has superceded that of Hull and Mehl.

1. Sidewise growth. To test the theory of sympathetic nucleation, Hillert devised an experiment in which a single pearlite colony is sectioned from the surface (by polishing) in 1 micron increments. The photographic images of each section were organized in a manner so that a movie could be made revealing the three-dimensional form of the pearlite colony. From this experiment, it became clear that the pearlite colony was not made up of alternating crystals (plates) of ferrite and cementite, but rather consisted of a single crystal of ferrite and a single crystal of cementite intricately interwoven. In the 1962 paper, Hillert gave the following description of the development of pearlite studied by the sectioning technique.

> 1. Cementite nucleates at the grain boundaries forming a network, thus displacing the austenite composition toward the hypoeutectoid side in the Fe-C diagram.
>
> 2. Ferrite nucleates at the interface between cementite and austenite and grows along this interface isolating the cementite from the remaining austenite.
>
> 3. When growing along the cementite-austenite interface,

the ferrite may reach a hole in the network or a sharp edge of the cementite. Here the ferrite may not be able to isolate the cementite completely from the austenite. An arm of cementite grows out from the network and retains contact with the austenite.

4. During the growth of ferrite, the austenite composition will move back toward the hypereutectoid side. The growth of the arm starts to grow along the interface between ferrite and austenite, now isolating the ferrite from the austenite.

5. Owing to the small volume fraction of cementite, this phase has more difficulty than ferrite in forming a complete layer and thus isolating the other phase. Consequently, there is now a good chance that a structure forms which contains alternating units of cementite and ferrite, with both of them in contact with austenite. This may be regarded as the first stage of branching.

6. During further growth, more branching occurs until the spacing is close to the value characteristic of the temperature.

Thus it was concluded that sidewise growth does not occur by repeated sympathetic nucleation. Instead, Hillert proposed that sidewise growth occurred by the "branching" of the ferrite and cementite lamellae.

2. Edgewise Growth. Smith (34) suggested that proeutectoid ferrite formed at an austenite:austenite grain boundary would have a definite orientation relationship with one grain, giving rise to a partially coherent interface. Usually, this would result in a high index orientation relationship with the other grain and an incoherent interface. At low undercoolings, Smith proposed growth occurs predominantly into the grain containing the incoherent ferrite:austenite boundary because partially coherent interfaces were considered to have low mobility. Smith believed pearlitic

ferrite behaved in the same manner as proeutectoid ferrite, whether it nucleated before or after the cementite constituent. By analogy to the theory of cellular growth, the hypothesis was given that the pearlite colony would only be able to grow into the grain which was unrelated crystallographically with the pearlitic ferrite, i.e., pearlite could grow only by the advance of an incoherent interface. Hillert, using similar arguments applied to the cementite phase, generalized Smith's hypothesis to read:

> The ferrite and cementite constituents of pearlite can have any orientation relationships to the matrix austenite except for those which allow the formation of interfaces which are partially coherent with the matrix austenite.. . . The lattice orientations of pearlitic ferrite and cementite are thus random with respect to the matrix austenite except for the avoidance of some orientations.

c. Contributions of Honeycombe

The work of Honeycombe (18) would tend to support the Smith/Hillert contention. Ferrite is known to form partially coherent interfaces with austenite when one of the three orientation relationships given in Table I pertain while cementite forms only one reproducible orientation relationship with austenite (see Table I).

Honeycombe used transmission electron microscopy to study the orientation relationship between the pearlitic phases and the retained austenite in a high manganese steel. As predicted by Smith and Hillert, at least one pearlitic phase was crystallographically related by one of the above orientation relationships to the parent grain while neither ferrite nor cementite was related in any

Table I

Orientation Relationships

Kurdjumov-Sachs	$(111)_A$	$(110)_F$
	$[\bar{1}10]_A$	$[\bar{1}11]_F$
Baker-Nutting	$(001)_A$	$(001)_F$
	$[100]_A$	$[\bar{1}10]_F$
Nishiyama-Wasserman	$(111)_A$	$(110)_F$
	$[\bar{1}10]_A$	$[001]_F$
Petch	$(1\bar{1}1)_A$	$(100)_C$
	$(110)_A$	$(010)_C$
	$(\bar{1}12)_A$	$(001)_C$

A = fcc austenite

F = bcc ferrite

C = orthorhombic cementite

reproducible manner to the grain into which growth was occurring. The lack of reproducible orientation relationships is usually taken, by most investigators, as an indication of precipitates having disordered interfaces.

B. Problems, Inconsistencies, and Unanswered Questions in the Theory of the Pearlite Transformation

a) The Pearlite:Austenite Interface and the Mechanism of Growth. All theories of pearlite growth assume that the pearlite:austenite interface is incoherent or disordered-like. There have been indications, however, that this view may be incomplete. Cahn (35) has suggested that the growth rate is determined by a complex interplay between diffusion and "interface mobility." Cahn and Hagel (36) indicated that growth is controlled in part by an "interface process." They felt that if diffusion was the only growth restraint, the ferrite:cementite:austenite three phase junction would grow extremely rapidly since the diffusion distances there are relatively short. Since this is not observed, it was concluded "that the rate (of growth) near the junction must also be influenced by the ability of the interface to move."

The thermionic emission micrographs published by Rathenau and Baas (37) indicate that grain boundaries and twin boundaries often affect the growth of pearlite, sometimes stopping or changing the directions of individual lamella. If the growth interface was truly incoherent, and thus insensitive to changes in crystallography, this type of behavior would not be observed. Since these results were obtained by isothermal transformation, it is interesting to note

that Verhoeven (38) found similar results during "forced velocity" growth experiments. It was observed that grain boundaries occasionally disrupt the lamellar nature of the pearlite by halting the advance of cementite lamella.

b) The Importance of the Ferrite:Cementite Orientation Relationship. It would seem from the literature that there is a great deal of disagreement concerning the importance of this point. Aaronson, Laird, and Kinsman (39) state that there should be a significant barrier to growth at the lamellar interfaces of pearlitic carbide and pearlitic ferrite in the form of a partially coherent boundary. This structure should strongly limit the ability of the lamellae to grow along wandering paths. Direct observations of the structure of such an interface had yet to be reported though good evidence for it can be seen in published TEM micrographs (18, 40, 41). All investigators are in agreement that the ferrite:cementite interfacial energy is or should be of low energy, thus giving rise to a lamellar morphology rather than a rod-like morphology (which is kinetically favored). Hillert (3), because of the branching mechanism, concluded the crystallography was unimportant. Kirkaldy, because he observed (optically) smoothly curving lamella with no spacing change, concluded that the ferrite:cementite interface is incoherent (42). These conclusions are quite inconsistent with Ohmari et al. (17), who reported that two ferrite:cementite orientation relationships are usually observed in pearlite, and that the boundary planes most often correspond to good atomic matching habit planes. It is apparent that the only way to resolve this conflict is by directly studying (via TEM) the ferrite:cementite interphase boundary.

c) The Ferrite:Cementite Interfacial Energy in Relation to Theories of Growth. Using recent experimental data, Ridley calculated the ferrite:cementite interfacial energy to be 930 ergs/cm^2 from Zener's maximum growth theory and 620 ergs/cm^2 from Kirkaldy's maximum rate of entropy production theory, both of which assume volume diffusion control as the rate controlling process. These energies appear too high for the type of partially coherent interface expected between lamellar pearlitic phases. Kirchner et al. (43) has recently suggested a value for the ferrite:cementite interfacial energy of 500 $\pm$ 360 ergs/cm^2, which would include energies significantly lower than the values predicted by the growth theories.

As pointed out by Ridley (44), if an interfacial energy more appropriate for a partially coherent interface is used to describe the interface, such as 400 ergs/cm^2, the ratio $S/S_c = 4.7$ results, where S and S_c are values for interlamellar spacing and critical interlamellar spacing. This is much higher than the accepted values $S/S_c = 2$ and $S/S_c = 3$. The fact that these values refer to experimentally determined minimum interlamellar spacings as opposed to mean interlamellar spacing indicates that S/S_c may be as high as 5.90, that is almost three times higher than the Zener criteria and twice as high as the Kirkaldy criteria. There certainly appears to be enough discrepancy to merit further investigation into the exact mechanism of the pearlite transformation.

III. EXPERIMENTAL PROCEDURES

A. Specimen Preparation

The choice of alloy is the key to much of the experimental design. In order to conduct the interfacial structural studies at the growth interface, which comprise the experimental heart of this program, it is absolutely vital that the austenite matrix, remaining untransformed during isothermal reaction, not decompose to martensite during quenching to room temperature, even in thin foils. Therefore, the alloy to be studied is the same as that used by Bain (45) and Bain, Davenport, and Waring (46) in 1932 and more recently by White and Honeycombe (47) and Dippenaar and Honeycombe (18), who found that this desideratum is met by Fe-0.8 w/o C-12 w/o Mn. To dispel doubts about the generality of the results obtained from pearlite in the high manganese alloy, a high purity Fe-C eutectoid steel will also be studied. Comparison can thus be made between the lamellar interfaces in both systems. The high purity Fe-C-Mn (Table II) alloy used in this investigation was provided by Bethlehem Steel Corporation. Bars, .03x.03x.01 m were encapsulated in a high purity nitrogen atmosphere and homogenized at 1300 C

Table II. Composition of the Alloy Used in This Investigation

Alloy composition (Wt %)				
C	Mn	P	S	Al
0.81	12.3	.0003	.0006	<.005

for three days. Subsequent heat treatments were performed on 3mm

discs, 2mm thick. These specimens were placed in a nickel basket and austenitized at 1000 C for 10 minutes followed by isothermal transformation in molten salt at temperatures ranging from 600 to 650 C. The isothermal reaction times varied from 5 to 18 hours and were followed by a rapid quench into iced brine. The three millimeter discs were carefully mechanically thinned to .016mm thickness using a holder designed in this laboratory. The discs were then dished using a Tenupole electropolishing unit with 10 vol% perchloric/acetic acid solution at room temperature and a potential of 65 volts. This assured perforation near the center of the disc to minimize magnetic effects. In an effort to reduce oxide formation, the dished specimens were not thinned to perforation until immediately prior to TEM examination. This was done in a 250 ml glacial acetic acid, 75 g anhydrous sodium chromate, 25g chromic oxide and 10 ml water at 10 C and 32 volts. It was occasionally necessary to ion mill the thin foils for 5 minutes at an accelerating voltage of 500 volts to remove a residue from the polishing process. This procedure produced foils in which the cementite, ferrite, and austenite phases were thinned at virtually identical rates.

The high purity Fe-0.8%C alloy (kindly provided by Professor H.I. Aaronson) was 50 percent rolled and cut into 10x20x.7mm sections. The specimens were austenitized for 30 minutes at 1100 ^{o}C in a dynamic argon atmosphere. They were then quickly transferred to a salt bath at 645 ^{o}C and isothermally heat treated for 12 seconds followed by quenching in iced brine. Discs for transmission electron microscopy (TEM) were chemically thinned using 80ml H_2O_2, 3ml Hf, 10ml H_2O and electropolished in a solution of 100g $NaCrO_4$

dissolved in 500ml of glacial acetic acid at 60 V and 20 °C using a twin jet polisher. All TEM was done using a Philips 400T.

B. TEM Analysis

a) Misfit dislocations. Brooks (48) and van der Merwe (49-51) have shown that the distance that the strain field of an interphase boundary dislocation extends normal to the plane of the array is approximately equal to one half the interdislocation spacing. Therefore, as the spacing decreases the volume of crystal available to produce diffraction strain contrast from individual dislocations is reduced, leading to decreased dislocation visibility. However, when the dislocations are too closely spaced there is still sufficient lateral overlap of their strain fields so that they cannot be resolved with either bright-field or conventional dark-field TEM. The weak-beam, dark-field (WBDF) technique of Cockayne (52), on the other hand, minimizes the overlap by tilting the foil slightly out of the exact Bragg condition, thereby restricting visibility to only the most severely strained region about a dislocation and thus permitting more closely spaced dislocations to be resolved at an acceptable loss in strain contrast intensity. The WBDF technique has been used to resolve misfit dislocations on the broad faces of ferrite plates as closely spaced as 1.3nm (21). Burgers vector analysis will be based upon the usual g.b invisibility criterion. As has been discussed by Aaronson (10) at least some component of the burgers vector must lie in the interface plane.

The appearance of a regularly spaced dislocation array can be

virtually identical to that of a moire' fringe pattern (53). Considerable care has been exercised to avoid this misinterpretation. Examination of the diffraction pattern corresponding to each image can reveal whether or not an extra, suitably positioned diffraction beam is near the primary imaging beam, since at least two beams contribute to the final image (21). Measurement and comparison of fringe spacing with that expected from the diffracting planes will also be useful in sorting out the origin of the arrays. Final elimination of the moire' pattern explanation for the interfacial structure will be obtained by imaging the structures with several different reflections from both phases involved and demonstrating that the spacing between adjacent lines of contrast is not changed.

b) Structural and growth ledges. Structural ledges are a combination of single or multi-atomic high ledges and misfit dislocations (19) whose presence allows improved matching across an interphase boundary. They are most likely immobile, since displacement of them would require too much simultaneous atomic movement to be feasible (except perhaps in fcc/hcp transformations (54)) and would change the structure of the boundary. Growth ledges, on the other hand, replicate the existing boundary structure as they migrate (Figure E1) and hence are the major mechanism for growth of partially coherent boundaries.

Strain field contrast (55) as well as topographical effects (56) are the mechanisms participating in the imaging of ledges. It has been found (10) that the strain fields of both structural ledges and growth ledges give rise to displacement vectors perpendicular to the plane of the interface.

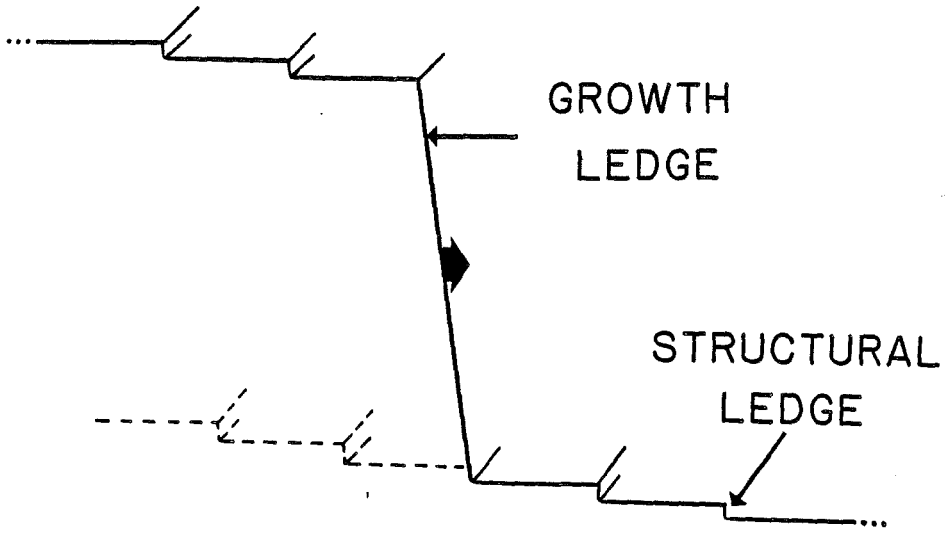

Figure E.1 Replication of interfacial structure by growth ledges.

Topographical ledge contrast results from changes in the relative thickness of the two phases (e.g. ferrite and carbide) at a ledge and is observed as a deflection of the extinction contours (56, 57). This contrast mechanism allows the determination of ledges spaced too closely for resolution by strain field contrast. The detection of extinction contour displacements is enhanced through use of the WBDF imaging technique due to the accompanying decrease in spacing and increase in sharpness of the extinction contours (21). Gleiter (56) has developed an equation (given below) which will allow the heights of ledges to be calculated from the magnitude of the extinction contour displacement.

$$h = m * \sin(a) * \sin(b)$$

h = ledge height
m = contour displacement
a = interface/foil surface angle
b = contour/ledge angle

A further test on growth ledges will be to make hot stage TEM observations of their movement. This type of experiment was successfully performed by Baro and Gleiter in fcc:bcc brass (58) and Hackney and Shiflet in their study of equilibrium theta plates in Al-5% Cu (59).

IV. RESULTS AND DISCUSSION

The results of this investigation will be presented in four sections. The first section will address the effects of crystallography at the ferrite:cementite lamellar interface and address the problem of curvature. Section two will consider experimental evidence suggesting that crystallography plays a major role in determining the behavior of the pearlite:austenite growth interface. This dependence will be investigated in greater detail in section three. On the basis of TEM observation of an interaction between the pearlite growth interface and the ferrite:cementite interphase boundary, section four will present an entirely new mechanism of pearlite growth based on the crystallographic effects explored in sections one through three.

1. CRYSTALLOGRAPHIC EFFECTS AT THE FERRITE:CEMENTITE INTERFACE

A. Introduction

Curvature of lamellae within a pearlite colony is a common observation with optical and electron microscopy in both high purity Fe-C steels and commercial alloys. Although strain effects following transformation have been invoked (60), Mehl's (2) suggestion that curvature occurs during the growth process is now generally accepted. Even though some type of low energy ferrite:cementite lamellae interface is often reported in pearlite (11-18) with orientation relationships of either the Bagaryatskii (11), Isaichev (61), or second Petch (13) (Table III), the presence of curved lamellae has been interpreted by Hillert (3) and Puls and Kirkaldy (42) as an indication that the ferrite:cementite interface is crystallographically insensitive. Other investigators, however, have suggested that lamellae curvature may occur by a mechanism deferential to a ferrite:cementite crystallographic relationship. Ohmori, Davenport, and Honeycombe (17) have suggested that the ferrite:cementite orientation relationship could alternate from the Bagaryatskii to the Isaichev within the same pearlite colony (They differ by an angle of 3.58° about cementite[010]). This would allow for the presence of a series of good fit habit planes parallel to cementite[010]. This situation could then give rise to a "corrugated habit plane that consisted of small alternate facets comprising these planes..." (17). This would allow a change in the habit plane while maintaining a relatively low energy interface.

In observing a surface replica with scanning electron

Table III

Ferrite:Cementite Orientation Relationships in Pearlite

Bagaryatskii	(001) //($\bar{1}2\bar{1}$) C F [010] //[111] C F [100] //[$\bar{1}$01] C F
2nd Petch	(001) //($\bar{2}\bar{1}$5) C F o [100] 2.6 //[3$\bar{1}\bar{1}$] C F o [010] 2.6 //[131] C F
Isiachev	(101) //(112) C F [010] //[11$\bar{1}$] C F

microscopy, Bramfitt and Marder (62, 63) interpreted striated cementite lamellae as being associated with a direction change during growth. They termed these striations "growth steps" and suggested that they could allow the growth direction to change without a change in the crystal orientation.

In these previous studies, however, no attempt to investigate the actual ferrite:cementite interface of lamellae which had changed habit planes during the growth process was made. When describing the ferrite:cementite interface, the important point which needs attention was clearly stated by Hillert in his classic 1962 paper on the pearlite transformation (3): ". . . the interesting question is not really whether any orientation relationship exists (or usually exists) between ferrite and cementite, but rather whether such a relationship is of any importance for the development or growth of pearlite." From the experimental evidence available at that time, Hillert concluded ". . . such a relationship is relatively unimportant." However, with the advent of higher resolution TEM techniques, it may be seen that the development of the morphology of the individual lamella is highly sensitive to the crystallographic relationship between the ferrite:cementite lamellae.

B. Results and Discussion

In the TEM investigation of lamellar curvature in both high purity Fe-0.8%C and Fe-12%Mn-0.81%C, it was observed that the change in the ferrite:cementite boundary plane does not occur smoothly. Instead, the high coincidence (112) ferrite:(101) cementite atomic habit plane is maintained during curvature by the presence of

discrete interfacial steps. Examples of this in the high purity Fe-C eutectoid are shown in Figure 1.1. In Figure 1.1a, b the termination of cementite lamella 1 results in the shifting over of the neighboring lamella. Note that the change in apparent habit plane does not occur smoothly, but rather by the presence of interfacial steps. From the micrographs, it is clear that lamella 2 deviates substantially from the (112) plane; however, closer inspection reveals that the change in direction is accomplished by means of interfacial steps approximately 25 angstroms in height with a spacing dependent on the angle by which the apparent habit plane varies from the ferrite (112). As may be discerned from Figure 1.1b, considerable variation in apparent habit plane may be accommodated by this mechanism. Variations in the thickness of cementite lamellae which would necessarily cause a change in the apparent habit plane can also occur in conjunction with interfacial steps, as shown in Figure 1.1c and in Figure 1.1d.

Although the cementite lamellae are often faulted (17), there does not appear to be any crystallographic incongruities associated with the steps in Figures 1.1a, b, c, or d. This would imply that the steps are purely structural, thereby ruling out the mechanism outlined by Ohmori et al. (17) in these instances. However as shown in the micrograph in Figure 1.1e, there are faults in some of the cementite lamellae which may be associated with changes in the ferrite:cementite habit plane.

Ferrite:cementite interfacial steps are also observed in pearlite formed in the Fe-12Mn-.8C steel. In Figure 1.2a, the ferrite:cementite interface is tilted parallel to the electron beam direction. Several steps (arrowed) of approximately 30 angstroms in

Figure 1.1 FCI interfacial steps in Fe-.8C pearlite with the Isaichev orientation relationship. Beam direction at (or near) $[111]_F$; $[010]_C$. Atomic habit planes corresponding to $(11\bar{2})_F$; $(101)_C$.

a. Ferrite:cementite interfacial steps in Fe-.8%C allowing lamellar curvature.

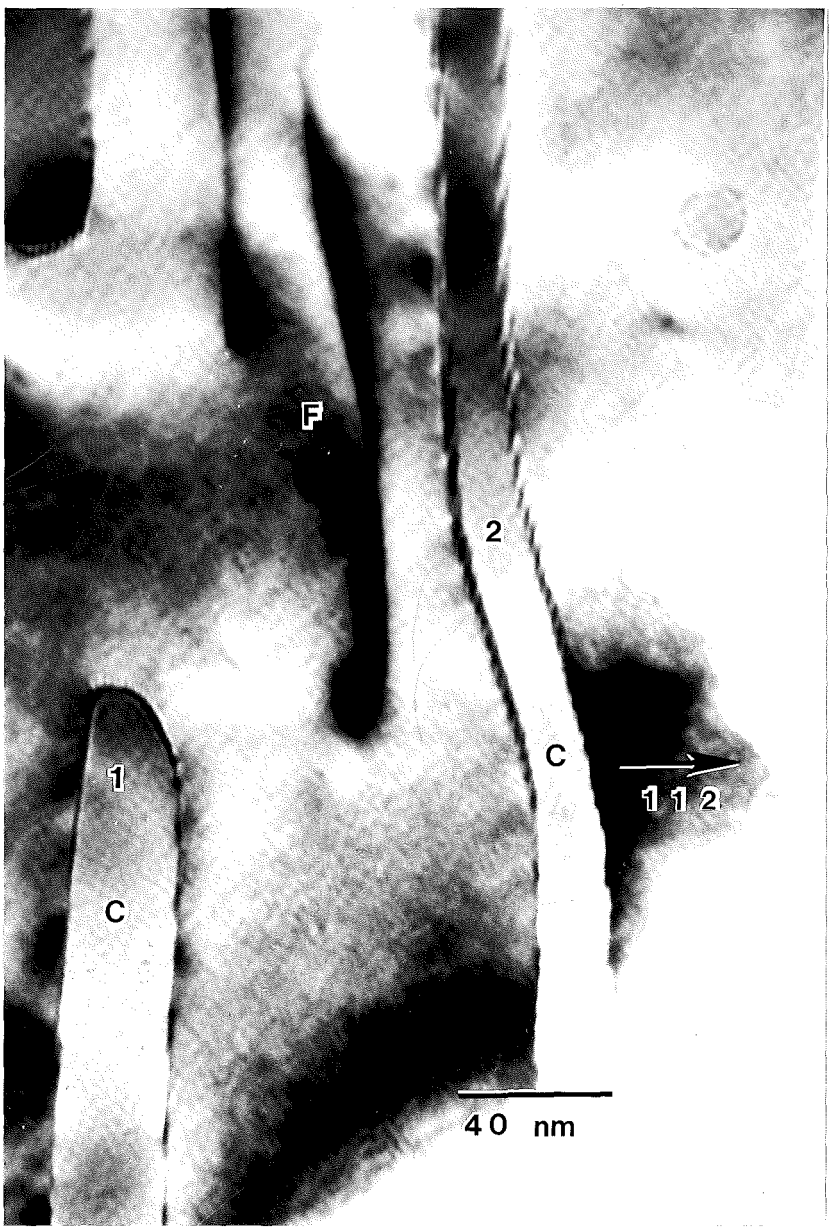

Figure 1.1 FCI interfacial steps in Fe-.8C pearlite with the Isaichev orientation relationship. Beam direction at (or near) $[11\bar{1}]_F$; $[010]_C$. Atomic habit planes corresponding to $(11\bar{2})_F$; $(101)_C$.

b. Ferrite:cementite interfacial steps in Fe-.8%C allowing lamellar curvature.

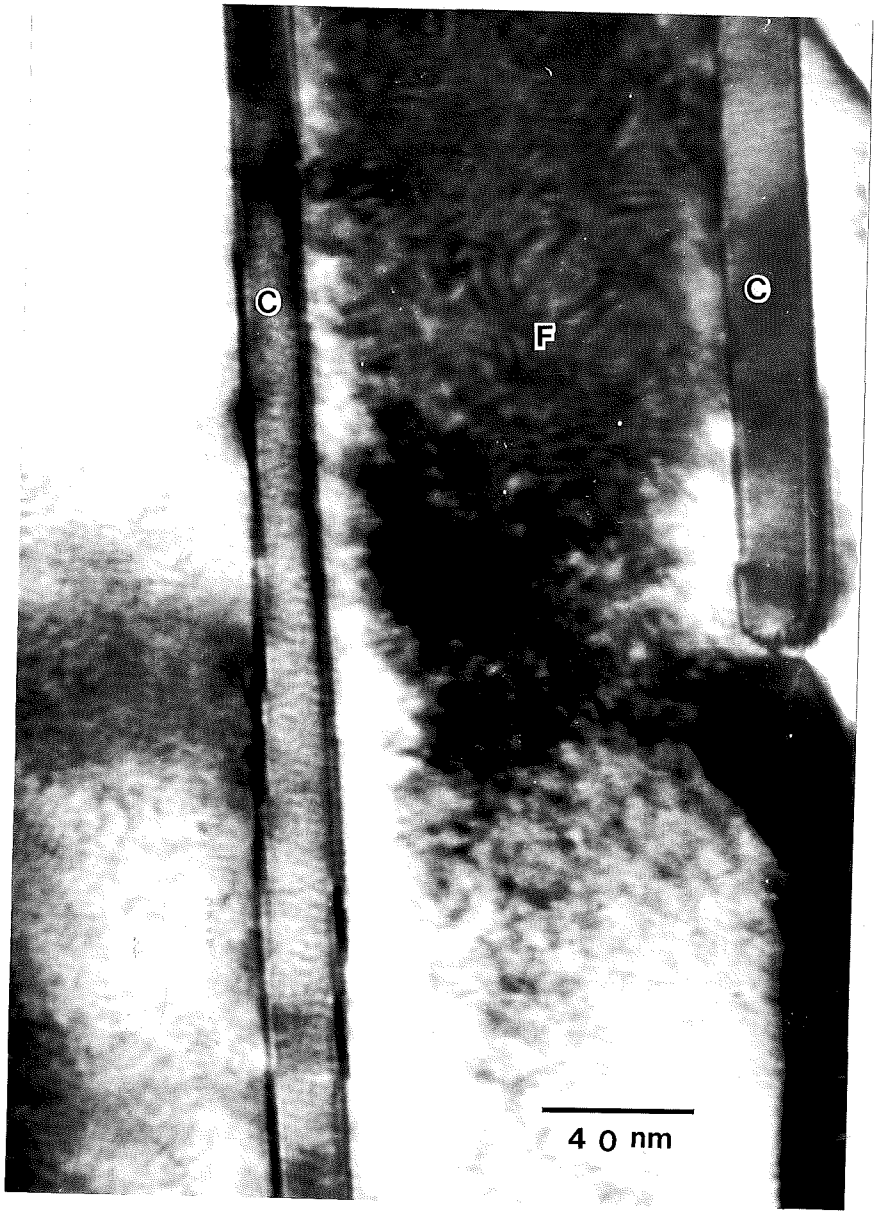

Figure 1.1 FCI interfacial steps in Fe-.8C pearlite with the Isaichev orientation relationship. Beam direction at (or near) $[111]_F$; $[010]_C$. Atomic habit planes corresponding to $(11\bar{2})_F$; $(101)_C$.

c. Ferrite:cementite interfacial steps in Fe-.8%C allowing lamellar thickness changes.

Figure 1.1 FCI interfacial steps in Fe-.8C pearlite with the Isaichev orientation relationship. Beam direction at (or near) $[111]_F$; $[010]_C$. Atomic habit planes corresponding to $(11\bar{2})_F$; $(101)_C$.

d. Ferrite:cementite interfacial steps in Fe-.8C allowing lamellar thickness changes.

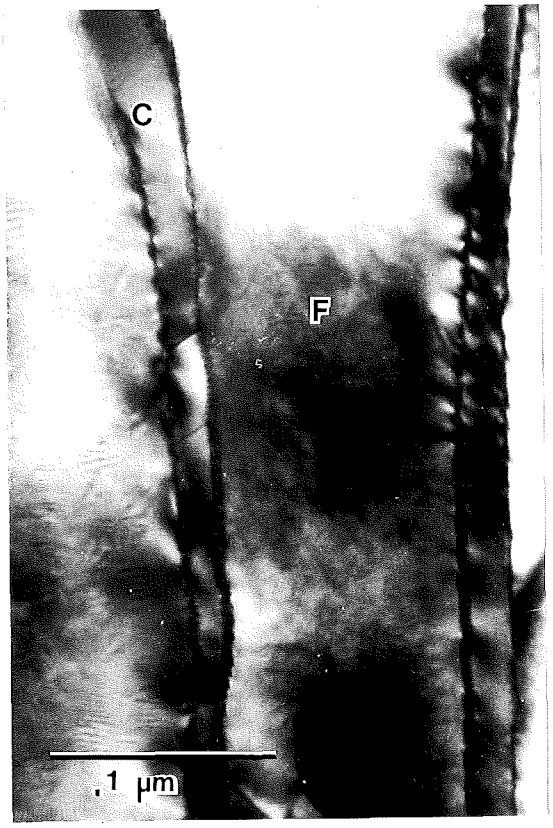

Figure 1.1 FCI interfacial steps in Fe-.8C pearlite with the Isaichev orientation relationship. Beam direction at (or near) $[111]_F$; $[010]_C$. Atomic habit planes corresponding to $(11\bar{2})_F$; $(101)_C$.

e. Structural fault in cementite lamella.

height may be observed. The associated selected area electron diffraction pattern in 1.2b shows that the steps allow changes in the boundary plane while maintaining the good fit Isiachev atomic habit plane. If the interface is tilted at an angle to the electron beam direction so that the defects might be imaged, as in Figure 1.2c, both white on black strain contrast and topographical contrast are observed. The ledges are the coarse defects (arrowed). The fine linear defects were shown to be moire' fringes.

The spacing of the ledges in Figure 1.2c is too large to have much effect on the position of the boundary plane. However, Figure 1.2d reveals substantial lamellar curvature may be obtained if the ledge spacing is decreased. Note once again the existence of both strain contrast and topographical contrast.

The TEM observations that have been discussed say nothing about the absolute surface energy of the ferrite:cementite interface. However, the fact that the boundary plane may rotate in response to growth influences without losing the (112)ferrite//(101)cementite atomic habit plane does imply that this plane is described by an energy cusp in the gamma-plot. This conclusion is based on the assumption that if a lower energy ferrite:cementite plane is present within the angle of deviation (measured from 1.1b to be 19 degrees about the ferrite [111]), then it would have been adopted rather than decreasing the distance between the interfacial steps. Stating this another way, it is energetically more favorable for the system to create interfacial defects (steps) which maintain the (112)ferrite//(101)cementite crystallography rather than adopt a different atomic habit plane. The manner by which pearlite maintains the ferrite:cementite habit plane during changes in

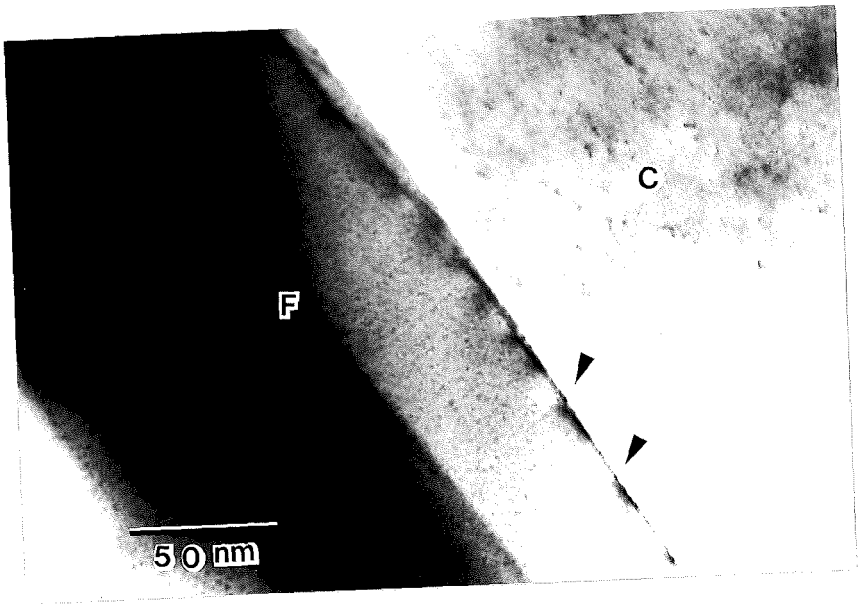

Figure 1.2 Boundary steps in Fe-12Mn-.81C.

a. Interfacial steps (arrowed) at the ferrite:cementite boundary. 18h, 610C.

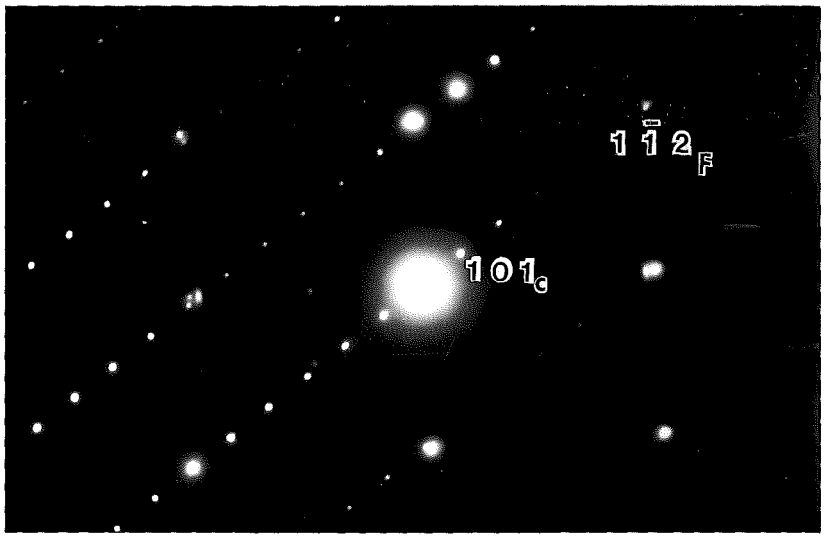

b. Ferrite [110] SADP showing ferrite $(1\bar{1}2)$ habit plane.

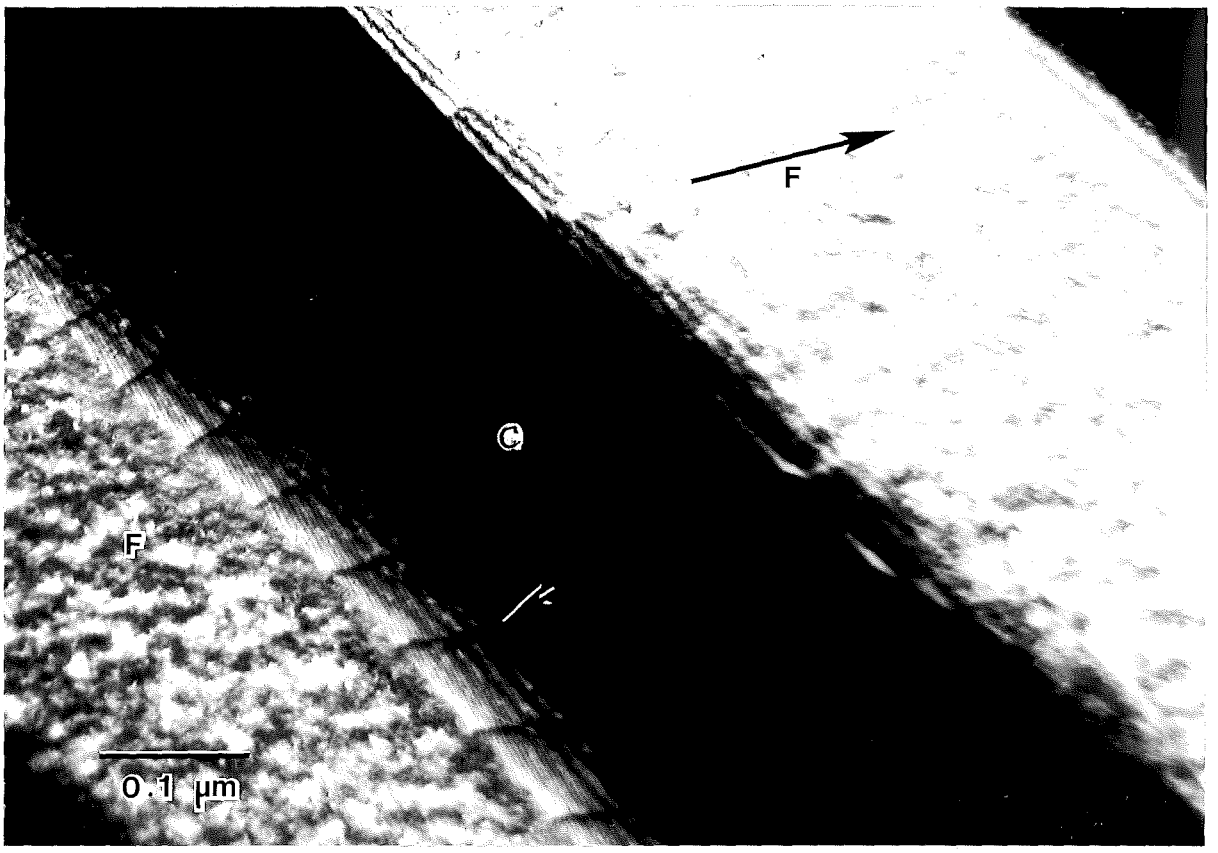

Figure 1.2 Boundary steps in Fe-12Mn-.81C.

c. Dark field image of steps in (a). $g = 002_F$.

Figure 1.2 Boundary steps in Fe-12Mn-.81C.

d. Curvature of lamellae accommodated by interfacial steps. $g = 110_F$. 12h, 600 C.

lamellar boundary plane strongly implies that the development and growth of individual lamellae within the pearlite colony is highly sensitive to the crystallographic relationship which exists between the ferrite and cementite lamellae.

2. INTERFACIAL STRUCTURE AT THE PEARLITE:AUSTENITE GROWTH INTERFACE

A. Introduction

As pointed out in the Background section, a disordered interface between the advancing pearlite phases (ferrite and cementite) and the matrix (austenite) is fundamental in current theories of pearlite growth. This belief of an incoherent growth interface is based primarily on the work of Mehl and coworkers in the 1940's (2) Rathenau and Baas in 1954 (37), and Hillerts' seminal 1962 paper (3).

In this section and results sections 3 and 4 an entirely new mechanism of pearlite growth will be developed which requires a dependence on crystallography at the growth interfaces. It will be demonstrated that this mechanism exists and suggest answers based on this new theory to resolve many long unanswered questions in pearlite growth.

B. Results and Discussion

Only the high manganese alloy could be used to study the pearlite growth interface because of the absence of the martensite transformation which, if it occurred, would destroy any interfacial structure formed at transformation temperatures. The optical micrograph in Figure 2.1a shows that the formation of pearlite occurs primarily along austenite grain boundaries with about 15% of the austenite transforming to pearlite. As this steel is

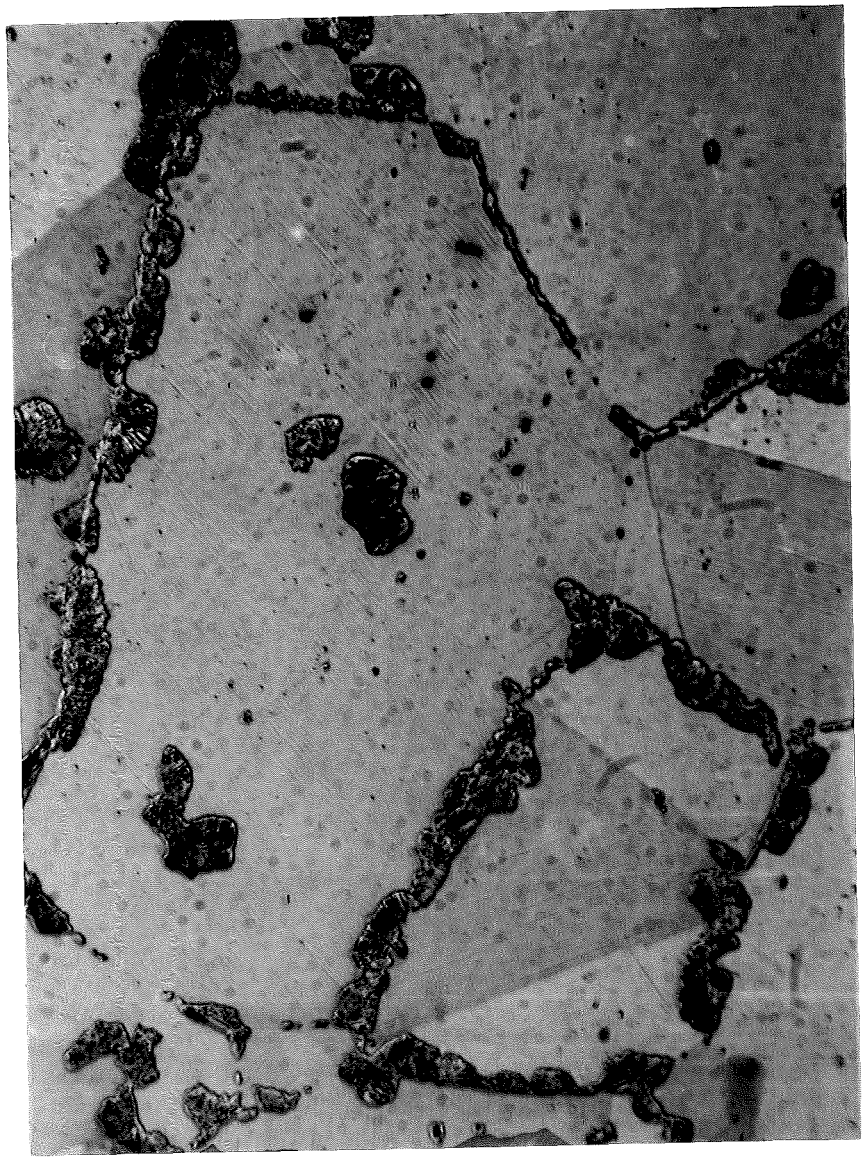

500X

Figure 2.1 Pearlite in Fe-12Mn-.81C.

a. Optical micrograph showing pearlite formation in Fe-12Mn-.81C. 12h, 610C.

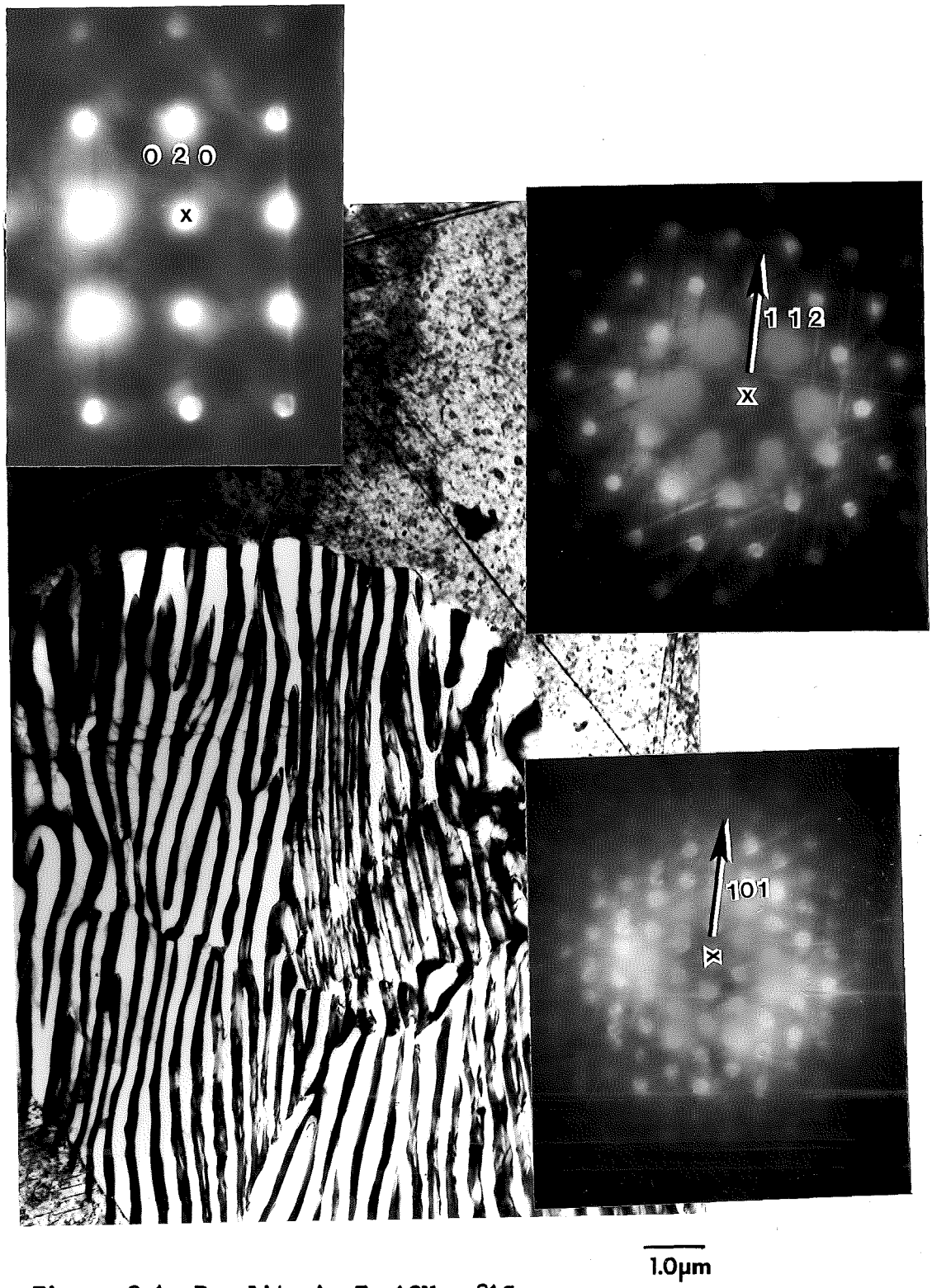

Figure 2.1 Pearlite in Fe-12Mn-.81C.

b. TEM micrograph of pearlite, with electron diffraction patterns showing bcc ferrite [111] , orthorhombic cementite [010], and fcc austenite [001] .

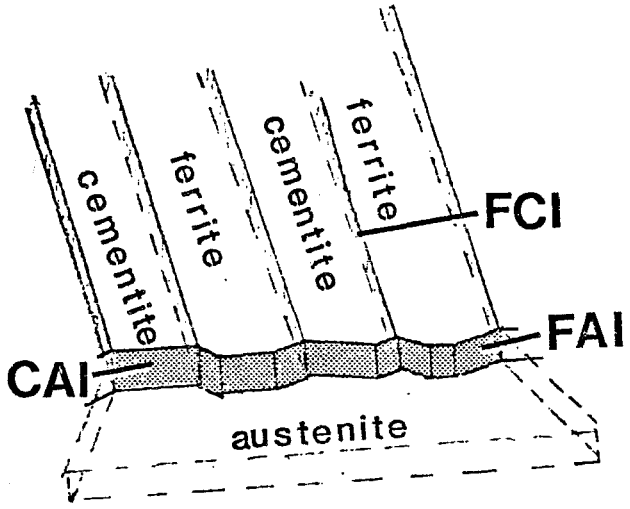

Figure 2.1 Pearlite in Fe-12Mn-.81C.

c. Schematic illustrating the various interphase interfaces in pearlite.

hypereutectoid, proeutectoid cementite is first formed with pearlite developing from it. The TEM micrograph in Figure 2.1b with corresponding convergent beam electron diffraction (CBED) patterns demonstrates that the pearlite consists of bcc ferrite and orthorhombic cementite growing synchronously into fcc austenite with no evidence of martensite. All of the colonies studied exhibited the Isaichev orientation relationship between the ferrite and cementite constituents. This crystallographic relationship is indicated by the CBED's in Figure 2.1. No reproducible, low index orientation relationship was observed between the austenite grain into which growth was occurring and either of the pearlitic phases. Figure 2.1c is a schematic illustrating the various interphase interfaces in the pearlite reaction. The two growth interfaces will be the subject of this section, namely the ferrite:austenite interface (FAI) and cementite:austenite interface (CAI).

a. Facetting

Facetting of precipitates has often been considered as evidence for crystallographic effects at an interphase boundary. It is an indication, though not proof, of the presence of partial coherency at the interface. Facets were observed regularly at the ferrite lamellae:austenite boundary (FAI) (Figure 2.2). The micrographs in this figure are each taken from a different colony growing into a different austenite grain and at several reaction temperatures. Therefore the observation is quite general. Note in Figs 2.2a and b the indicated parallel facetting of the growing edge of adjacent ferrite lamella. The cementite lamella, are generally, though not always, composed of a single facet rather than the multiple facets observed in the ferrite (Figures 2.2a, b and c). If, based on

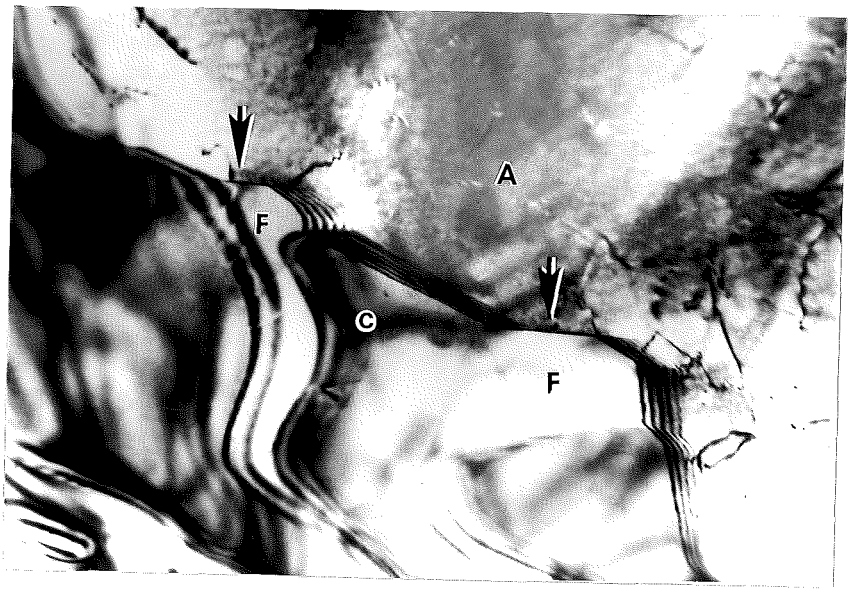

Figure 2.2 Facetting at the pearlite:austenite growth interface.

a. Parallel planar ferrite facets. 12h, 640C.

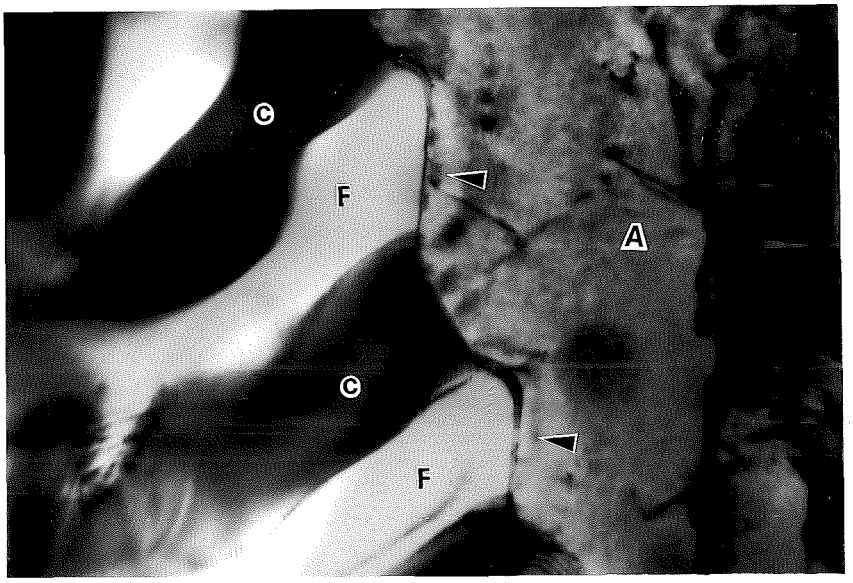

b. Parallel planar ferrite facets. 12h, 600C.

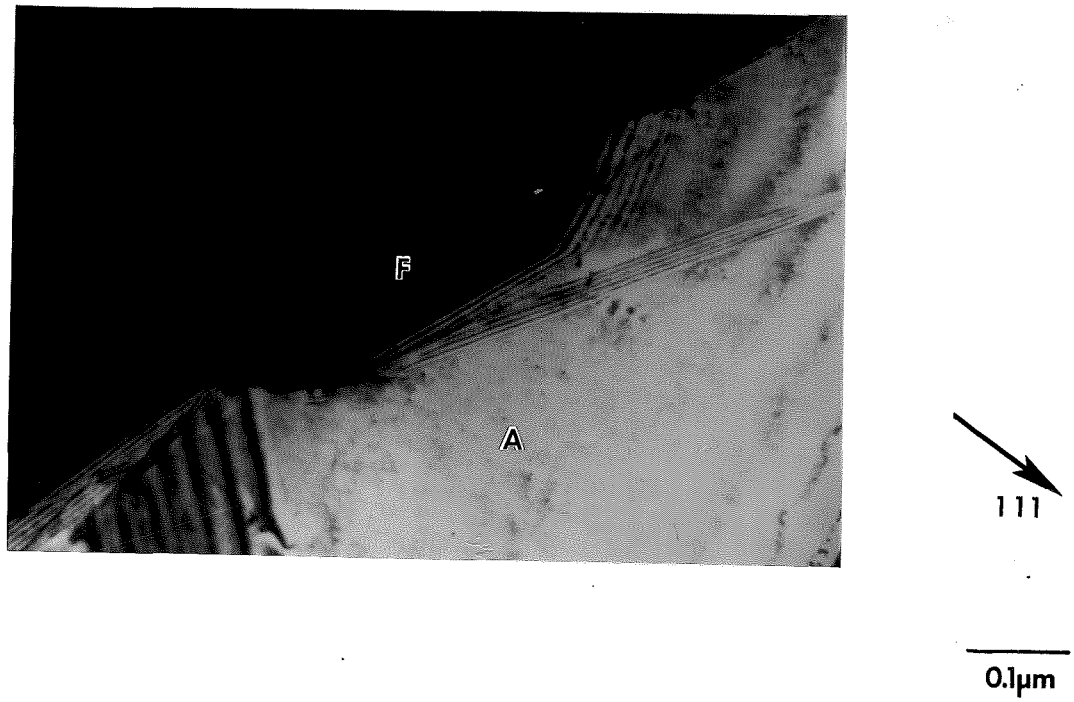

Figure 2.2 Facetting at the pearlite:austenite growth interface.

c. Austenite dark field showing ferrite facetting. 12h, 640C.

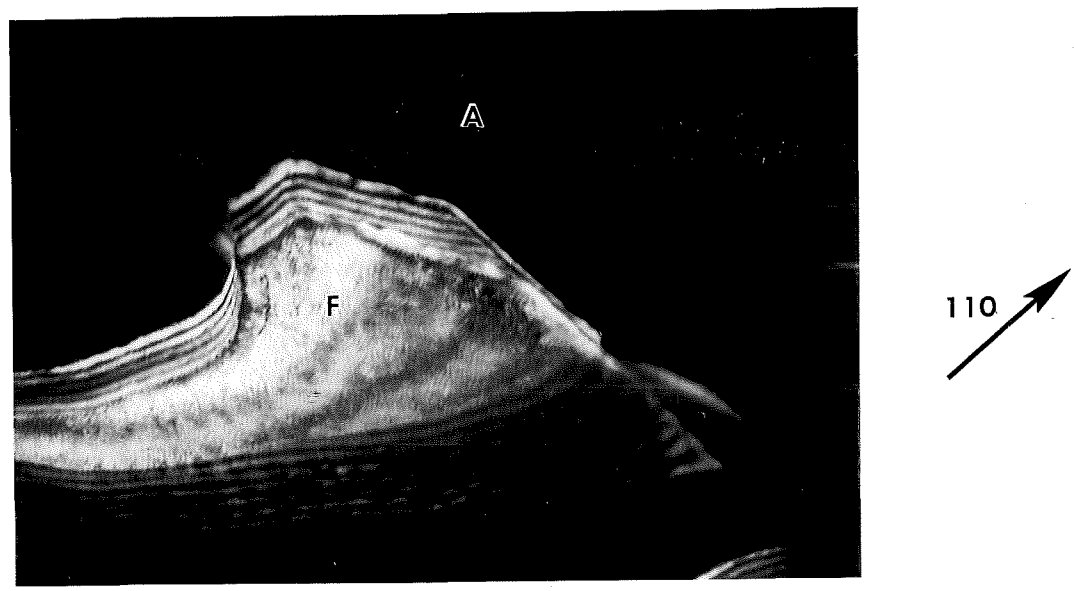

d. Ferrite dark field showing facets. 12h, 640C.

facetting evidence alone, we assume that the growth interface is partially coherent, then from the theories of advancement of these types of interfaces by Aaronson and coworkers (14,15), growth ledges and other interfacial structures such as misfit dislocations and/or structural ledges should be present.

b. Ferrite:Austenite Growth Interface

Using TEM to image the pearlitic ferrite:austenite growth interface (FAI, Figure 2.1c) illustrates ledges (Figure 2.3) at several different FAI's. In Figure 2.3a, a ferrite lamella is imaged in the dark field mode using a 110 ferrite reflection. The FAI is tilted nearly parallel with the beam direction and two ledges (arrowed) are immediately apparent, having heights of 85 and 40 angstroms. A second example of ledges at the FAI is shown in Figure 2.2b. Once again, the interface plane is tilted parallel to the beam direction. Imaging in the bright field mode reveals ledges of 60 and 40 angstroms. Further examples of FAI ledges are given in Figures 2.3c-e. These micrographs reveal the type of contrast observed at the ledge defects when the interface plane is tilted at some angle to the beam direction. As expected, there is strong "topographical" contrast caused by the inflection of the extinction contours, particularly in Figure 2.3c where a FAI ledge is imaged using an austenite 111 reflection. Figures 2.3d and e reveal that significant "strain" contrast exists for the interfacial ledges in addition to topographical contrast. Figure 2.3d is a bright field in which the ledges show "black-on-white" strain contrast, while 2.3e is a dark field using the ferrite [200] g vector showing "white-on-black" strain contrast. Using the Gleiter method (18) the ledge heights are calculated for Figures 2.3c-e and combined with

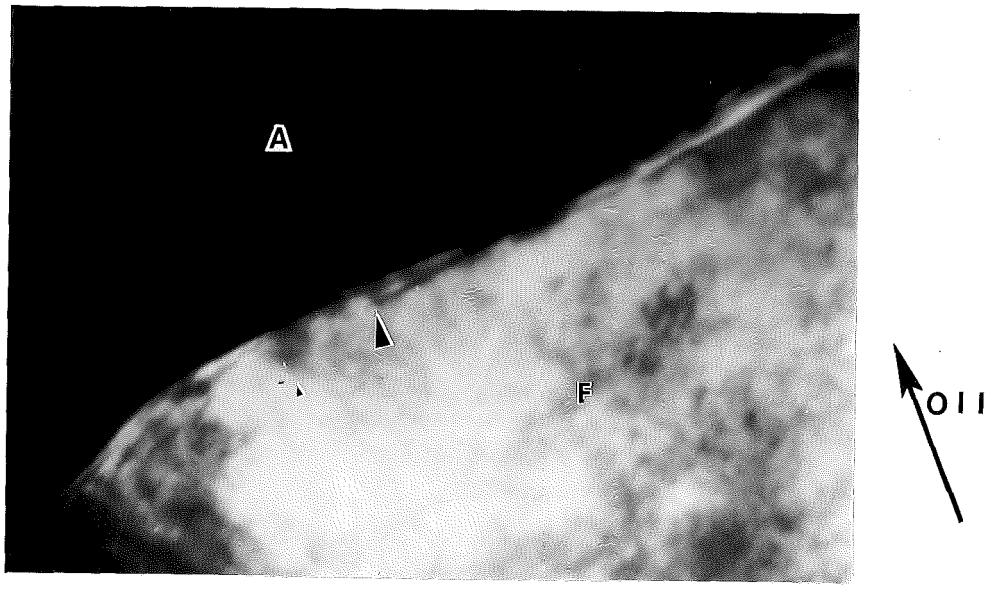

(a)

Figure 2.3 Examples of ledges (arrowed) at the pearlitic ferrite: austenite growth interface (see Table IV).

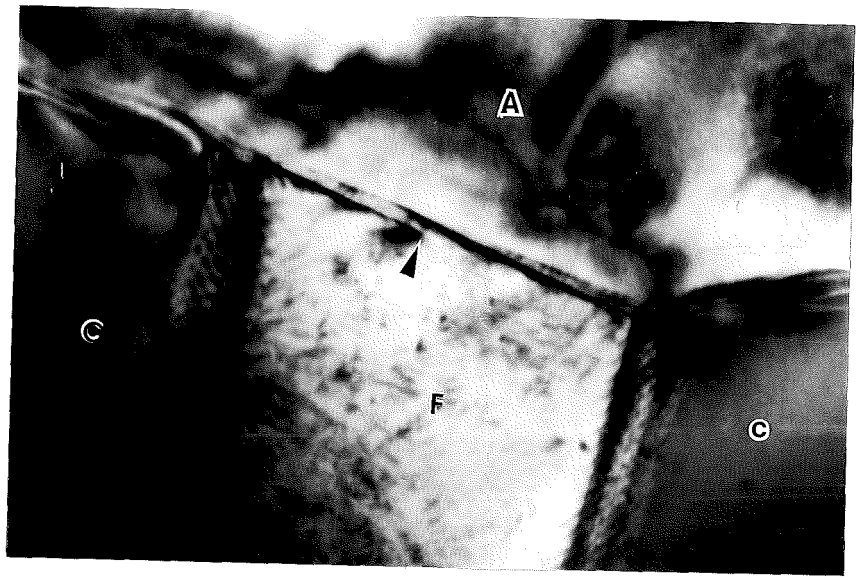

(b)

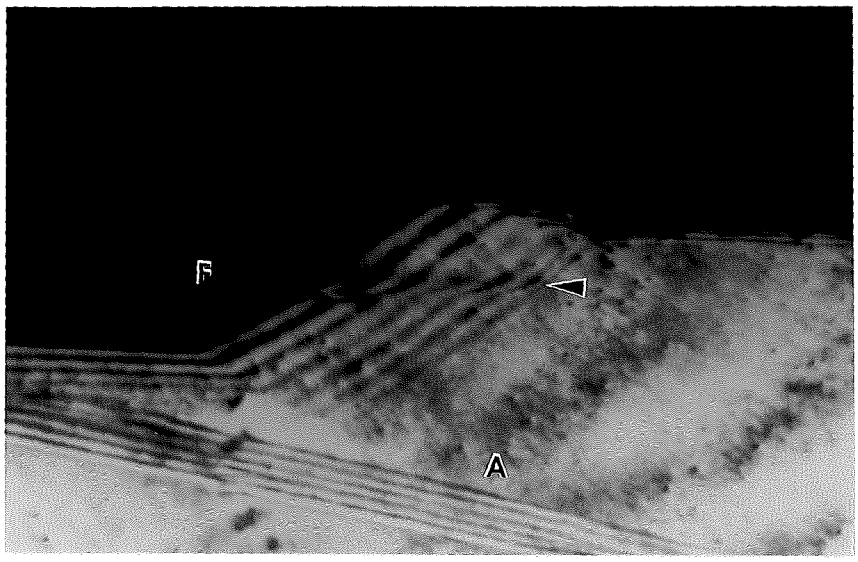

(c)

Figure 2.3 Examples of ledges (arrowed) at the pearlitic ferrite: austenite growth interface (see Table IV).

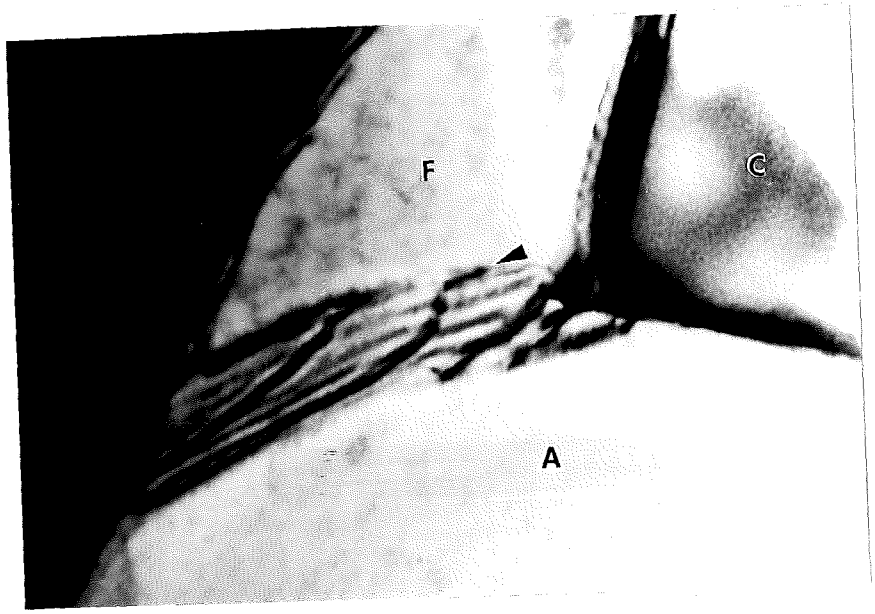

(d)

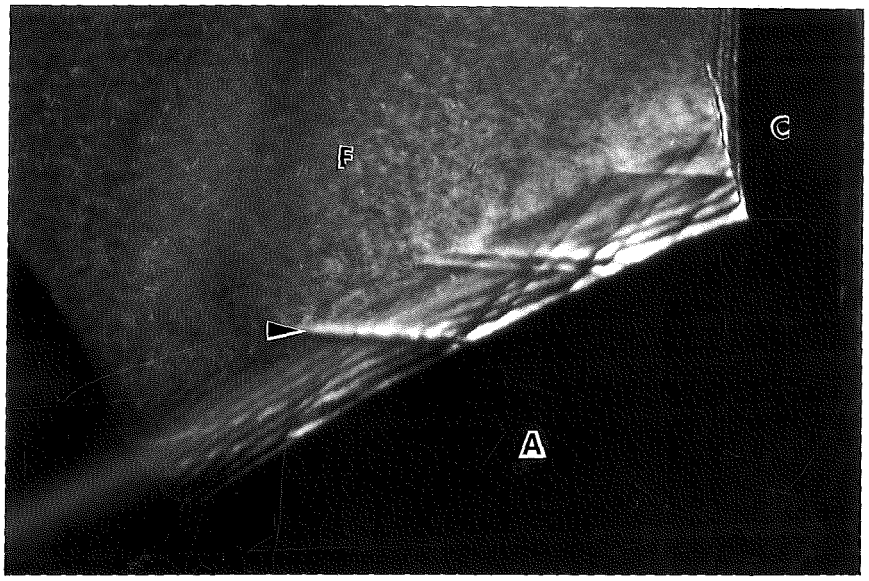

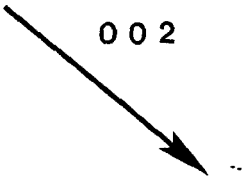

0.1μm

(e)

Figure 2.3 Examples of ledges (arrowed) at the pearlitic ferrite: austenite growth interface (see Table IV)

the data from Figures 2.3a and b and other figures from later sections in Table IV. It is apparent from the micrographs and Table IV that ledges are present at the FAI at reaction temperatures ranging from 600 to 650 C, and during both the initial stages (Figure 2.3d) and later stages (Figure 2.3b) of the transformation.

A more complete analysis of FAI ledges is shown in Figure 2.4. In 2.4a, the flat ferrite:austenite interphase boundary plane is parallel to the beam direction. A number of interfacial ledges are observed (inset) with heights of ~40-60 angstroms. The ledges are numbered so that specific identification can be made in each micrograph. If the FAI is tilted so that the interphase boundary may be imaged using weak beam dark field (WBDF) techniques (9) the defects are seen to exhibit strain contrast and topographical contrast. The "white on black" strain contrast of the ledges is obvious in Figures 2.4b,c. The topographical contrast is manifested by the inflection of the extinction contours at the intersection with the ledges. This can be seen in 2.4 b,c but is most obvious in the inset in 2.4d, where a no strain contrast condition is obtained but the topographical contrast remains.

The no (strain) contrast condition is found for the g vector almost parallel to the trace of the interfacial plane. This is consistent with the theory of ledge defect contrast discussed in the experimental section.

In order to investigate the possibility of resolving finer structure at the FAI, the WBDF technique was employed by which interfacial dislocations having small spacings might be resolved. Because the appearence of moire' fringes resembles closely that of misfit dislocations (Figure 2.5a) great care was taken to assure the

Table IV

Heights of FAI Growth Ledges

Figure	Ledge Height Angstroms	Reaction Time Hours	Reaction Temperature Degrees C
2.3a	90 40	12	630
2.3b	60 40	18	610
2.3c	70*	12	640
2.3d	40*	6	650
2.3e	10*	12	610
2.4a	60 40	18	610
3.1a	15	12	600
4.1a	15*	12	610
4.1e	30*	7	600

*Determined by the Gleiter method.

Figure 2.4 Analysis of ledge contrast. 18h, 610C.

a. Ledges at the ferrite:austenite growth interface.

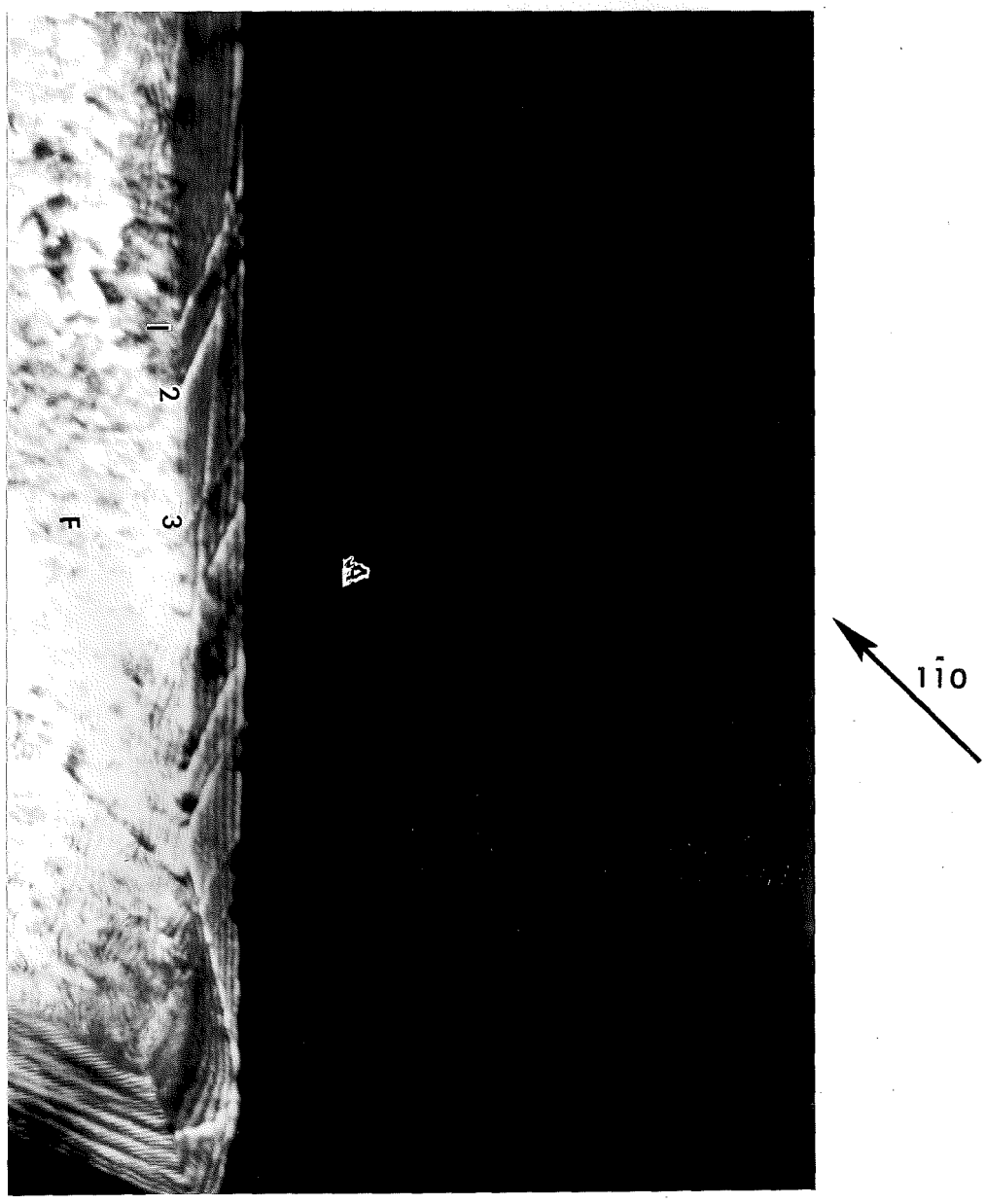

Figure 2.4 Analysis of ledge contrast. 18h, 610C.

b. Ledges from (a) imaged in dark field using ferrite [1$\bar{1}$0].

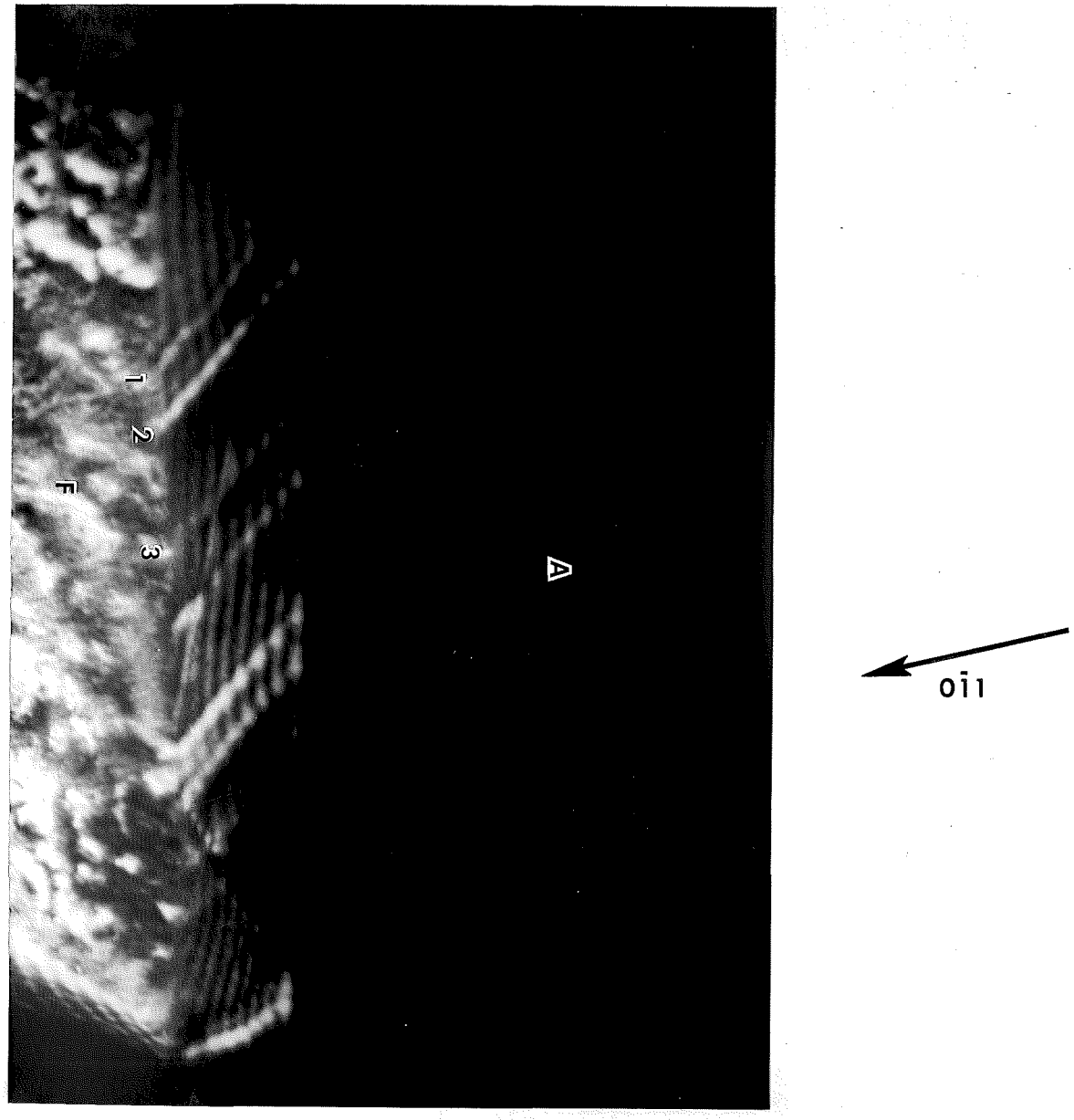

Figure 2.4 Analysis of ledge contrast. 18h, 610C.

c. Ledges from (a) imaged in dark field using ferrite [0ī1] .

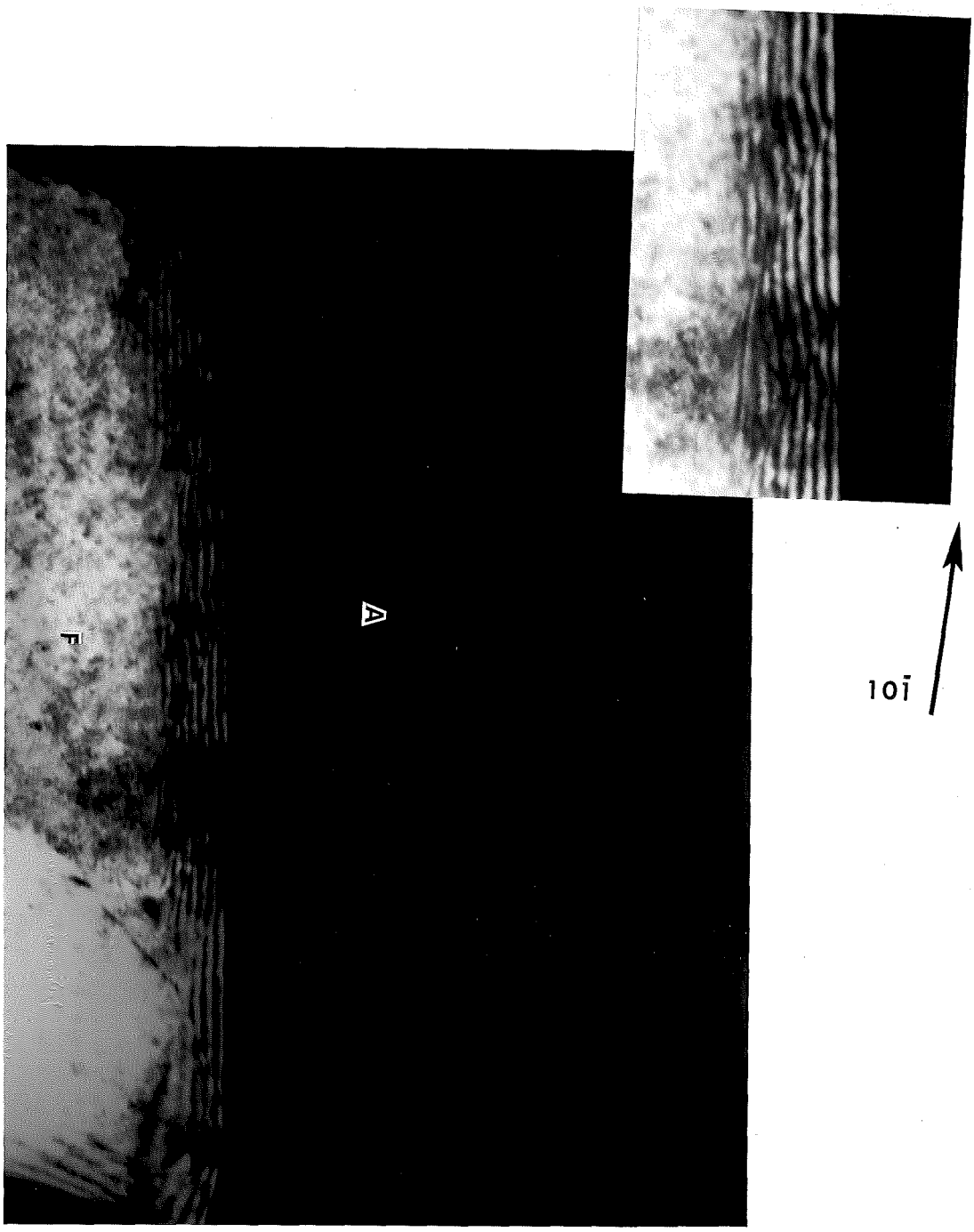

Figure 2.4 Analysis of ledge contrast. 18h, 610C.

d. No strain contrast obtained for ledges in (a) using ferrite [10$\bar{1}$]. Topographical contrast is still visible (see inset).

images obtained were those of structural defects and not an imaging artifact. The results of these experiments are shown in Figures 2.5b, c, and 2.6a-c with 2.6a-c corresponding to the FAI ledge analysis in Figure 2.4. In Figure 2.5b, the linear defects between the pearlitic ferrite and matrix austenite are seen to lie in at least three crystallographic directions (marked) with spacings between 20 and 30 angstroms. Note also the presence of a growth ledge (arrowed). Several contrast and one no contrast condition was found for this interface. The g vector for the no contrast condition in Figure 2.5c indicates that the displacement vector associated with these defects lies in or close to the interfacial plane, suggesting that these structures are misfit dislocations.

The Figures 2.6a-c show misfit dislocations in that interface. It is observed in Figure 2.6c that these defects are still visible while the ledges have a no strain contrast condition. This indicates that the b for these defects is not perpendicular to the interface and that some component must lie in the interface plane. Thus, the dislocations shown in the 2.6a-c insets would seem to have at least some misfit correcting function.

c. Cementite:Austenite Growth Interface

Although the FAI is frequently facetted, the pearlitic cementite:austenite interface (CAI) (Figure 2.1c) is seldom sharply facetted, but is often seen as a flat plane lying between two facetted FAI's (Figure 2.2b and c). However, ledge structures analogous to those on the FAI are also found at the CAI. This is seen in Figure 2.7a where the CAI is tilted so that the interfacial plane is parallel to the beam direction. The cementite dark field reveals ledges with heights between 30 and 40 angstroms. The bright

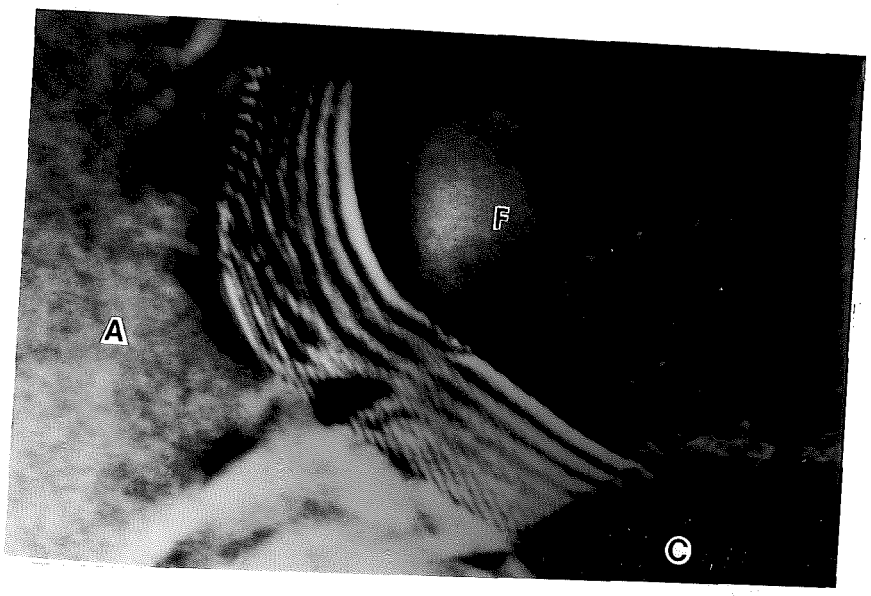

Figure 2.5 Interfacial dislocations at the ferrite:austenite interface. 12h, 630C.

a. Moire' fringes.

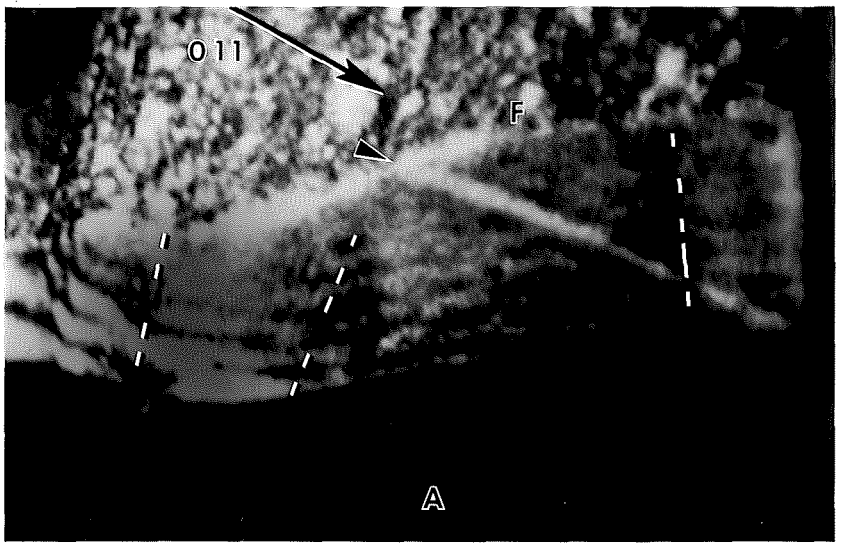

50 nm

Figure 2.5 Interfacial dislocations at the ferrite:austenite interface. 12h, 630C.

b. WBDF of ferrite:austenite interface using ferrite [011].

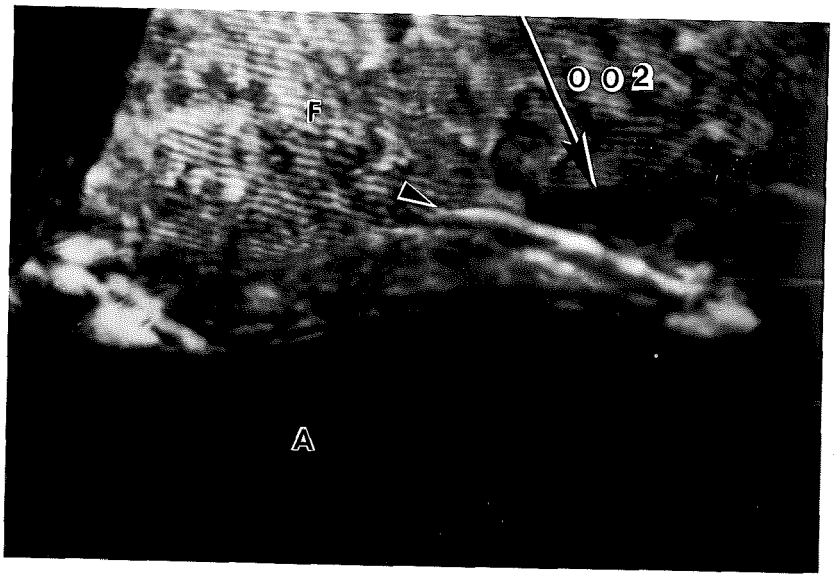

50 nm

c. WBDF of ferrite:austenite interface using ferrite [002]. Ledge in contrast. Dislocations out of contrast.

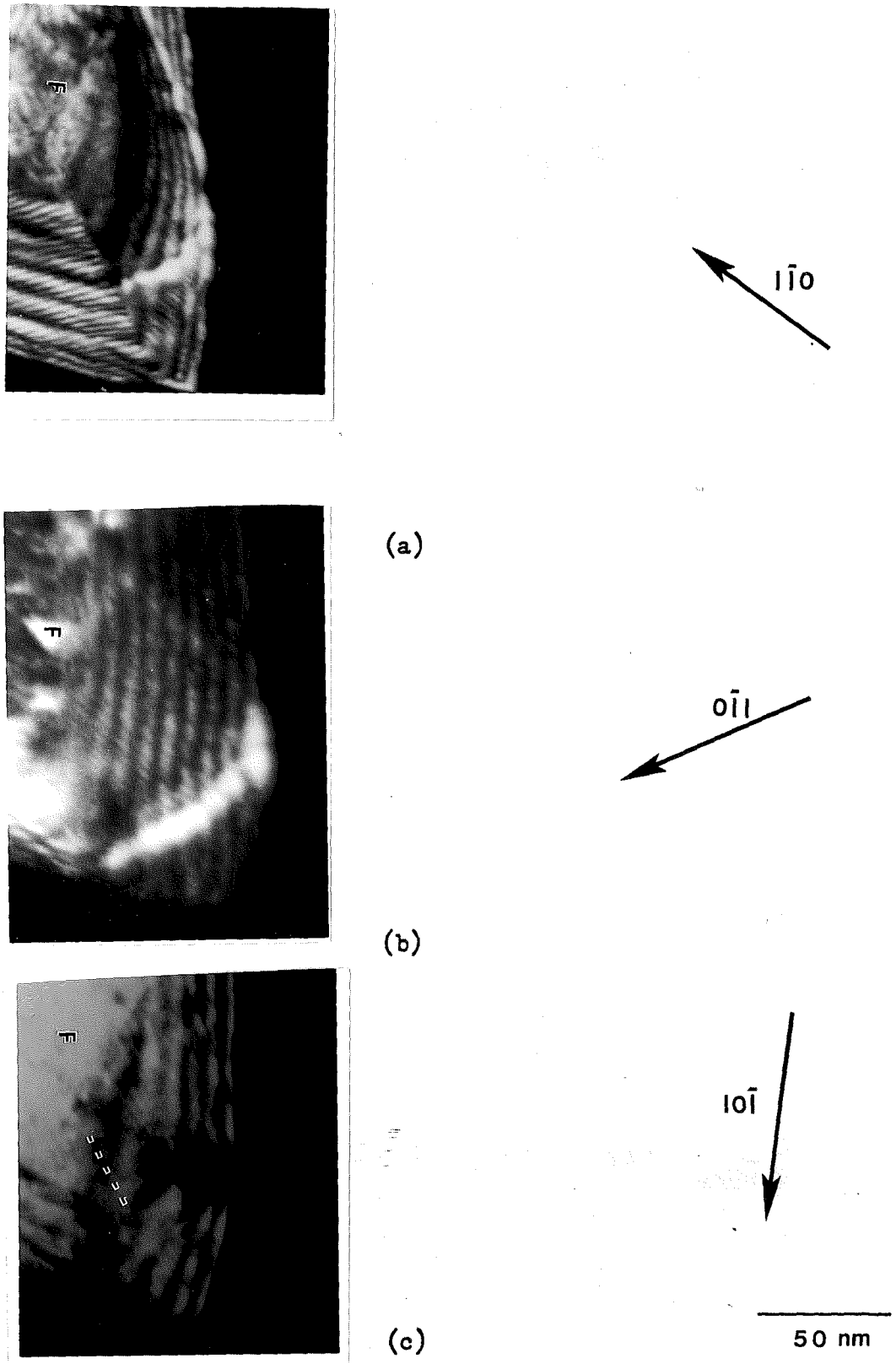

Figure 2.6 Linear defects with at least some misfit correcting function. 18h, 610C.

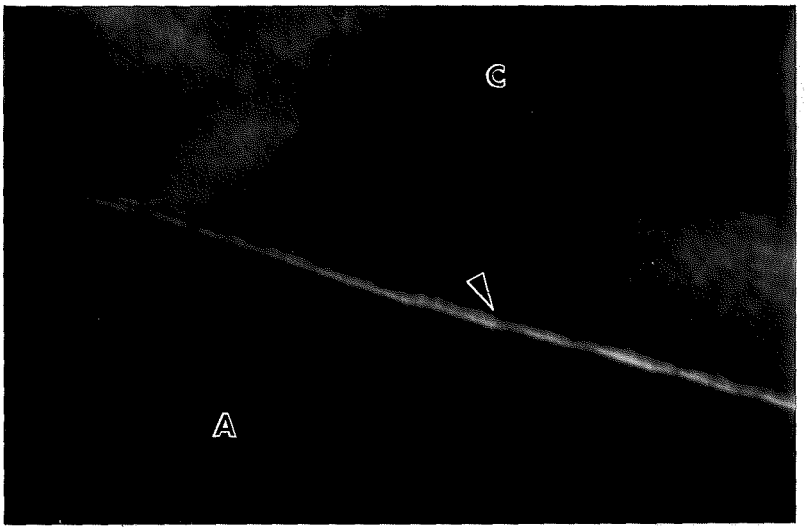

Figure 2.7 Cementite:austenite interfacial ledges.

a. Cementite dark field showing 30 angstrom ledges. 12h, 640C.

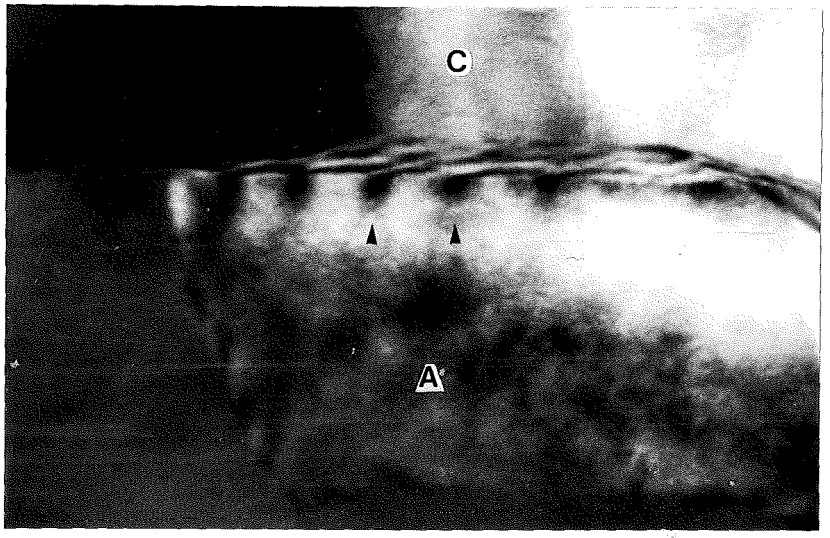

b. Bright field micrograph of (a) showing substantial strain fields at interfacial ledges.

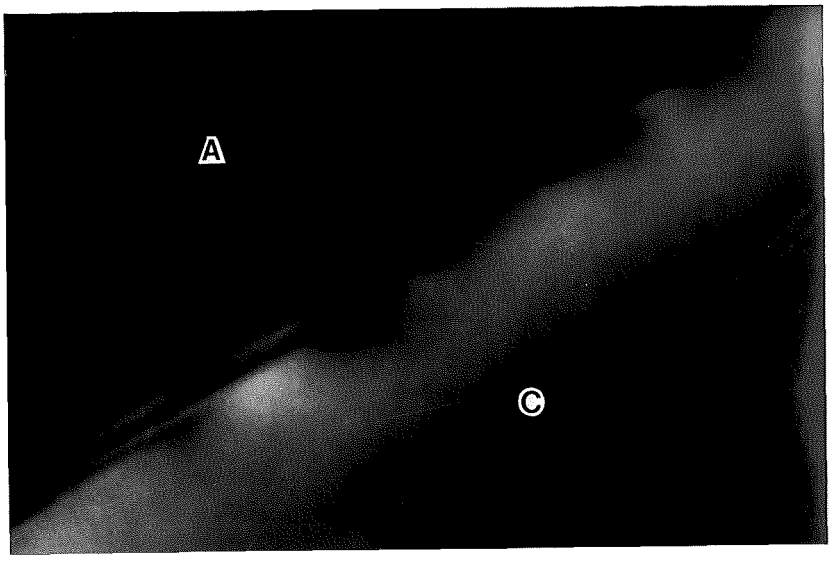

50 nm

Figure 2.7 Cementite:austenite interfacial ledges.

c. Cementite dark field showing 40 angstrom ledges. 18h, 610C.

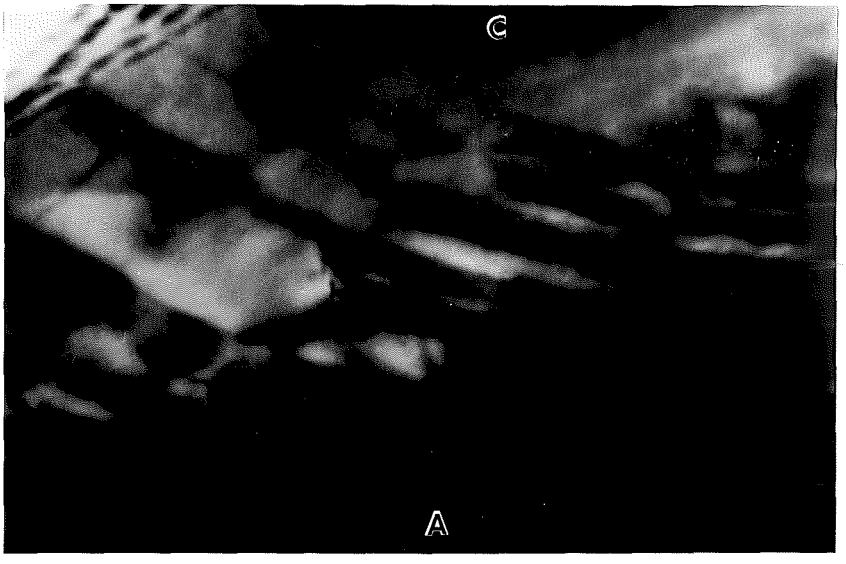

70 nm

d. Cementite dark field showing complex ledge configuration. 18h, 610C.

field of 2.7a is shown in 2.7b. Note that substantial strain fields associated with the interfacial ledges may be seen emanating from the interface into the austenite. This type of strain field contrast has also been observed for structural ledges and growth ledges on partially coherent interfaces of in Al-Cu (59). Two other examples of CAI ledge defects are imaged using cementite reflections in 2.7c and 2.7d.

In Figure 2.8a-d, the interface from Figure 2.7a and b has been imaged using several austenite reflections. The "black on white" strain contrast and coinciding topographical contrast are observed for 2.8a-c at three different contrast conditions. A no strain contrast condition is obtained for g=002 (Figure 2.8d), which is parallel to the trace of the CAI, although the topographical contrast is still present. This is, as expected, the same result obtained for the visibility of ledges on the FAI and is consistent with the theory of growth and structural ledge contrast. Once again, the presence of interfacial defects expected to exist on partially coherent interfaces is found on interfaces which, until now, have been considered to be "disordered-like" or incoherent.

d. In-situ Hot Stage TEM

It has been clearly demonstrated that ledges exist on the advancing edges of both the pearlitic ferrite and cementite:austenite interfaces. Close examination of Figures 2.2 and 2.3 for the FAI and Figures 2.7 and 2.8 for the CAI show that boundary advancement would result with movement of these ledges across the interface (as schematically illustrated in Figure B8). The question remains as to whether these defects are structural ledges or growth ledges. There is often confusion as to the role of

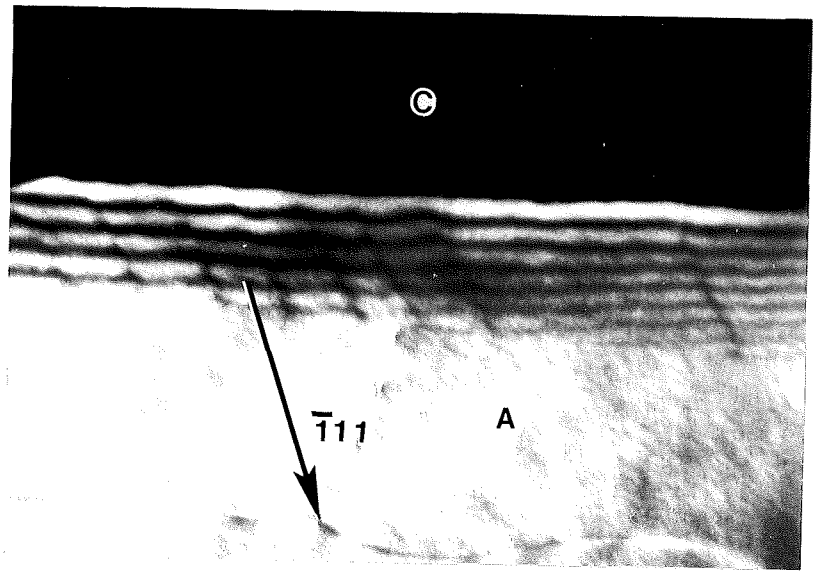

Figure 2.8 Analysis of cementite:austenite interfacial ledges. 12h, 610C.

a. Ledges from 2.7(a) imaged using austenite $[\bar{1}11]$ dark field.

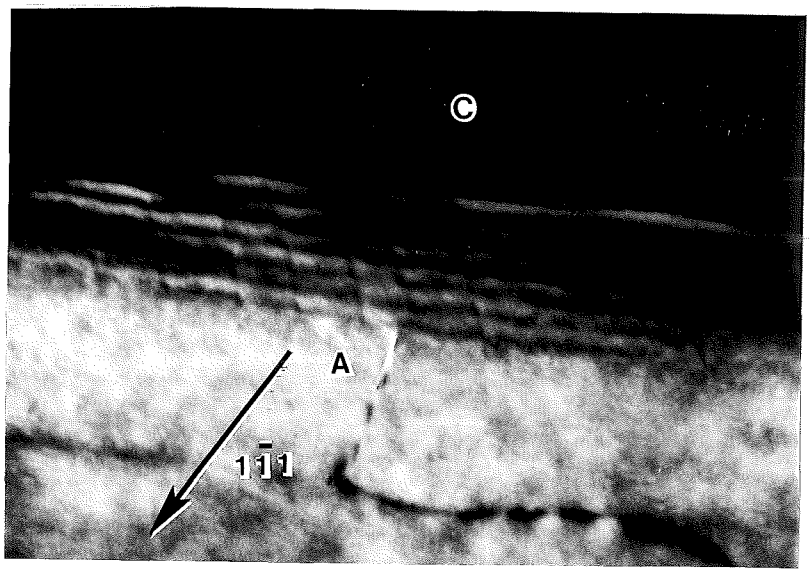

b. Ledge contrast using austenite $[\bar{1}11]$.

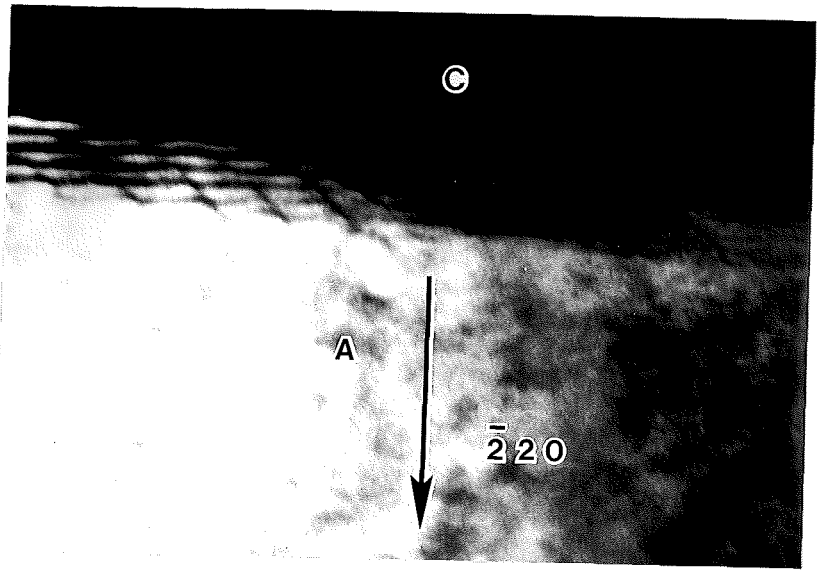

Figure 2.8 Analysis of cementite:austenite interfacial ledges. 12h, 640C.

c. Ledge contrast using austenite [$\bar{2}20$].

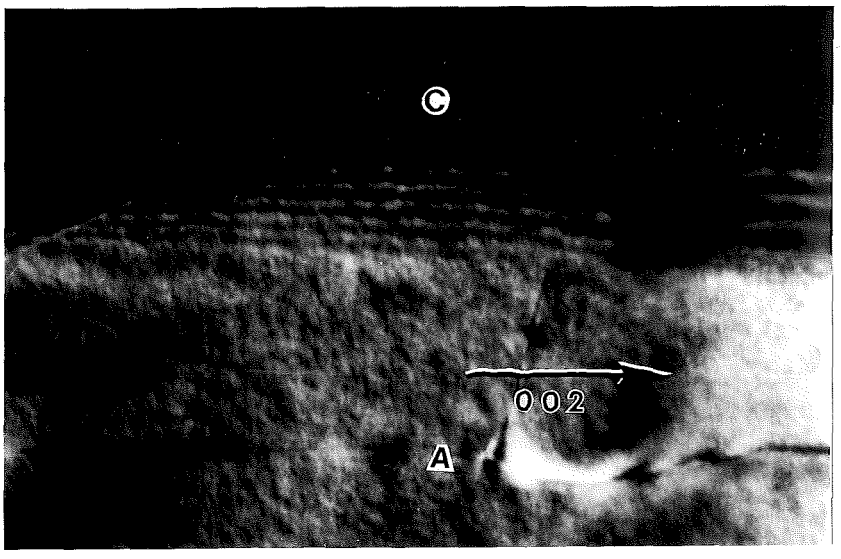

d. No strain contrast condition using austenite [002].

structural and growth ledges in partially coherent interfacial structure. A structural ledge exists on the interface only to lower energy by improving coherency (21). The mobility of these structures is predicted (19) and has been shown via hot stage TEM (58) to be limited if not completely immobile. The growth ledge, on the other hand, is the primary mechanism for the advancement of a partially coherent interface and therefore has a high mobility (14,15). A previous study by Rigsbee and Aaronson (20, 21) has shown that structural ledges are generally small (triatomic in their study of bcc:fcc interfaces in an Fe-C-Si alloy) with a somewhat regular spacing where the interface is microscopically flat. Growth ledges occurring on a variety of precipitate phases (including grain boundary allotriomorphs, Widmanstatten plates, precipitate plates, etc., in ferrous and non-ferrous systems) on the other hand, have been observed to be relatively large (10), tens, hundreds or even thousands of angstroms high, with a variable, unpredictable, spacing even on microscopically flat interfaces. The heights of the ledges in Figures 2.2, 2.3, and 2.7, which may vary from 30 angstroms to about 90 angstroms (Table IV), would indicate that these structural defects are growth ledges rather than structural ledges and are thus present for the purposes of advancement of the pearlite interface. The most convincing and direct method to demonstrate the difference between growth and structural ledges is with in-situ hot stage TEM experiments. In this manner, the specimen may be heated inside the microscope and the determination may be made as to whether the ledges are mobile. This technique has been used by Baro and Gleiter (58) to demonstrate growth ledge mobility in alpha-brass and the present author has used in-situ hot stage experiments to distinguish

immobile atructural ledges from mobile growth ledges on partially coherent θ:k interfaces in Al-5Cu (59). The obvious requirement is that the high temperature phase be retained throughout the experiment. Because the untransformed austenite is retained on quenching, it should be possible to locate ledges on either the ferrite or cementite lamellae formed in the bulk and observe their behavior when the specimen is heated to appropriate temperatures. If they are growth ledges they should remain mobile.

The results of this experiment are illustrated in Figure 2.9. Several ledges are indicated in Figure 2.9a which is a micrograph of a FAI before the specimen was heated. Figures 2.9b-e show the results of heating the foil to 380 C for ca. 30 secs., cooling, and recording the image four separate times. It is clear that the ferrite growth ledges (arrowed) have systematically shifted across the interface. A jog in the ledge developing in Figure 2.9c (arrowed) is also visible. This could be due to its intersection with another ledge which at this diffracting condition is out of contrast. It is possible to determine the distance the ledges moved on the interphase boundary during each temperature spike by using the stacking fault in Figure 2.9a to first determine the foil thickness. Using this technique the foil thickness is determined to be ~300 nm and the approximate distances of ledge migration is recorded in Table V. The ledges moved a total of 130 nm with an average displacement of 33 nm per heat treatment spike. Heating the foil to higher temperatures for longer times resulted in the nucleation of cementite plates within the austenite, Figure 2.10a (a good indication that the steel specimen was not being decarburized) and sympathetic nucleation of new lamellae of pearlite with much

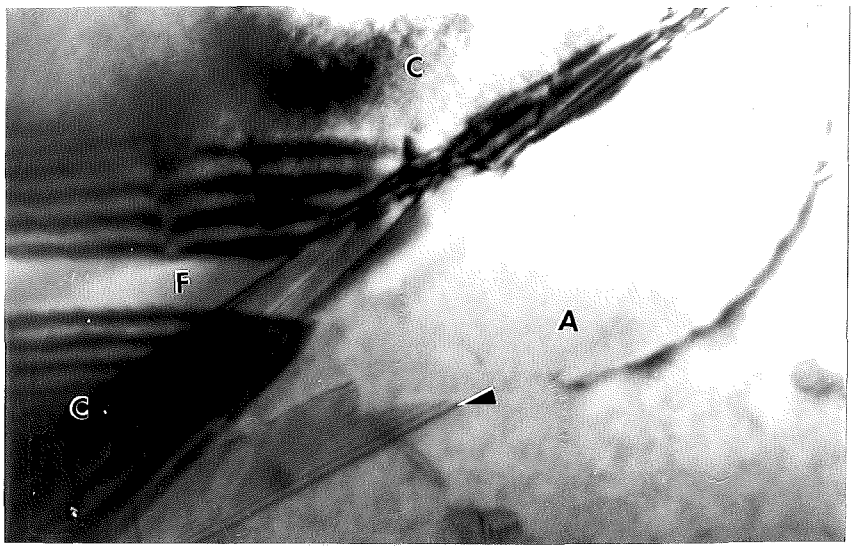

0.1μm

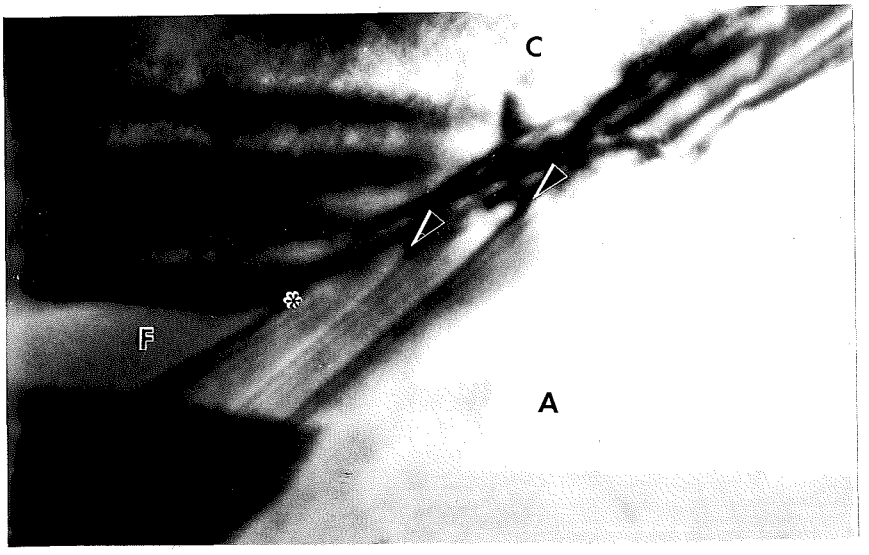

0.1μm

Figure 2.9 Hot stage microscopy experiment.

a. Interface prior to heating. 12h, 610C.

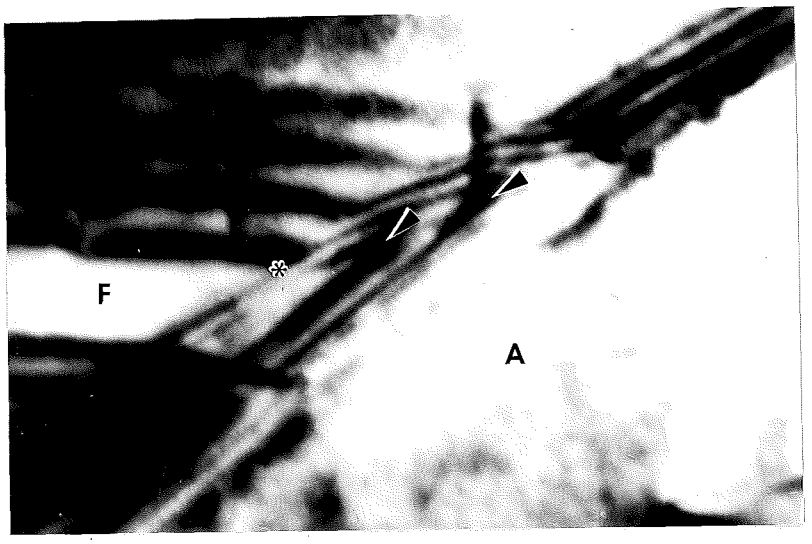

Figure 2.9 Hot stage microscopy experiment.

b. After heat no. 1.

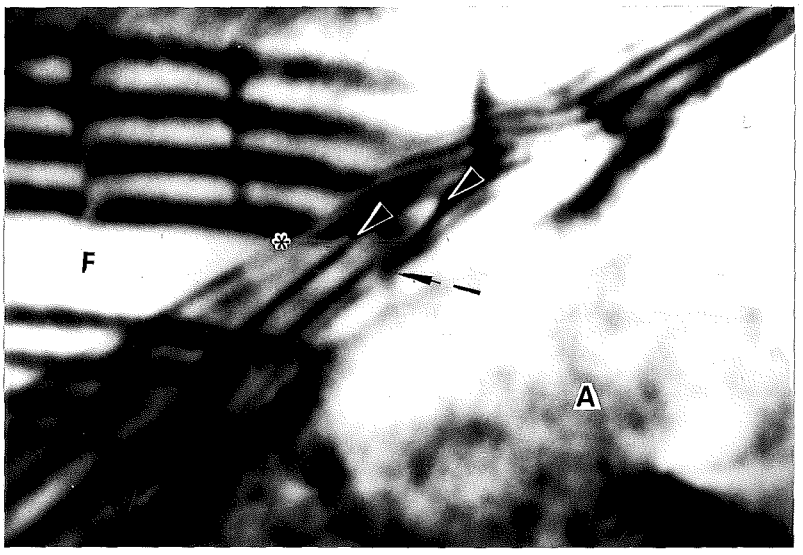

c. After heat no. 2.

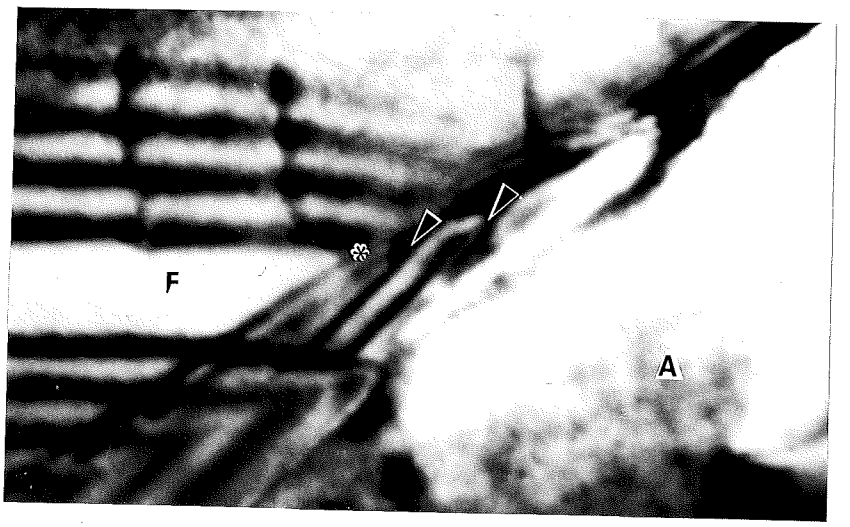

Figure 2.9 Hot stage microscopy experiment.

d. After heat no. 3.

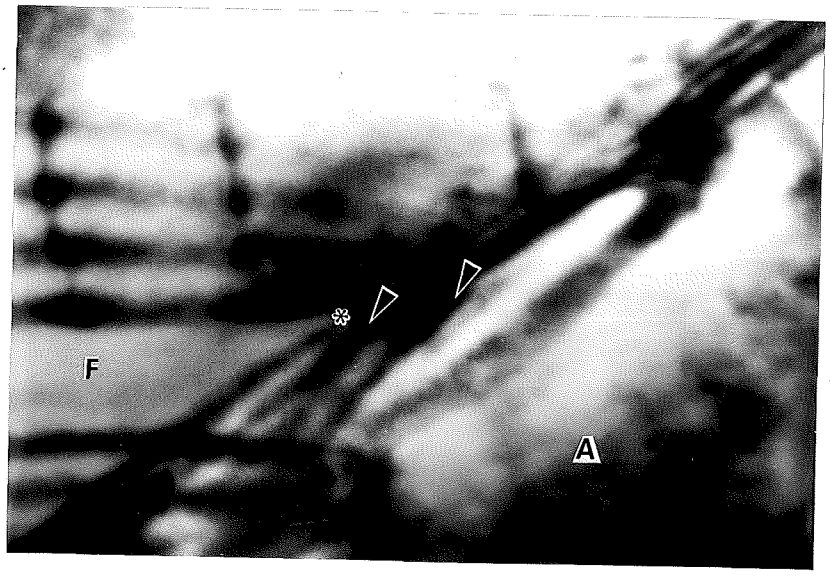

e. After heat no. 4.

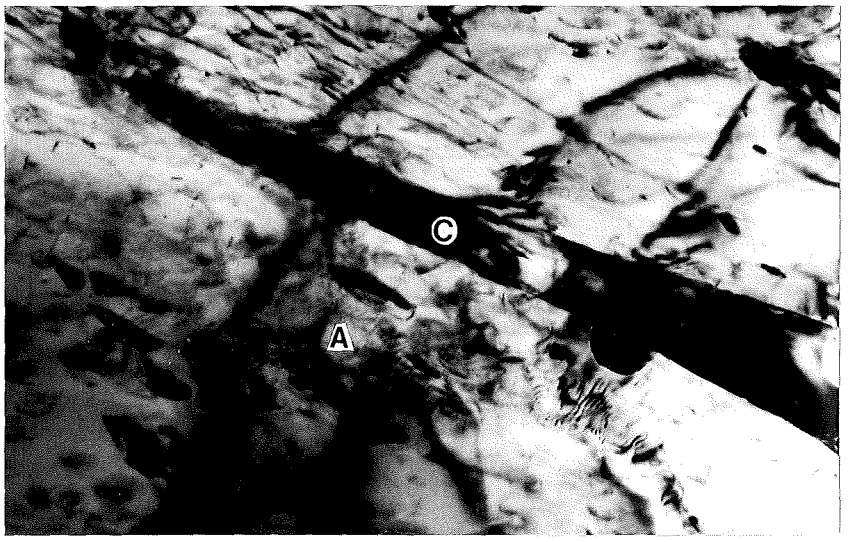

Figure 2.10 Austenite decomposition reactions in TEM hot stage.

a. Cementite plate formation during hot stage experiment.

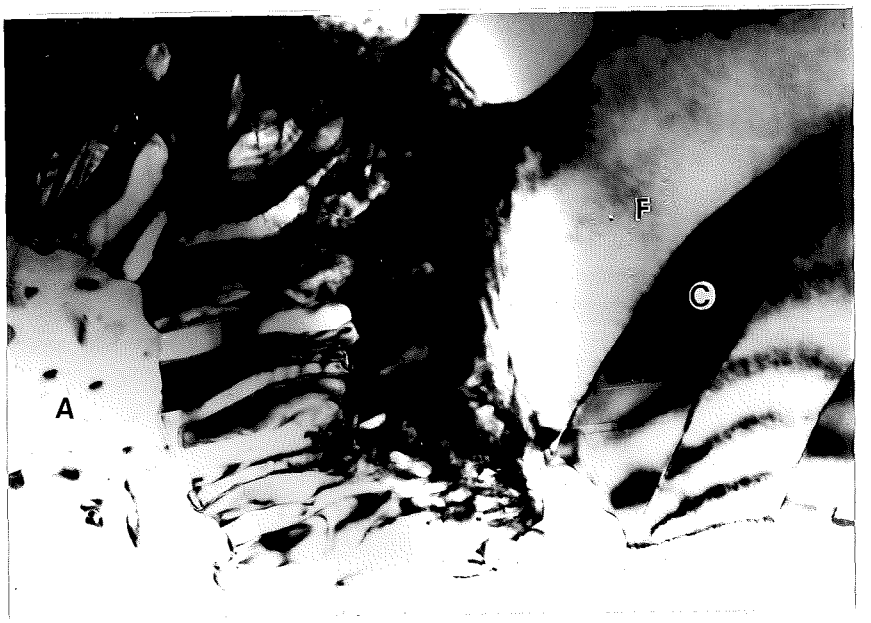

b. Growth of pearlite with much reduced spacing formed <u>after</u> heat no. 4.

reduced spacing (Figure 2.10b). It should also be noted that the hot stage employed had only one tilt direction which greatly limits the obtainable contrast. The combined evidence of facetting and, more importantly, the presence of growth ledges confirms that the FAI and CAI in pearlite are not crystallographically insensitive as currently believed. This implies that partial coherency exists at this interface despite the fact that rational orientation relationships are seldom, if ever, developed between pearlitic phases and the austenite grain into which they are growing (18). This crystallographic dependence will be discussed further in the following section.

Table V

Growth Ledge Displacement

heat no.	displacement (nm)
1	26
2	37
3	42
4	26

3. CRYSTALLOGRAPHIC EFFECTS AT THE PEARLITE:AUSTENITE GROWTH INTERFACE

A. Crystallography at the Growth Interface

Throughout the previous section, a "crystallographic effect" has been alluded to several times. Certainly, the observation of facetting and growth by the ledge mechanism is indicative of crystallographic dependence. However, Honeycombe (18) has previously shown that no reproducible orientation relationship is formed between the pearlite constituents and the retained austenite grain into which growth occurred. This conclusion is, in fact, supported by the work done in the present investigation. The lack of rational orientation relationships would seem to indicate a minimum effect of crystallography in obstensible disagreement with the results presented in the previous section. Once again, the experimental approach will be relied upon to examine this paradox.

In order to determine the exact crystallographic relationship at the growth interface, attempts were made to tilt this interface exactly parallel to the beam direction. If these attempts were successful (and occasionally they were) convergent beam electron diffraction was applied to obtain the relative orientations. It will be shown that although rational, low index orientation relationships seldom exist, there is a tendency for the pearlite:austenite growth interface to form facets parallel to a low index plane of at least one of the three phases involved. Several examples of facetting will be presented in the following figures and

summarized in Table VI. The experimental details of the g-vector determination are given in appendix 2.

Table VI

Pearlite:Austenite Facet Planes

Figure	Facet planes HI = high index but undetermined	Error (in degrees rotation)
3.1a	$(1\bar{1}\vec{1})_A$ // $(\bar{1}2\bar{1})_F$	1//0
3.1b	$(\bar{1}\bar{1}\vec{1})_A$ // $(312)_F$	1//5
3.2	$(220)_A$ // $(411)_C$	2//1
3.3	$(022)_A$ // $(HI)_F$	3//-
3.3	$(HI)_A$ // $(011)_F$	-//5
3.4	$(220)_A$ // $(311)_F$	1//6
3.5	$(120)_A$ // $(HI)_F$	0//-
3.5	$(200)_A$ // $(HI)_F$	0//-
3.6	$(442)_A$ // $(1\bar{1}0)_F$	3//4
3.7	$(731)_A$ // $(011)_C$	3//3
3.8	$(022)_A$ // $(5\bar{1}2)_F$	1//3

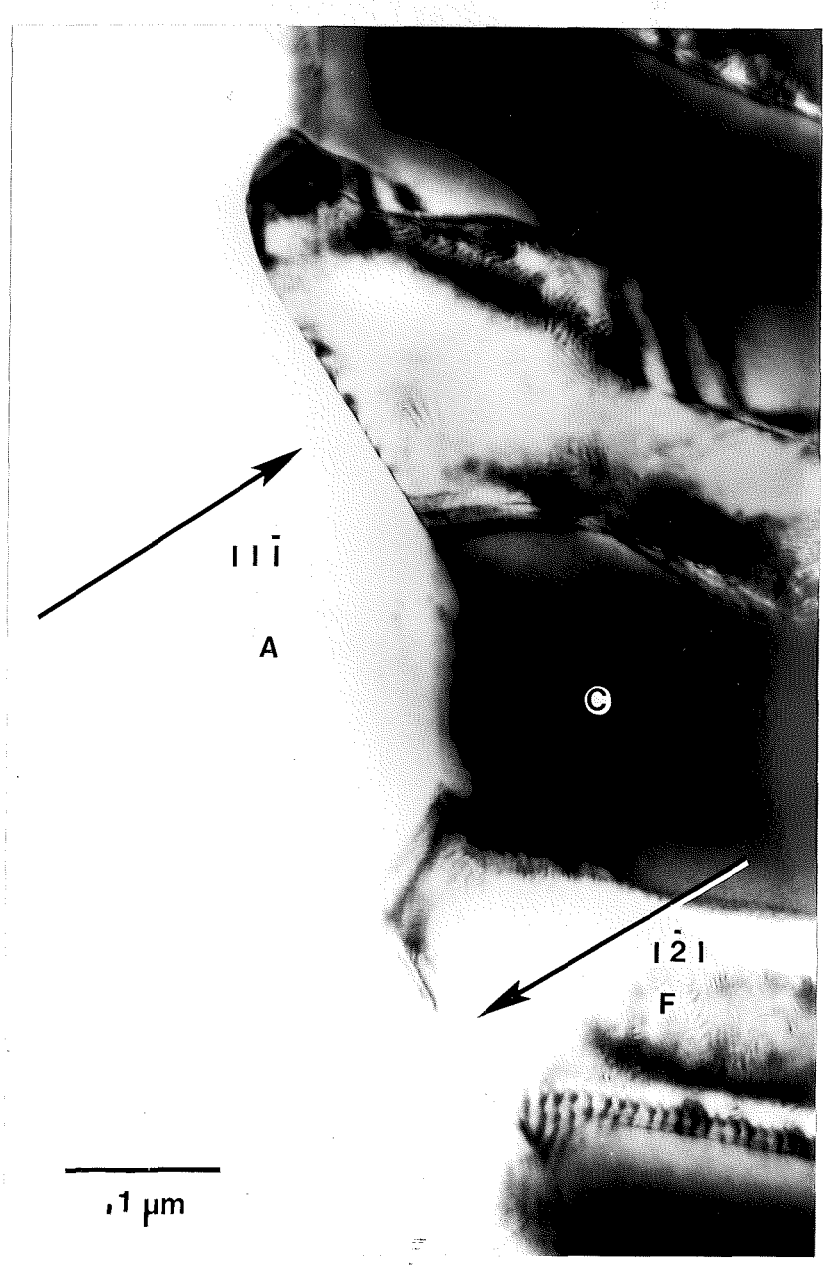

Figure 3.1 Low index facetting. 12h, 600C.

a. Parallel facets on ferrite lamella. Facet lies on $(1\bar{2}1)_F$; $(11\bar{1})_A$.

Figure 3.1 Low index facetting. 12h, 600C.

b. Same colony as (a); parallel facets on ferrite and cementite lamella on $(\bar{1}1\bar{1})_A$.

Figure 3.2 Parallel facets on ferrite and cementite lamella. Facet lies on $(220)_A$; $(411)_C$. 12h, 600C.

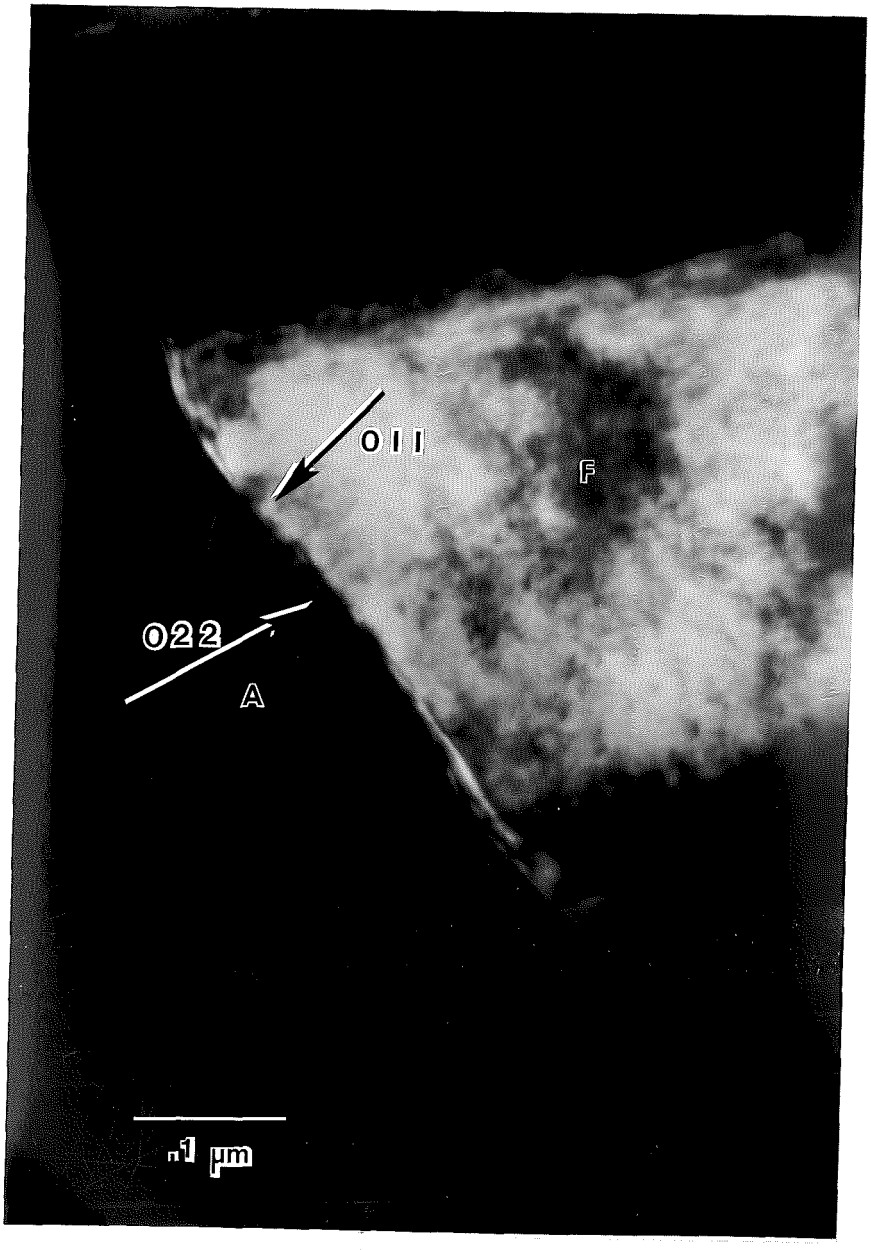

Figure 3.3 Two facets on a single ferrite lamella. Facet (1) lies on $(011)_F$. Facet (2) lies on (022). 12h, 630C.

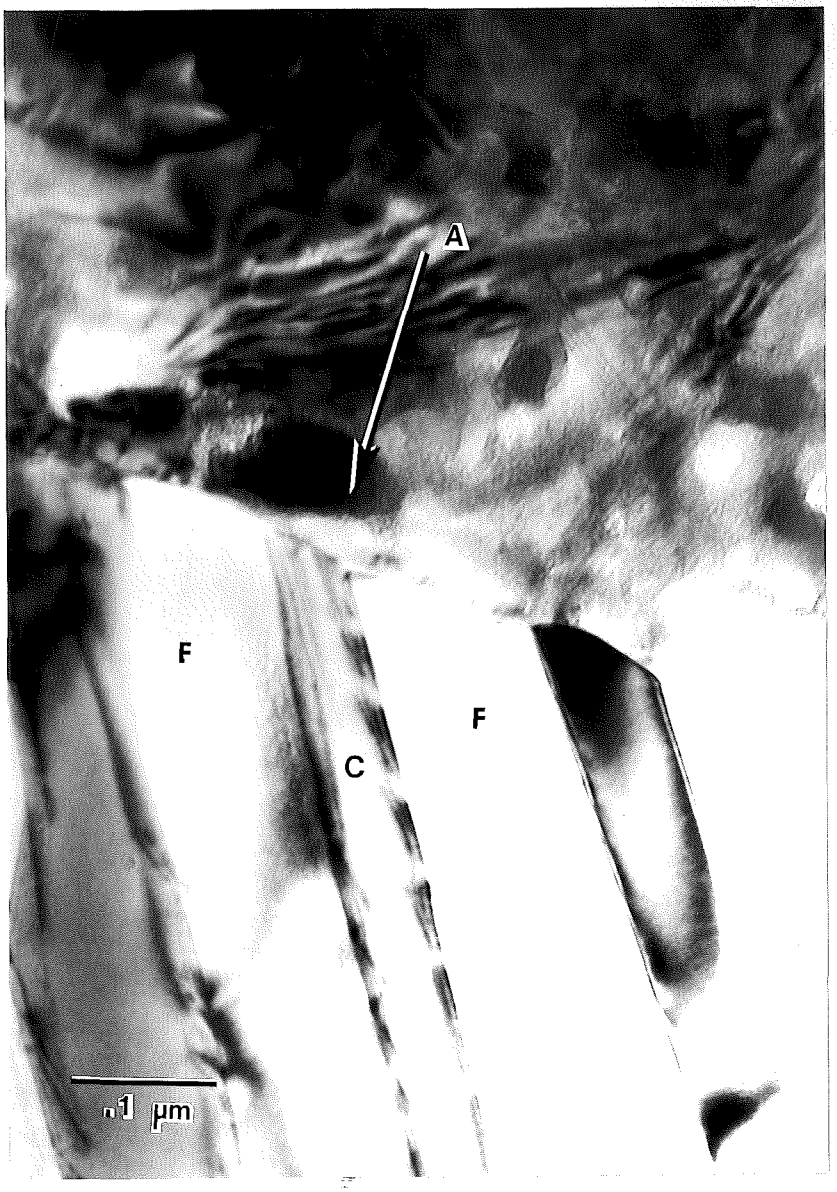

Figure 3.4 Planar ferrite and cementite interfaces on $(022)_A$. 18h, 610C.

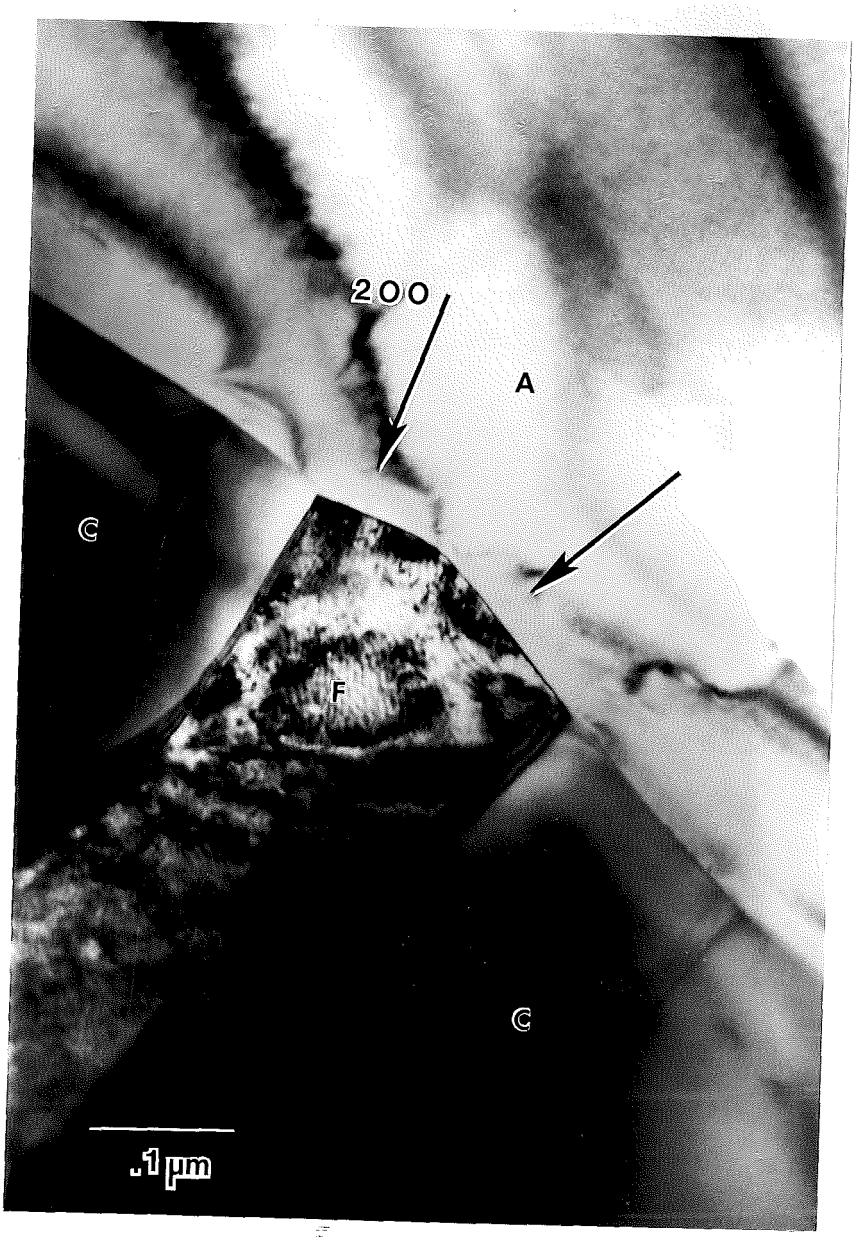

Figure 3.5. Two facets on a single ferrite lamella. Facet (1) lies on $(200)_A$. Facet (2) lies on (120). 18h, 610C.

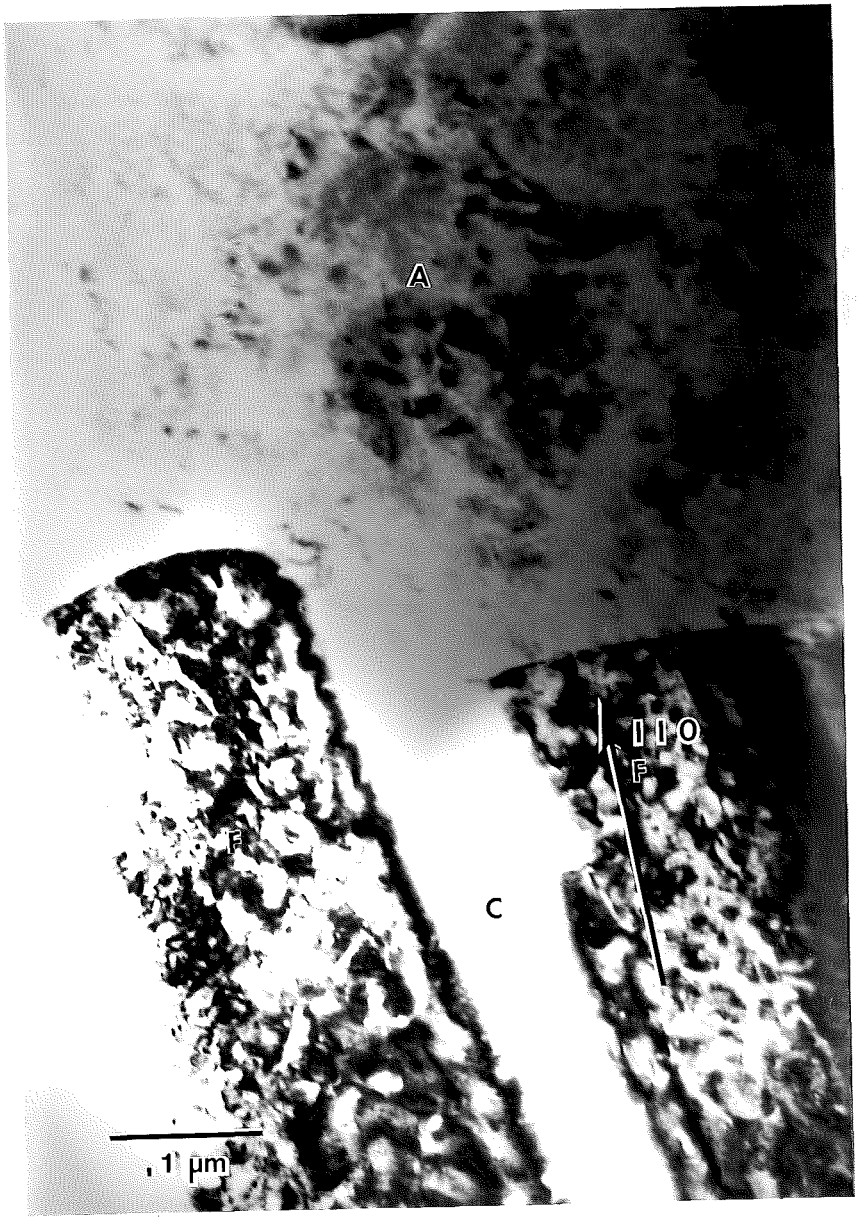

Figure 3.6 Planar ferrite facet on $(1\bar{1}0)_F//(44\bar{2})_A$. 12h, 600C.

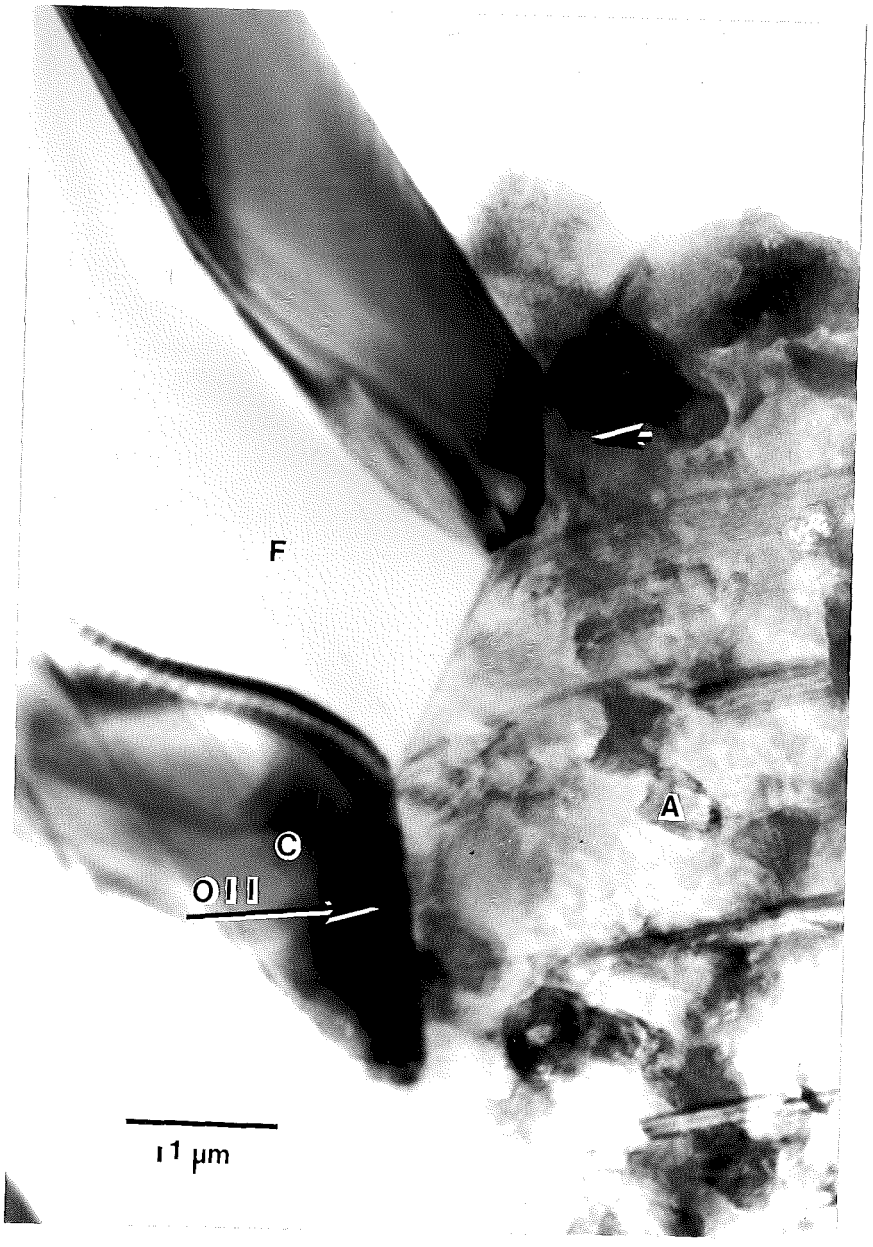

Figure 3.7 Parallel facets on cementite lamella on $(011)_\alpha$ 12h, 600C.

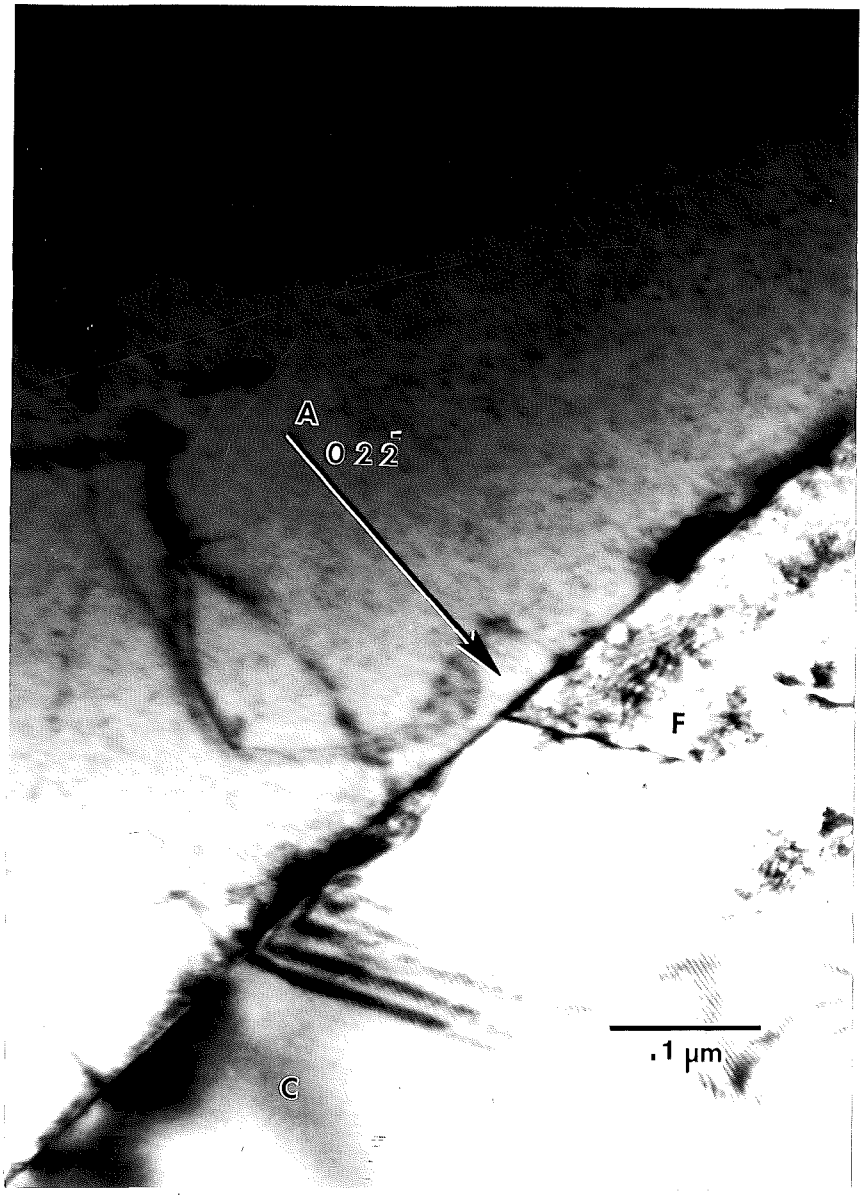

Figure 3.8 Planar ferrite and cementite interface on $(02\bar{2})_A$. 18h, 610C.

From these observations, it would appear that a given ferrite (cementite) lamella has a propensity to facet on a low index austenite plane and/or a low index ferrite (cementite) plane. It is apparent that adjacent ferrite (cementite) lamella may facet in a similar manner, although this is certainly not always observed. From this limited study, it would seem that within a given colony there exists a great deal of freedom concerning which planes will form facets. This being the case, it would be difficult to state that a given lamella would maintain the same facetted morphology throughout the growth process. The implication here is that the growth interface morphology is in a continuous state of flux. The formation of low index facets, however, indicates that surface energy considerations (and thus crystallography) are important during the dynamic condition of growth.

Given the current state of the theoretical relationship between crystallography and surface energy, there does not appear to be any reliable quantitative argument to explain why facets form on low index:high index planes. However, speculative statements concerning the nature of this phenomena can be made if the facets are assumed to correspond to shallow cusps in the gamma-plot. Recent studies by Baluffi and coworkers (unpublished results presented at the TMS-AIME Fall meeting, 1984) have shown that small bicrystals having high angle grain boundaries will rotate so that high coincidence (or deep cusp) interfaces may be formed. During this rotation process, there are experimentally measurable discontinuities in rotation velocity. It has been proposed that these discontinuities correspond to shallow cusps which cannot satisfy the condition

$$\int \gamma dA = \text{minimum}$$

where A is the surface area.

However these shallow cusps do act to temporarily "trap" the boundary plane in a shallow energy well. It is suggested that this trapping effect could have significance to the facetting phenomena observed at the pearlite:austenite growth interface. If there are indeed shallow energy cusps corresponding to low index planes, these results indicate that the pearlite growth interfaces may coincide with them. Since these cusps are assumed to be shallow (small torque terms), it is certainly conceivable that the influences of growth might act to "dislodge" the interface. However, given the hypothesis that each low index plane is associated with a shallow cusp, it is apparent that there are numerous available cusps for the interface to "move" into. Baluffi's results indicated that this type of movement in bicrystals occurred via grain boundary ledges. It is unknown whether or not a similar mechanism is active here.

As alluded to previously, the experimental approach has been emphasized in this dissertation; however, initial attempts have been made at modelling the atomic arrangement at the pearlitic ferrite:austenite growth interface. Essentially, a computer program has been written which will allow the unrelaxed atomic positions at the interface to be plotted. It is expected that future theoretical efforts by the pearlite research group will significantly further these efforts.

B. Computer Program for Determining Atomic Positions

If one is only concerned with low index planes in simple

```
10 DIM A1(3,25)
20 DIM J(3,8)
30 DIM W(3,100,2)
40 DIM H(3,500)
50 DIM P(3,3)
60 DIM O(3,100)
70 DIM G(3)
80 DIM R2(3,3)
90 DIM R5(3,3)
100 DIM R7(3,3)
110 DIM R3(3,3)
120 DIM R4(3,3)
130 DIM K(3)
140 DIM W1(3,100,2)
150 DIM Y(3)
160 FOR B8=1 TO 2
170 GOSUB 220:REM DATA SUBRTN
180 GOSUB 1000:REM LATTICE MATRIX GENERATION
190 GOSUB 1910:REM PLANE ROTATION
200 NEXT B8
210 GOTO 3570
220 REM LINES 580,590,600 HAVE BEEN RES ERVED FOR THE INPUT OF THE ORTHNORMAL CO
ORDINATES OF THE ATOMS CONTAINED WITHIN THE UNIT CELL.ENTER THE X,Y,Z COORDINATE
S BEGINNING WITH POSITION 0,0,0.
230 Z5=0
240 PRINT "INPUT THE # OF ATOMS IN OR ONTHE UNIT CELL.EXAMPLE:BCC=9"
250 INPUT N
260 IF B8=2 THEN 360
270 FOR O5=1 TO N
280 FOR O6=1 TO 3
290  READ A1(O6,O5)
300 PRINT A1(O6,O5)
310 NEXT O6
320 NEXT O5
330 DATA 0,0,0,0,1,0,0,0,1,1,0,0,0,1,1
335 DATA 1,0,1,1,1,0,1,1,1,0,.5,.5,.5,0,.5
340 DATA .5,.5,0,.5,1,.5,1,.5,.5,.5,.5,1
360 IF B8=1 THEN 450
370 FOR I=1 TO N
380 FOR P=1 TO 3
390  READ A1(P,I)
395 PRINT A1(P,I)
400 NEXT P
410 NEXT I
425 DATA 1,0,1,0.5,0.5,0.5,0,1,0
430 DATA 1,0,0,0,0,1,1,1,1,1,1,0
440 DATA 0,1,1,0,0,0
450 J(1,1)=1
460 J(2,1)=1
470 J(3,1)=1
480 J(1,2)=1
490 J(2,2)=-1
500 J(3,2)=1
510 J(1,3)=1
520 J(2,3)=-1
530 J(3,3)=-1
540 J(1,4)=-1
550 J(2,4)=-1
560 J(3,4)=1
570 J(1,5)=1
580 J(2,5)=1
```

```
590 J(3,5)=-1
600 J(1,6)=-1
610 J(2,6)=1
620 J(3,6)=-1
630 J(2,7)=1
640 J(1,8)=-1
650 J(3,7)=1
660 J(1,7)=-1
670 J(2,8)=-1
680 J(3,8)=-1
690 Z1=0
700 Z2=0
710 PRINT "INPUT ORTHONORMAL UNIT CELL  DIMENSIONS a,b,c"
720 PRINT "INPUT a"
730 INPUT B1
740 PRINT "INPUT b"
750 INPUT B2
760 PRINT "INPUT c"
770 INPUT B3
800 PRINT "INPUT PLANE OF INTEREST (HKL)"
810 PRINT"INPUT h"
820 INPUT C1
830 PRINT "INPUT k"
840 INPUT C2
850 PRINT "INPUT l"
860 INPUT C3
870 PRINT "INPUT CRYSTALLOGRAPHIC DIRECTION (H,K,L) WHICH YOU WISH TO BE PARALLEL
TO THE X-AXIS IN THE PLOT"
880 PRINT "INPUT H"
890 INPUT D1
900 PRINT "INPUT K"
910 INPUT D2
920 PRINT "INPUT L"
930 INPUT D3
940 X8(1)=B1
950 X8(2)=B2
960 X8(3)=B3
980 Z2=1
990 RETURN
1000 REM SUBROUTINE GENERATION
1010 Z2=0
1020 X6=1
1030 GOTO 1060
1040 X6=X6+1
1050 PRINT "X6",X6
1060 FOR A=0 TO X6
1070 FOR B=0 TO X6
1080 FOR C=0 TO X6
1090 FOR M=1 TO N
1100 E(1)=A1(1,M)+A
1110 E(2)=A1(2,M)+B
1120 E(3)=A1(3,M)+C
1130 FOR F1=1 TO 8
1140 FOR F2=1 TO 3
1150  G(F2)=E(F2)*J(F2,F1)
1160 NEXT F2
1170 REM SUBROUTINE EVALUATION
1180 C4=C1
1190 C5=C2
1200 C6=C3
1202 C7=B1*G(1)
1204 C8=B2*G(2)
1206 C9=B3*G(3)
1210 D4=(C4*C7)+(C5*C8)+(C6*C9)
1215 D=D4/SQR(C4^2+C5^2+C6^2)
1220 REM EQUATION FOR DISTANCE OF POINT FROM PLANE
```

```
1230 REM POINT CONSIDERED OFF PLANE IF  /D/)1 ANGSTROM
1240 IF D).1 THEN 1830
1245 IF D(-1.24 THEN 1830
1250 Z2=Z2+1
1260 FOR I1=1 TO 3
1270  H(I1,Z2)=G(I1)
1280 NEXT I1
1290 IF Z2)1 THEN 1320
1300 IF H(1,1)=H(2,1)=H(3,1)=0 THEN 1440
1310 REM:SINCE PRIMITIVE CELLS ARE NOT USED THIS LOOP
1320 REM: WILL ELIMENATE REDUNDANT POINTS
1330 FOR V=1 TO Z5
1340  IF H(1,Z2)=H(1,V) THEN 1380
1350  C9=1
1360 NEXT V
1370 GOTO 1440
1380  IF H(2,Z2)=H(2,V) THEN 1400
1390 GOTO 1350
1400  IF H(3,Z2)=H(3,V) THEN 1420
1410 GOTO 1350
1420 GOTO 1810
1430 REM SUBROUTINE EVALUATION
1440 Z5=Z5+1
1450 FOR I=1 TO 3
1460  H(I,Z5)=H(I,Z2)
1470 NEXT I
1480 REM RENUMBERS ACCEPTED COORDINATES
1490 IF Z5)99 THEN 1900
1500 PRINT "Z5";Z5
1505 LPRINT "D";D
1510 LPRINT G(1),G(2),G(3)
1520 K(1)=C1
1530 K(2)=C2
1540 K(3)=C3
1550 K1=K(1)
1560 K2=K(2)
1570 K3=K(3)
1580 L=(K1^2)+(K2^2)+(K3^2)
1590 P(1,1)=1-((K1^2)/L)
1600 P(2,2)=1-((K2^2)/L)
1610 P(3,3)=1-((K3^2)/L)
1620 P(1,2)=-1*((K1*K2)/L)
1630 P(2,1)=P(1,2)
1640 P(1,3)=-1*((K1*K3)/L)
1650 P(3,1)=P(1,3)
1660 P(2,3)=-1*((K2*K3)/L)
1670 P(3,2)=P(2,3)
1680 IF D=0 THEN 1750:REM D=0 WHEN POINT IS ON PLANE
1690 REM LOOP TO * D()1;H MATRIX WITH PROJ MATRIX
1700 FOR V=1 TO 3
1710  O(V,Z5)=X8(1)*H(1,Z5)*P(V,1)+X8(2)*H(2,Z5)*P(V,2)+H(3,Z5)*P(V,3)*X8(3)
1720 NEXT V
1730 GOTO 1780
1740 REM LOOP TO REDEFINE D=0;H MATRIX TO O MATRIX
1750 FOR F=1 TO 3
1760  O(F,Z5)=H(F,Z5)*X8(F)
1770 NEXT F
1780 LPRINT O(1,Z5),O(2,Z5),O(3,Z5)
1790 GOTO 1830
1800 GOTO 1830
1810 Z2=Z5
1820 Z2=Z5
1830 Z2=Z5
1840 NEXT F1
1850 NEXT M
1860 NEXT C
```

```
1870 NEXT B
1880 NEXT A
1890 GOTO 1040
1900 RETURN
1910 REM SUBROUTINE ROTATION
1920 REM MUST ROTATE PLANE NORMAL C1,C2,C3, TO Z AXIS 0,0,B3
1930 REM FIRST TAKE THE POSITIVE CROSS PRODUCT OF THE NORMALIZED VECTORS
1940 REM THIS ALLOWS THE ANGLE OF ROTATION TO BE DETERMINED
1950 REM ALONG WITH THE AXIS OF ROTATION
1960 REM NORMALIZATION FACTOR
1970 L1=SQR(K(1)^2+K(2)^2+K(3)^2)
1980 K1=K(1)
1990 K2=K(2)
2000 K3=K(3)
2010 Y(1)=0
2020 Y(2)=0
2030 Y(3)=1
2040 D5=(Y(1)*K1+Y(2)*K2+Y(3)*K3)/(SQR(Y(1)^2+Y(2)^2+Y(3)^2)*SQR(K1^2+K2^2+K3^2)
)
2045 LPRINT "*D5*";D5
2050 IF D5=0 THEN 2110
2055 D6=D5+100
2060 IF D6)100 THEN 2110
2070 K(1)=K1*-1
2080 K(2)=K2*-1
2090 K(3)=K3*-1
2100 REM CROSS PRODUCT
2105 LPRINT "*";K1;K2;K3
2110 Q=(K(2)*Y(3)-K(3)*Y(2))*(1/L1)
2120 R=(K(3)*Y(1)-K(1)*Y(3))*(1/L1)
2130 S=(K(1)*Y(2)-K(2)*Y(1))*(1/L1)
2140 LPRINT "Q";Q,"S";S,"R";R
2150 T=(SQR(Q^2+R^2+S^2))
2160 IF T<1 THEN 2190
2170 T=T-.0000001
2180 REM ANGLE OF ROTATION
2190 PRINT "T";T
2200 T1=ATN(T/SQR(1-(T^2)))
2210 LPRINT "T";T
2220 LPRINT "T1";T1
2240 Q=Q*L1
2250 R=R*L1
2260 S=S*L1
2261 L2=SQR(Q^2+R^2+S^2)
2263 Q=Q/L2
2265 R=R/L2
2267 S=S/L2
2270 LPRINT "Q";Q,"S";S,"R";R
2280 R2(3,3)=COS(T1)
2290 R2(2,2)=COS(T1)
2300 R2(1,1)=COS(T1)
2310 R2(1,2)=R2(1,3)=R2(2,1)=R2(3,1)=R(3,2)=R(2,3)=0
2320 R3(1,1)=Q^2
2330 R3(2,1)=Q*R
2340 R3(2,2)=R^2
2350 R3(3,1)=Q*S
2360 R3(3,3)=S*S
2370 R3(1,3)=R3(3,1)
2380 R3(1,2)=R3(2,1)
2390 R3(3,2)=R*S
2400 R3(2,3)=R3(3,2)
2410 R4(1,1)=R3(1,1)*(1-COS(T1))
2420 R4(1,2)=R3(1,2)*(1-COS(T1))
2430 R4(2,1)=R3(2,1)*(1-COS(T1))
2440 R4(2,2)=R3(2,2)*(1-COS(T1))
2450 R4(3,2)=R3(3,2)*(1-COS(T1))
```

```
2460 R4(2,3)=R4(3,2)
2470 R4(3,3)=R3(3,3)*(1-COS(T1))
2480 R4(3,1)=R3(3,1)*(1-COS(T1))
2490 R4(1,3)=R4(3,1)
2500 R5(1,1)=0
2510 R5(2,2)=0
2520 R5(3,3)=0
2530 R5(1,2)=-1*S*SIN(T1)
2540 R5(1,3)=R*SIN(T1)
2550 R5(2,1)=S*SIN(T1)
2560 R5(2,3)=-1*Q*SIN(T1)
2570 R5(3,1)=-1*R*SIN(T1)
2580 R5(3,2)=Q*SIN(T1)
2590 R2(1,2)=0
2600 REM THE ROTATION MATRIX IS GIVEN BELOW
2610 FOR U=1 TO 3
2620 FOR V=1 TO 3
2630  R7(U,V)=R2(U,V)+R4(U,V)+R5(U,V)
2640 LPRINT "R2";U;V;"=";R2(U,V)
2650 LPRINT "R4";U;V;"=";R4(U,V)
2660 LPRINT "R5";U;V;"=";R5(U,V)
2665 LPRINT "R7";U;V;R7(U,V)
2670 NEXT V
2680 NEXT U
2690 FOR Z=1 TO Z5
2700 FOR V=1 TO 3
2710  W(V,Z,B8)=O(1,Z)*R7(V,1)+O(2,Z)*R7(V,2)+O(3,Z)*R7(V,3)
2720 NEXT V
2730 NEXT Z
2740 FOR M=1 TO 3
2750  K(M)=D1*R7(M,1)+D2*R7(M,2)+D3*R7(M,3)
2760 NEXT M
2770 K1=K(1)
2780 K2=K(2)
2790 K3=K(3)
2800 LPRINT K1;K2;K3;"*";X
2810 L1=SQR(K1^2+K2^2+K3^2)
2820 Y(1)=1
2830 Y(2)=0
2840 Y(3)=0
2850 GOTO 2890
2860 Y(1)=D1*B1
2870 Y(2)=D2*B2
2880 Y(3)=D3*B3
2890 D5=(Y(1)*K1+Y(2)*K2+Y(3)*K3)/(SQR(Y(1)^2+Y(2)^2+Y(3)^2)*SQR(K1^2+K2^2+K3^2)
)
2900 IF D5=0 THEN 2970
2905 D6=D5+100
2910 IF D6>100 THEN 2960
2920 PRINT D5
2930 K(1)=K1*-1
2940 K(2)=K2*-1
2950 K(3)=K3*-1
2960 REM CROSS PRODUCT
2970 Q=(K(2)*Y(3)-K(3)*Y(2))*(1/L1)
2980 R=(K(3)*Y(1)-K(1)*Y(3))*(1/L1)
2990 S=(K(1)*Y(2)-K(2)*Y(1))*(1/L1)
3000 T=(SQR(Q^2+R^2+S^2))
3010 IF T<1 THEN 3040
3020 T=T-.00000001
3030 REM ANGLE OF ROTATION
3040 PRINT "T";T
3050 T1=ATN(T/SQR(1-(T^2)))
3054 S=S*L1
3055 Q=0
3056 R=0
```

```
3057 L2=SQR(S^2)
3058 S=S/L2
3060 R2(3,3)=COS(T1)
3070 R2(2,2)=R2(3,3)
3080 R2(1,1)=R2(2,2)
3090 R2(1,2)=R2(1,3)=R2(2,1)=R2(3,1)=R(3,2)=R(2,3)=0
3100 R3(1,1)=Q^2
3110 R3(2,1)=Q*R
3120 R3(1,2)=R3(2,1)
3130 R3(2,2)=R^2
3140 R3(1,3)=R3(3,1)=Q*S
3150 R3(2,3)=R3(3,2)=R*S
3160 R3(3,3)=S*S
3170 R4(1,1)=R3(1,1)*(1-COS(T1))
3180 R4(1,2)=R3(1,2)*(1-COS(T1))
3190 R4(2,1)=R3(2,1)*(1-COS(T1))
3200 R4(2,2)=R3(2,2)*(1-COS(T1))
3210 R4(3,2)=R3(3,2)*(1-COS(T1))
3220 R4(2,3)=R4(3,2)
3230 R4(3,3)=R3(3,3)*(1-COS(T1))
3240 R4(3,1)=R3(3,1)*(1-COS(T1))
3250 R4(1,3)=R4(3,1)
3260 R5(1,1)=0
3270 R5(2,2)=0
3280 R5(3,3)=0
3290 R5(1,2)=-1*S*SIN(T1)
3300 R5(1,3)=R*SIN(T1)
3310 R5(2,1)=S*SIN(T1)
3320 R5(2,3)=-1*Q*SIN(T1)
3330 R5(3,1)=-1*R*SIN(T1)
3340 R5(3,2)=Q*SIN(T1)
3350 R2(1,2)=0
3360 REM THE ROTATION MATRIX IS GIVEN BELOW
3370 FOR U=1 TO 3
3380 FOR V=1 TO 3
3390  R7(U,V)=R2(U,V)+R4(U,V)+R5(U,V)
3400 LPRINT "R2";U;V;R2(U,V)
3410 LPRINT "R4";U;V;R4(U,V)
3420 LPRINT "R5";U;V;R5(U,V)
3425 LPRINT "R7";U;V;R7(U,V)
3430 NEXT V
3440 NEXT U
3450 FOR Z=1 TO Z5
3460 FOR V=1 TO 3
3470  W1(V,Z,B0)=W(1,Z,B0)*R7(V,1)+W(2,Z,B0)*R7(V,2)+W(3,Z,B0)*R7(V,3)
3480 NEXT V
3490 NEXT Z
3500 FOR I=1 TO Z5
3510 LPRINT W(1,I,B0),W(2,I,B0),W(3,I,B0)
3520 NEXT I
3530 FOR U=1 TO Z5
3540  LPRINT W1(1,U,B0),W1(2,U,B0),W1(3,U,B0)
3550 NEXT U
3560 RETURN
3570 OPEN "FCC111" FOR OUTPUT AS #1
3580 FOR I=1 TO Z5
3590 FOR J=1 TO 3
3600  WRITE #1,W1(J,I,1)
3610 NEXT J
3620 NEXT I
3630 CLOSE #1
3640 OPEN "BCC242"FOR OUTPUT AS #2
3650 FOR U=1 TO Z5
3660 FOR V=1 TO 3
3670  WRITE #2,W1(V,U,2)
3680 NEXT V
```

crystal structures, the atomic positions on these planes may be easily visualized. However, if the planes are high index and/or the crystal structure is complex, the visualization process may be more difficult. In such cases, it may be necessary to consider atoms which lie just above or just below the geometric plane. Clearly, the computer becomes more necessary as the complexity of the situation increases. The program written to describe the unrelaxed atomic positions at the interphase boundary is discussed in this section. The general approach was to consider one crystal at a time, determine the positions of the atoms on the plane of interest, then rotate onto a reference cartesian coordinate system. Thus, if one wishes to study the unrelaxed atomic matching at an interface described by the crystallography $(111)_A // (110)_B ; [110]_A // [001]_B$, the program will consider the A crystal first, determine atomic positions on the $(111)_A$ plane, then rotate to the reference coordinate system with $[110]_A$ parallel to the reference x-axis. The same process would then occur for the B crystal plane except the $[001]_B$ will be parallel to the reference x-axis.

The verbal flowchart for the program is given below:

1. Generate the crystal lattice.
2. Determine what lattice points will lie "on" the xy reference plane.
3. Perform a perpendicular projection onto the plane for those atoms which lie just above or just below the plane.
4. Rotate the plane of interest parallel to the xy reference plane.
5. Rotate the crystal direction of interest parallel to the y-axis.
6. Repeat procedure for the second crystal structure.

Each of the above steps will now be considered in detail.

1) The easiest method for generating a three-dimensional crystal lattice is to determine the primitive unit cell (one atom per unit cell) and propagate this cell in three dimensions. However, since it is often difficult to determine the primitive cell for complex crystal structures, the program was generalized so that the entire unit cell could be used for obtaining the crystal lattice. Thus for bcc, there would be nine data points: 0,0,0; 0,1,0; 0,0,1, 1,0,0; 1,1,0; 1,0,1; 0,1,1; 1,1,1; .5,.5..5. These points belong to the crystal coordinate system and will be transformed to the orthonormal cartesian coordinate system later in the program. Having the crystal coordinates available in the data statements (lines 330-340, 425-440) the three-dimensional lattice is generated by the loops in lines 1020-1160, 1840-1890.

2) As each crystal coordinate is generated, it is transformed to cartesian coordinates (lines 1202-1206), then evaluated to determine if it lies "on" the plane. This is done by using the equation for a plane, the particular plane being designated by the user. This equation is given in lines 1180-1215. Essentially, the distance between the point and the plane is calculated. If this distance is zero, then mathematically speaking, the point lies on the plane. However, for low index planes, it may be necessary to allow points which are numerically just below the plane to interact across the interface with atoms from the second crystal. This may be done by giving the interface a "thickness" designated in lines 1240 and 1245.

Once a point is found to lie on the plane, it must be compared

with the previous points. Since we are not using a primitive lattice, it is possible to have redundant points. If the coordinates of this point are equivalent to a previously determined point, then it is discarded. This is accomplished by the loops in 1330-1420. The value in line 1490 determines the size (number of points) in the plot.

3) If there are indeed points which are just below the mathematical plane which need to be considered, then it is necessary to project these points onto the mathematical plane for the purposes of both plotting and consideration of interaction. This is accomplished by a matrix operation and is discussed quite eloquently in (64). The projection matrix for this operation is given in 1580-1670. The matrix multiplication occurs in 1750-1770.

4 and 5) The rotation operations are discussed in detail in (64). Only the rudiments will be considered here. For the purposes of transforming the two interfacial planes to a reference coordinate system so that the atomic positions at the interface might be investigated, it is necessary to rotate both plane normals onto a common axis in the reference coordinate system. This axis has arbitrarily been chosen as [0,0,1] (2010-2030). The dot product to determine the sign of the plane normal to give an angle positive and less than 90 degrees is determined in 2040-2090. The cross product to determine the rotation axis is given in 2110-2130. The angle of rotation is calculated in 2150-2200. The rotation matrix is determined in 2263-2680 and the rotation operation is carried out in 2690-2730.

Once the two plane normals are parallel, it is still necessary (usually) to make experimentally determined crystal directions,

which lie on the interfacial plane parallel. If this is not determined, then the crystallographic description of the interface is incomplete. Assuming all pertinent data are available, an operation similar to the previously discussed rotation is carried out to make both the experimentally determined crystal directions parallel to the reference [1,0,0] direction, and thus parallel to one another. This rotation operation is identical to the plane rotation except the crystal directions are rotated onto [1,0,0] rather than [0,0,1].

An example of the projection and rotation operations will now be considered using the bcc$(1\bar{2}1)$ plane to illustrate the procedure. The $(1\bar{2}1)$ plane containing the origin will be considered, thus the equation for the distance of a point (x,y,z) from a plane (a,b,c) reduces to:

$$(1) \quad D = (ax + by + cz)/\sqrt{a^2 + b^2 + c^2}$$

or

$$(2) \quad D = (x - 2y + z)/\sqrt{6}$$

If D = 0, then the point is considered to lie on the plane. However, for the purposes of considering atomic interactions across the interfacial plane, a point which lies less than one half a nearest neighbor interatomic distance below the mathematical plane will be considered "on" the plane. For the bcc crystal structure, this value is $(\sqrt{3}/4)a_o$. The crystal coordinates for bcc have been given earlier. From these, the cartesian coordinates may be obtained by multiplying through by the lattice parameter by a_o,

which will be chosen as 3 angstroms. The one half interatomic distance is thus 1.30 angstroms. Now, consider two atoms with coordinates (3, 0, -3) and (0, 0, -3), respectively. Inserting these values into equation (2), D = 0 for (3, 0, -3) and is thus mathematically defined to lie on the plane. For (0, 0, -3), however, D = -1.22 angstroms. Mathematically, this point is below the plane. However, it will be considered to interact with atoms across the interphase boundary since it is less than one-half of the nearest neighbor interatomic distance below the interface plane. To consider the position of this atom on the boundary, it is necessary to perform a perpendicular projection onto the mathematically defined plane. This may be carried out via a matrix operation as shown below:

$$\underline{X}_1 = \underline{P} * \underline{X}_0$$

where the projection matrix is given by:

$$P = \begin{bmatrix} 1-(a)(a)/n & -(a)(b)/n & -(a)(c)/n \\ -(b)(a)/n & 1-(b)(b)/n & -(b)(c)/n \\ -(c)(a)/n & -(c)(b)/n & 1-(c)(c)/n \end{bmatrix}$$

and (a,b,c) are the coordinates of the plane and
$n=a^2+b^2+c^2$ giving:

$$P * X = \begin{bmatrix} .83 & .33 & -.17 \\ .33 & .33 & .33 \\ -.17 & .33 & .83 \end{bmatrix} * \begin{bmatrix} 0 \\ 0 \\ -3 \end{bmatrix}$$

The new coordinates of the point projected onto the plane is given by the matrix multiplication rule (row vector * column vector).

$$x = (0)(.83) + (0)(.33) + (-3)(-.17) = .51$$

$$y = (0)(.33) + (0)(.33) + (-3)(.33) = -.99$$

$$z = (0)(-.17) + (0)(.33) + (-3)(.83) = -2.49$$

By substituting these values into equation (2), it is found that D=0 for the projected point, confirming that it is now mathematically defined to lie on the plane.

As discussed in step 4 of the flowchart, it is necessary to rotate the plane of interest parallel to the reference xy plane. This may be accomplished by rotating the plane normal into the reference [001] direction. The matrix operation to accomplish this task is considered below, using the projected point on the (121) plane for illustration.

Before the [121] can be rotated into the [001], the axis of rotation and the angle of rotation must be calculated. This information may be obtained by the normalized cross product between the two directions. In this manner, the rotation axis is determined to be (-2, -1, 0), which is indeed orthogonal to both directions. The angle of rotation is calculated as 65.9 degrees. For the matrix rotation

$$\underset{1}{\underline{X}} = \underline{R} * \underset{0}{\underline{X}}$$

the rotation matrix is determined to be:

$$R = \cos 65.9 \begin{bmatrix} 1 & 0 & 0 \\ 0 & 1 & 0 \\ 0 & 0 & 1 \end{bmatrix} + (1 - \cos 55.9) \begin{bmatrix} 4/5 & 2/5 & 0 \\ 2/5 & 1/5 & 0 \\ 0 & 0 & 0 \end{bmatrix} + \sin 65.9 \begin{bmatrix} 0 & 0 & -1/5 \\ 0 & 0 & 2/5 \\ 1/5 & -2/5 & 0 \end{bmatrix}$$

or

$$R = \begin{bmatrix} .882 & .237 & -.408 \\ .237 & .526 & .816 \\ .408 & -.816 & .408 \end{bmatrix}$$

The matrix multiplication with the projected point may be written as:

$$x' = (.51)(.882) + (-.99)(.237) + (-2.49)(-.408) = 1.23$$

$$y' = (.51)(.237) = (-.99)(.526) + (-2.49)(.816) = -2.43$$

$$z' = (.51)(.408) + (-.99)(-.816) + (-2.49)(.408) = 0$$

The point (1.23, -2.43, 0) is, of course, mathematically defined to lie on the (0,0,1) reference plane. The projection/rotation operation is now complete.

C. Atomic Positions at the FAI Facets

As an initial probe into the physical principles governing the formation of facets across low index/high index plane facets, the computer program just described will be used to search for high coincidence regions at the interface. As discussed in Chapter II.1.C, the presence of good atomic matching regions is thought to energetically favor growth by the ledge mechanism. Thus, the presence of such regions might explain both the predominance of growth ledges at the pearlite:austenite interface and, assuming good fit regions do lower the interfacial energy, the presence of facetting might also be explained.

Three facet boundaries for which the crystallography was completely determined will be considered. As indicated in part B of this section, it will be assumed that atoms less than one-half nearest neighbor atomic distance below the boundary plane will interact across the interface. This assumption has been used successfully in previous studies (17, 65) to explain partial coherency between phases with different crystal structures. In Figure 3.9, the configuration $(\bar{1}\bar{1}1)_A$ //$(1\bar{2}1)_F$; $[235]_A$ //$[012]_F$ is plotted. The squares coincide with atoms from the austenite fcc crystal structure while the crosses correspond to the bcc ferrite atoms. The good matching, high coincidence region is immediately obvious. A similar configuration, though somewhat smaller coherent region, is observed for the $(22\bar{1})_A$ //$(1\bar{1}0)_F$; $[\bar{1}22]_A$ //$[\bar{1}\bar{1}1]_F$ interface in Figure 3.10. In Figure 3.11, where the $(0\bar{1}1)_A$ //$(5\bar{1}2)_F$; $[0\bar{1}\bar{1}]_A$ //$[11\bar{2}]_F$ interface is plotted, there are not two-dimensional cells of high coincidence. It is apparent, however, that "strips"

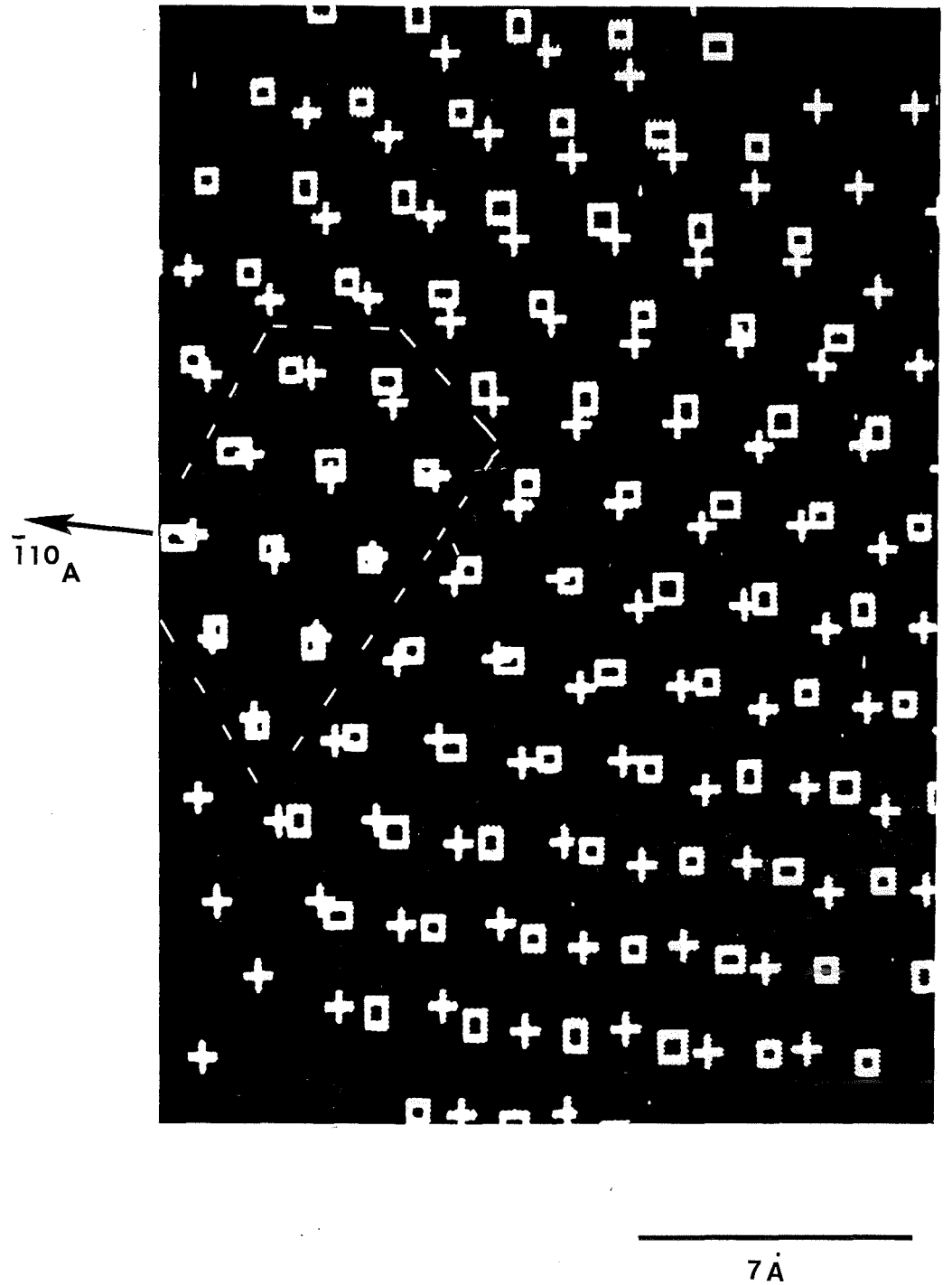

Figure 3.9 Coherent region for $(\bar{1}\bar{1}1)_A//(1\bar{2}1)_F$; $[235]_A//[012]_F$. Coincident point spacing is 65.5 angstroms along $[\bar{1}10]_A$.

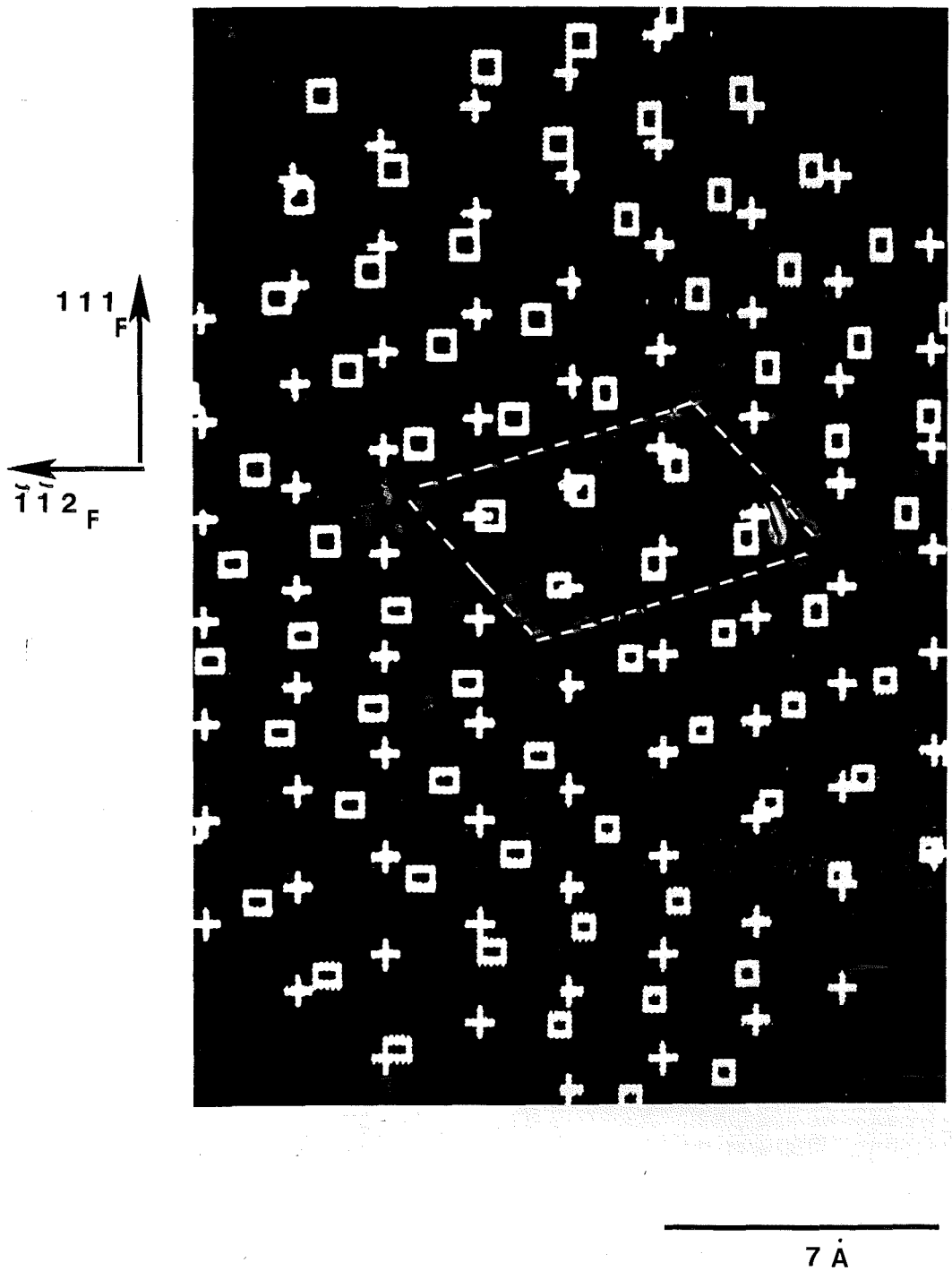

Figure 3.10 Good matching region for $(22\bar{1})_A // (1\bar{1}0)_F$; $[\bar{1}22]_A // [\bar{1}\bar{1}\bar{1}]_F$. Coincident point spacing is 1078 angstroms along $[111]_F$ and 1075.59 angstroms along $[\bar{1}\bar{1}2]_F$.

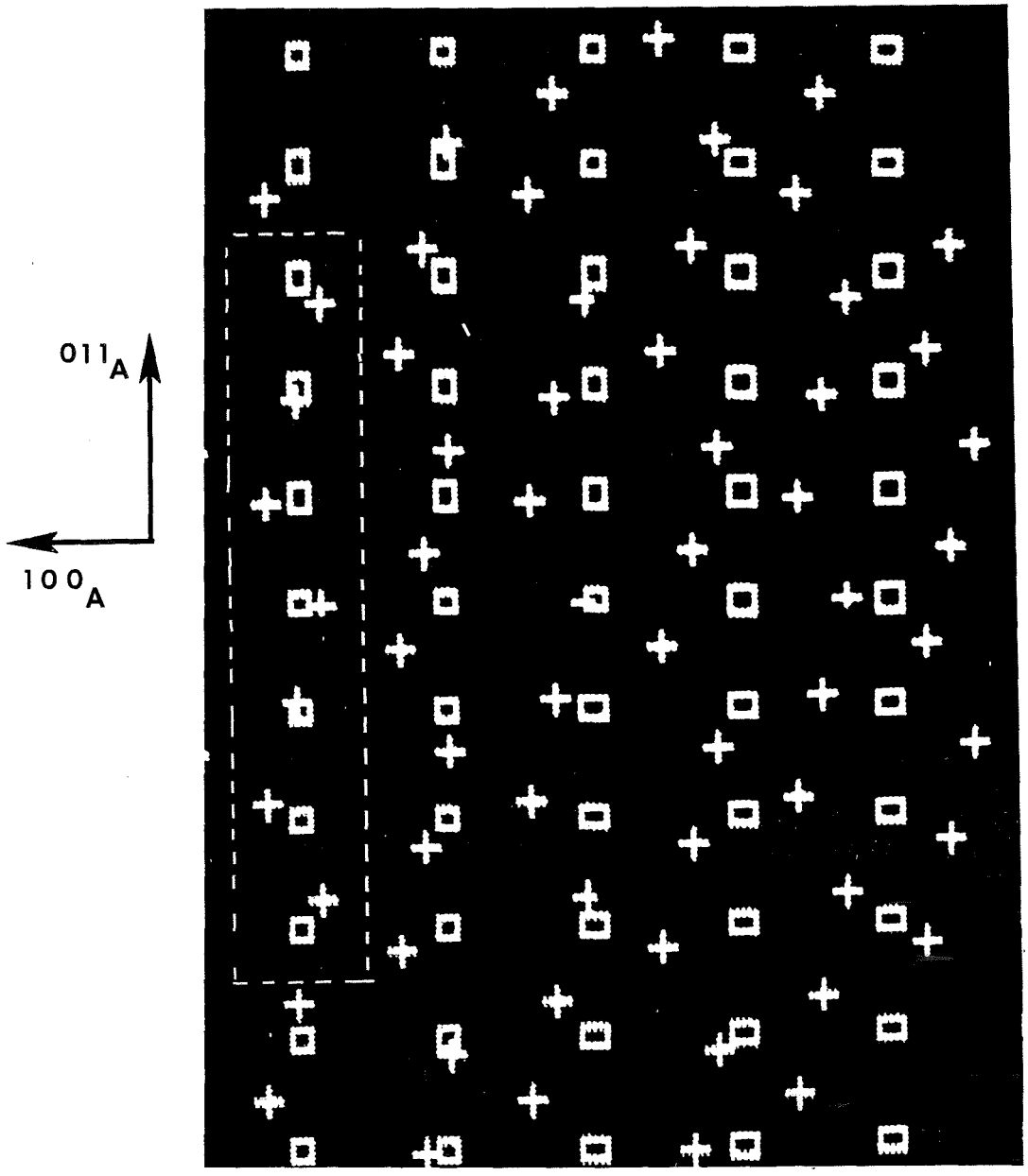

Figure 3.11 Good matching strip for $(0\bar{1}1)_A // (5\bar{1}2)_F$; $[01\bar{1}]_A // [11\bar{2}]_F$. Coincident point spacing is 320.4 angstroms along $[100]_A$ and 351 angstroms along $[011]_A$.

of good matching lie along [011]$_A$.

4. A NEW MODEL FOR THE PEARLITE GROWTH MECHANISM

A. Introduction

Most investigators believe that the pearlite lamellar spacing is determined by some type of optimization principle. However, as pointed out by Cahn and Hagel in 1962:

> The physical principles involved are not understood well enough to formulate a mechanism which would explain the ease with which pearlite maintains a spacing characteristic of the temperature at which it is growing.

This statement could as easily be applied to many of the other phenomena associated with the pearlite transformation, such as synchronous growth of the ferrite and cementite constituents, lamellar curvature (Mehl) and lamellar branching (Hillert). Based on the three previous sections and new experimental evidence presented in this paper, an atomic mechanism for the growth and development of lamellar pearlite will be proposed. From this model, considerable insight may be gained into the physical principles involved with each of the aforementioned phenomena.

B. Experimental Results

Careful examination of the FCI reveals boundary steps in an Fe-.8C alloy (Figure 1.1) and the ternary Fe-C-Mn steel (Figure 1.2). These were first observed by Bramfitt and Marder (62) with SEM and more recently in results section 1 using TEM. The application of

TEM techniques to the study of the ledges allowed their role in direction changes of lamella to be analyzed in terms of the crystallographic relationship between ferrite and cementite. Hence, these interfacial steps are denoted "direction steps." It was shown conclusively in section 1 that these steps permit the growth direction of individual lamella to change while still maintaining a low energy ferrite:cementite interface. How they originate and their relationship with the growth interface was not discussed at that point. If, however, the FCI and the FAI are imaged simultaneously (Figure 4.1a, b) structure at both interfaces can be clearly identified. Several growth ledges are indicated (open arrows) at the FAI. If they are traced along the growth interface until they intersect the ferrite:cementite:austenite triple junction (see Figure 4.1c), it is apparent that the growth ledges are continuous with the direction steps at the FCI (solid arrows). This implies that the lateral movement of growth ledges (discussed in section 2) is directly involved in the formation of the interfacial direction steps on the FCI. Imaging the growth interface in the dark field mode, a second set of growth ledges is revealed (Figure 4.1b). This set is about 90 degrees to the first, which at this orientation is out of contrast. Figure 4.1c is a schematic based on the micrographs and it illustrates the growth ledge and direction step association. The TEM micrographs in Figure 4.1d-e give further examples of this growth ledge/directional step continuity at the FAI/FCI intersection. This association will be discussed in greater detail later.

It would be reasonable to expect that the growth ledges on CAI would also be associated with the direction steps on FCI. As shown

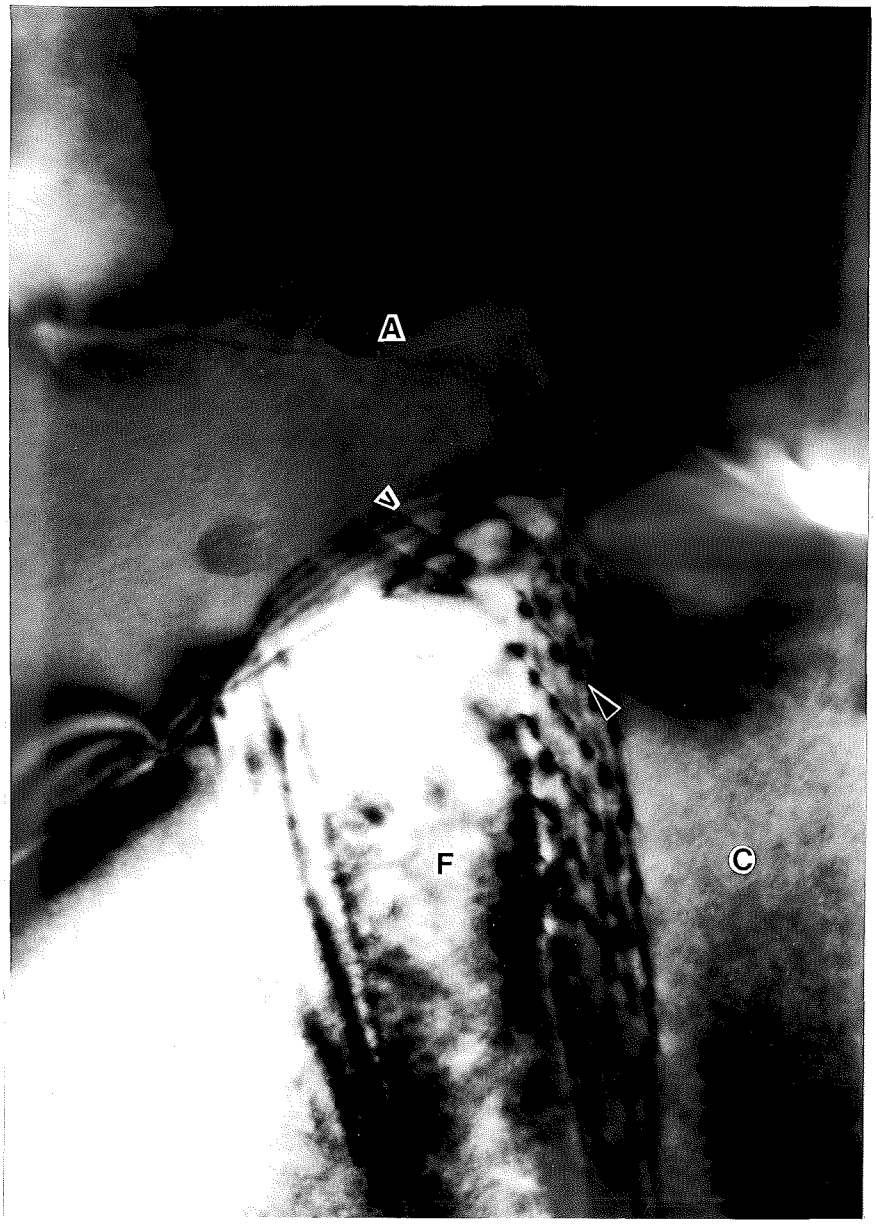

Figure 4.1 Growth ledge/direction step association.

a. Bright field micrograph showing continuity between FAI growth ledges and FCI direction steps. 12h 610C.

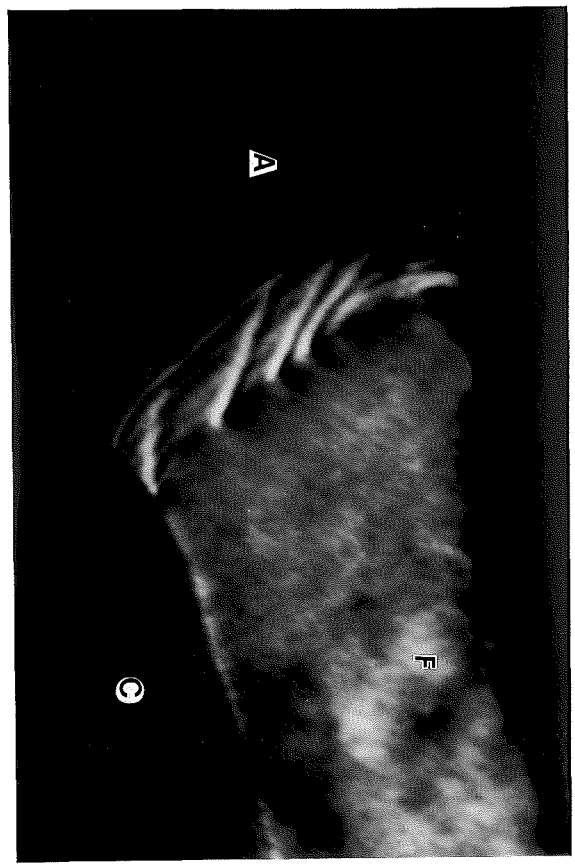

0.1μm

Figure 4.1 Growth ledge/direction step association.

b. Dark field micrograph showing a second set of FAI growth ledges not parallel to those in (a).

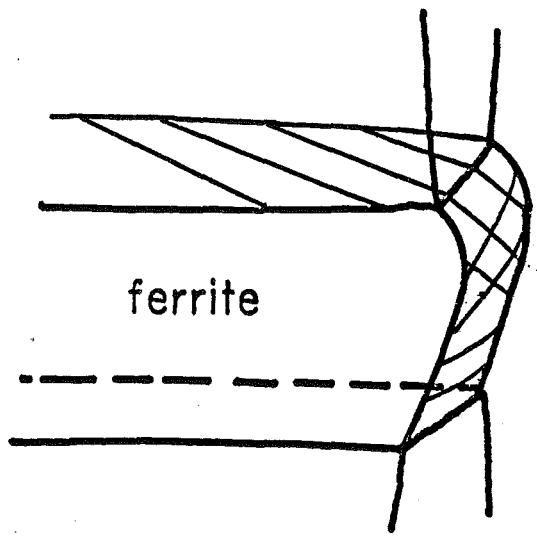

Figure 4.1 Growth ledge/direction step association.

c. Schematic based on (a); (b).

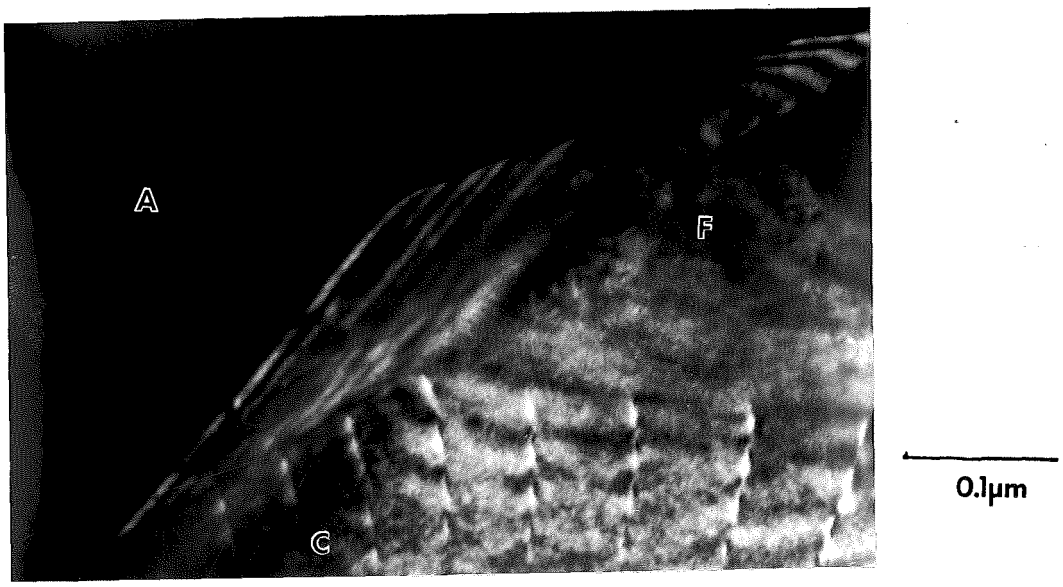

(d)

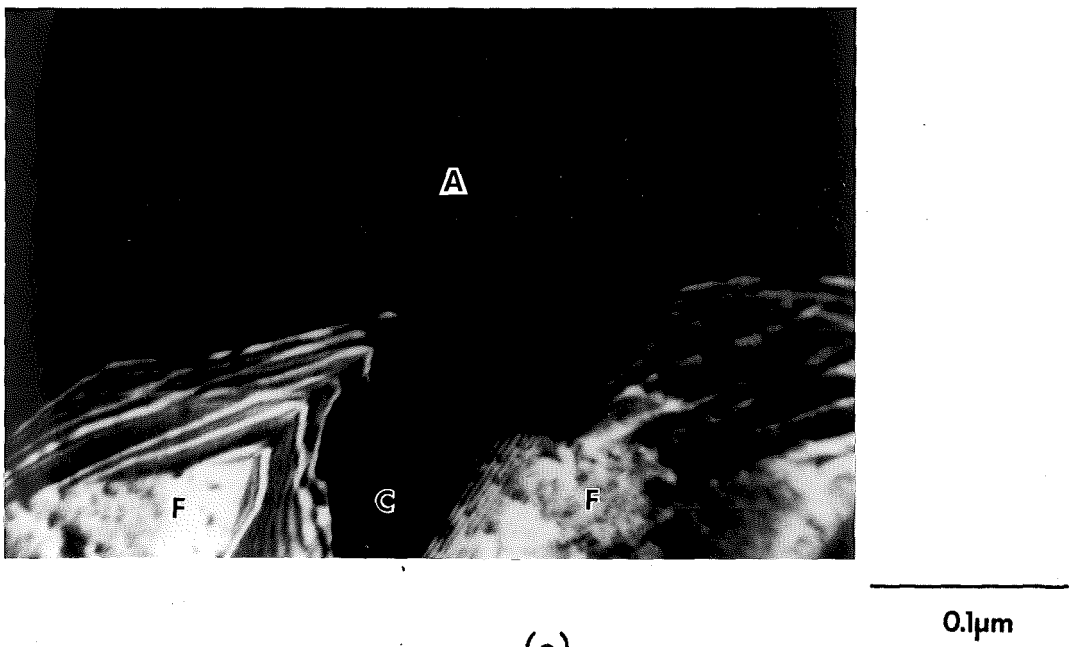

(e)

Figure 4.1 Growth ledge/direction step association.

d), e) Ferrite dark field micrographs showing growth ledge/direction step association.

in Figures 4.2a-c this is actually observed. The cementite lamella imaged in the dark-field mode (Figure 4.2a) shows two sets of non-parallel growth ledges at the CAI and direction steps at the FCI. Figures 4.2b and c are enlargements of the ferrite:cementite:austenite triple junction indicated in regions 1 and 2, respectively. It is again apparent that the growth ledges (open arrows) are continuous with the interfacial steps (closed arrows), indicating that the direction step formation mechanism is operative during the growth of both pearlite constituents.

Continuous Growth Ledges

The results just presented and shown in section 2 indicate that both the ferrite and cementite phases of pearlite grow by the ledge mechanism. This would be expected if the two constituents are truly "equal partners" (Hillert) in the formation of pearlite. This raises some interesting questions about the formation of growth ledges at the FAI and CAI. Since the crystal structures are so radically different, it might be expected that each lamella would have a "unique" set of ledges. However, experimentally, the situation has been found to be quite different. When both the FAI and adjacent CAI are successfully imaged (that is, with appropriate contrast), it is usually found that a single growth ledge may extend continuously through several FAI's and CAI's. In Figure 4.3a four adjacent lamella are imaged at their growth interface with austenite. Two non-parallel sets of growth ledges are visible marked 1 and 2. If we follow one of these ledges in set 1 (open arrows) starting at the CAI at the left we see it crosses one triple

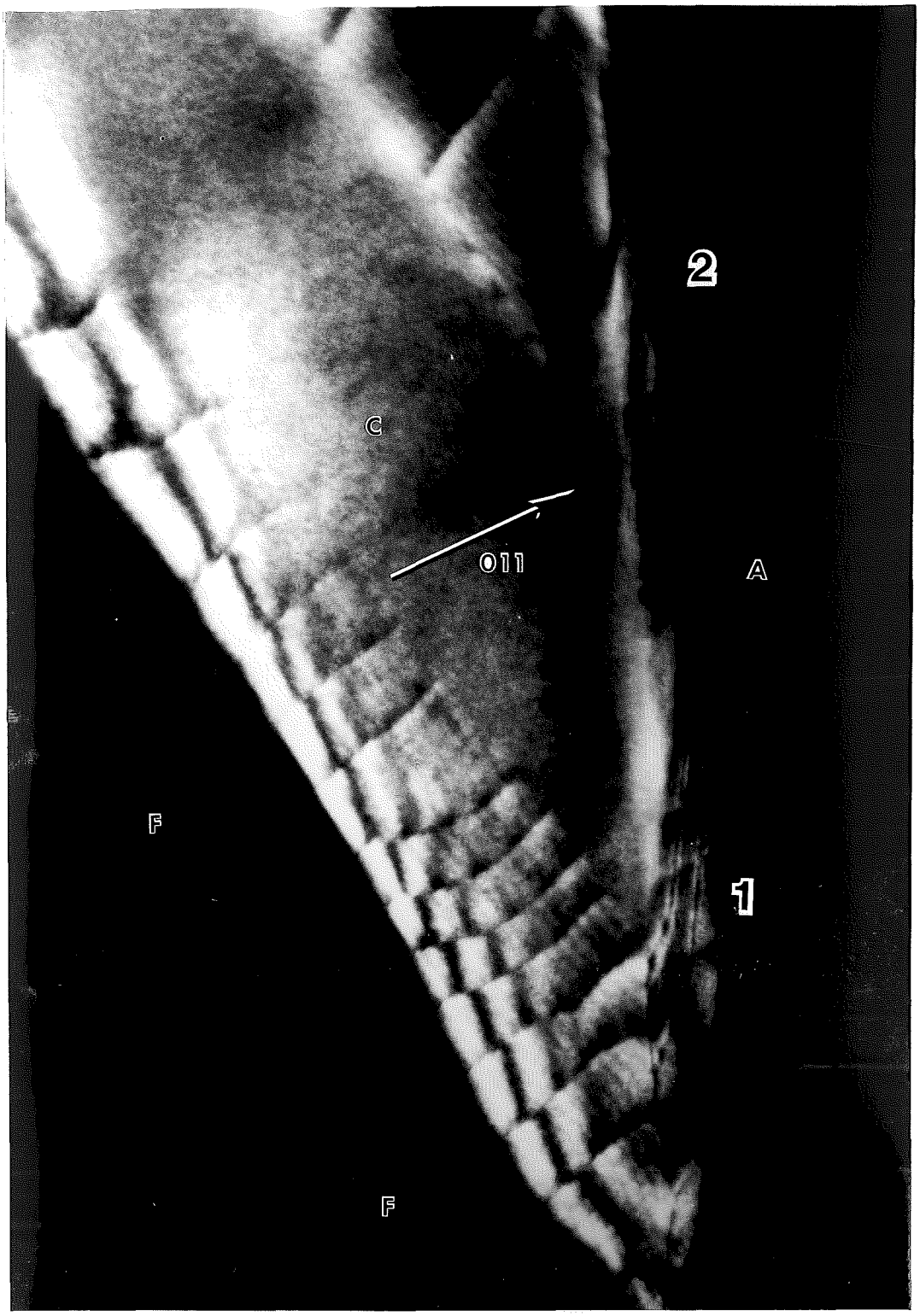

Figure 4.2 Growth ledge/direction step association. 12h, 610C.

a. Cementite dark field showing continuity between CAI growth ledges and FCI direction steps.

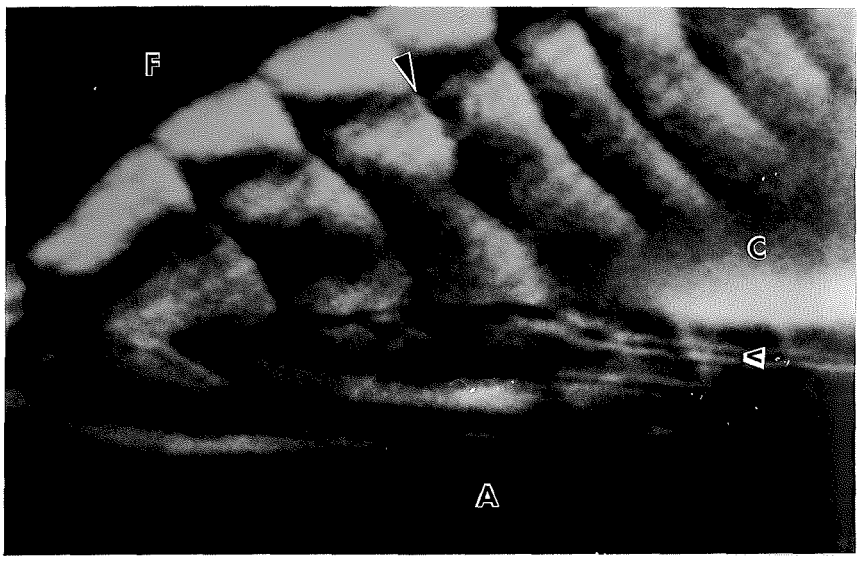

Figure 4.2 Growth ledge/direction step association. 12h, 610C.

b. Blow up of triple junction 1.

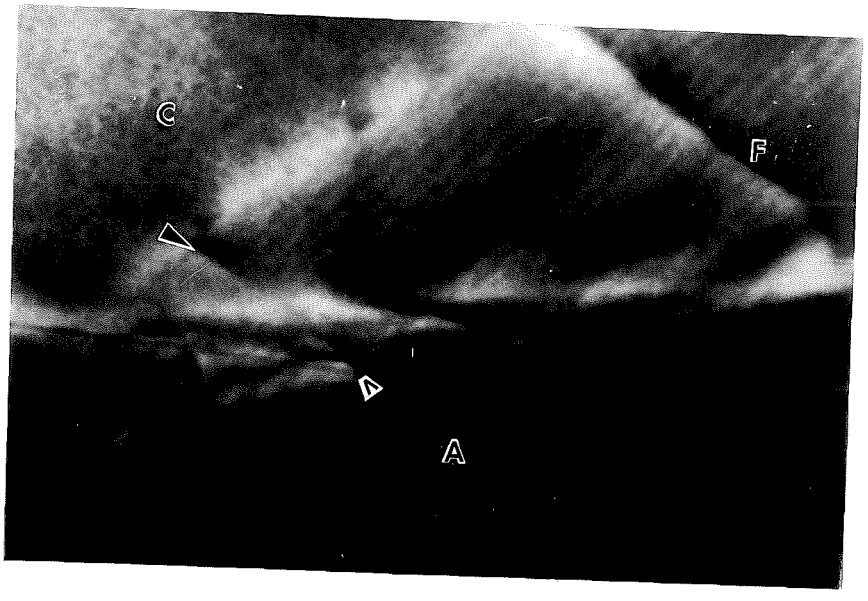

c. Blow up of triple junction 2.

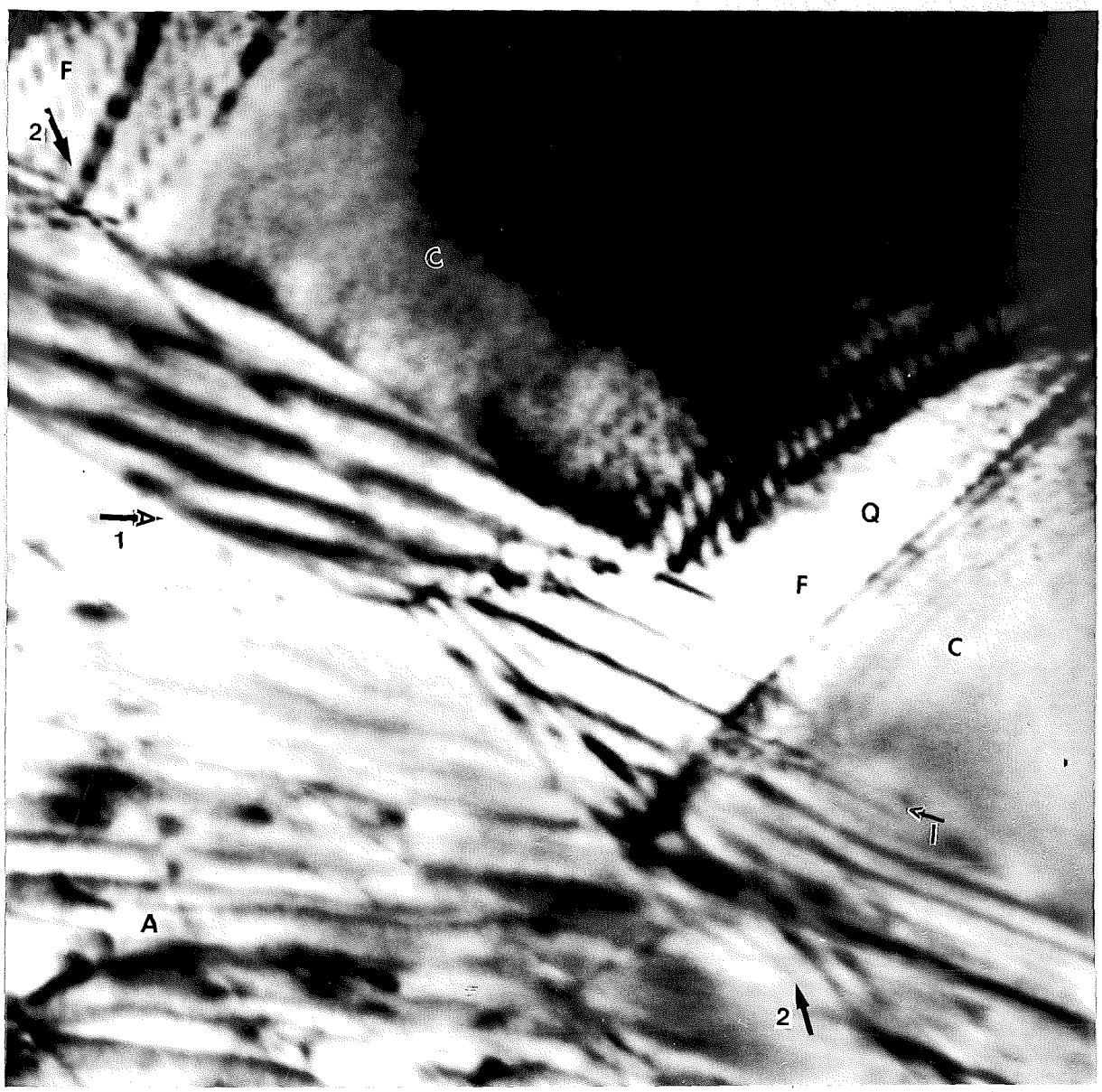

Figure 4.3 Continuous growth ledges.

a. Individual growth ledges extending across both CAI's and FAI's. 12h, 610C.

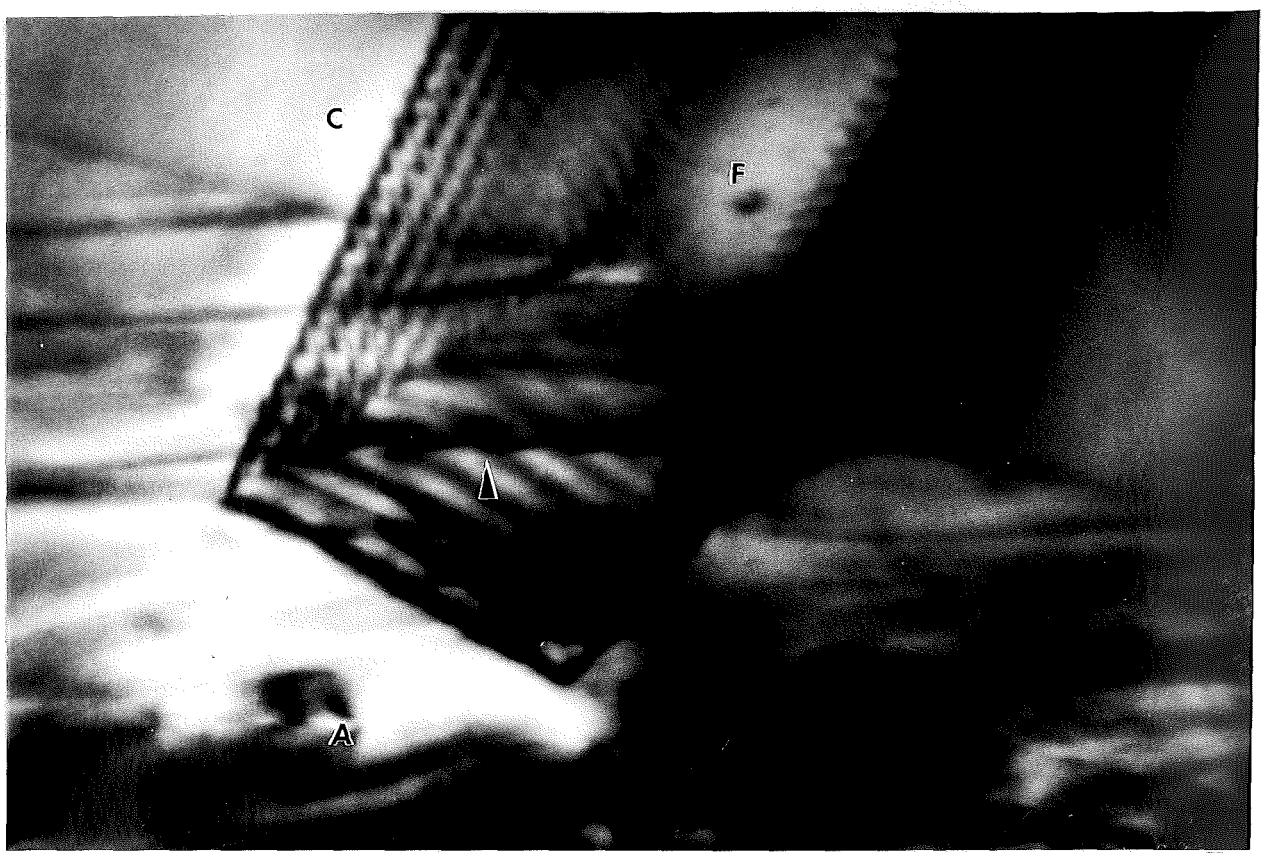

Figure 4.3 Continuous growth ledges.

b. A second orientation showing the topography and jogs on the growth ledges from (a).

0.1μm

Figure 4.3 Continuous growth ledges.

c. A second example. 12h, 600C.

junction, is extended into the FAI, crosses a second triple junction and is once again in a CAI. The growth ledges in set 2 (closed arrows) may be traced in a similar manner.

Figure 4.3b is another orientation of the ferrite lamella marked Q in Figure 4.3a. Jogs are visible at these growth ledges where they intersect with a second set of growth ledges now out of contrast. The topological contrast enhanced by the extinction contours is also visible.

C. Model and Discussion

Simultaneous imaging of the ferrite:cementite lamellar interface with the adjacent ferrite:austenite growth interface has shown that the direction steps are continuous with the growth ledges on the FAI and CAI. This suggests that the lateral movement of growth ledges is directly involved in the formation of the interfacial direction steps on the FCI. Figures 4.1-4.3 as well as many other observations also reveal at least two sets of non-parallel growth ledges. Based on these observations, we will develop a new model for pearlite growth.

A schematic of two lamellae is illustrated in Figure 4.4a' where a single set of parallel growth ledges moving right to left is shown on the lamellae growth interface. Figure 4.4a' has one ledge drawn isometrically with reference point x on its riser. With increasing time the reference point moves across the ferrite:austenite interface perpendicular to the plane of the ledge. When the point on the growth ledge intersects the ferrite:cementite interfacial plane (defined as ABCD), the increased

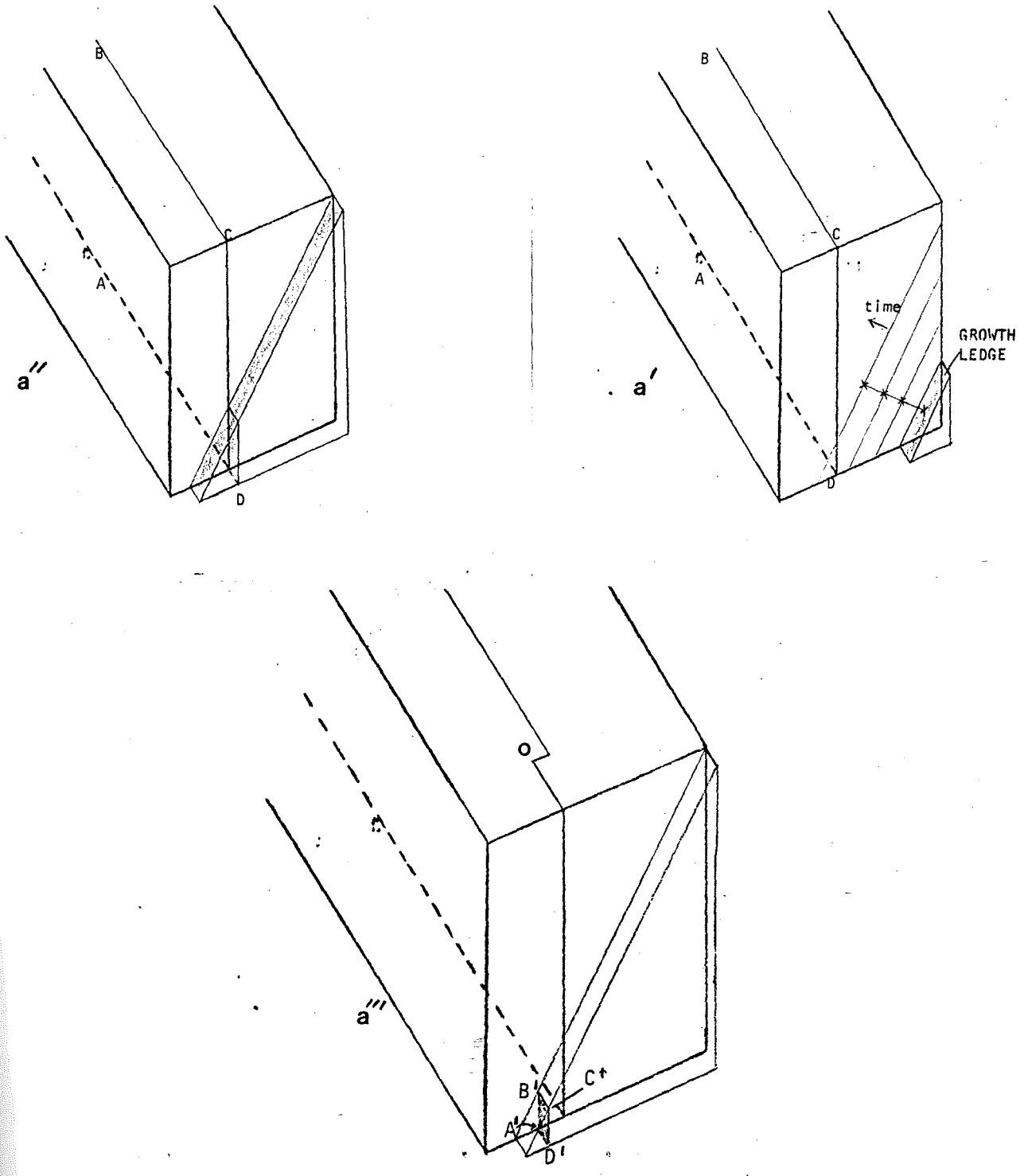

Figure 4.4 Schematics of proposed growth mechanism.

a. Schematic showing FCI step formation by pearlite growth ledge.

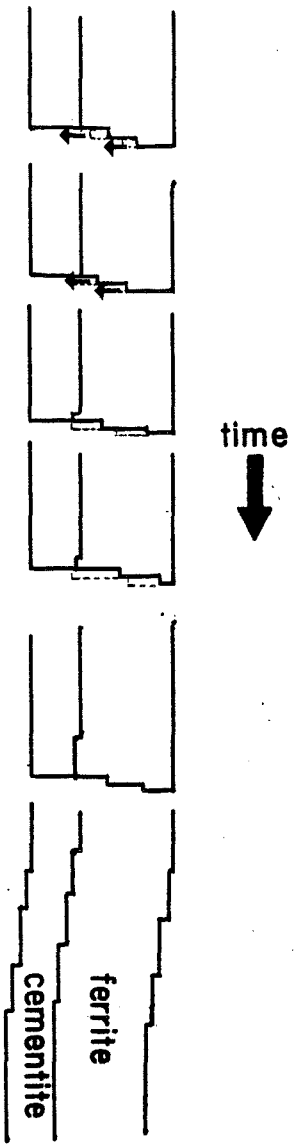

Figure 4.4 Schematic of proposed growth mechanism.

b. Schematic showing curvature resulting from a single set of parallel growth ledges.

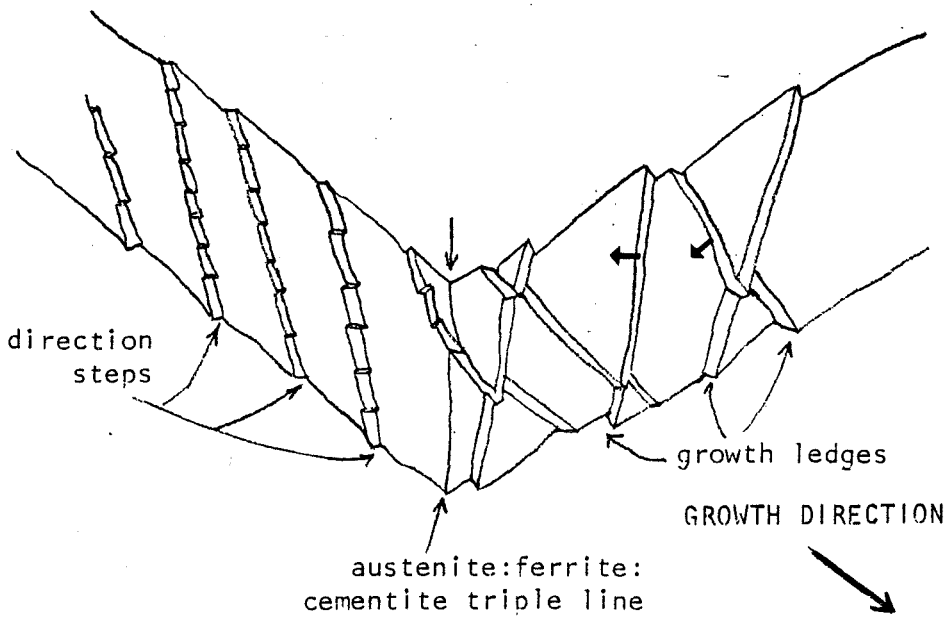

Figure 4.4 Schematic of proposed growth mechanism.

c. Schematic showing the growth ledge/direction step configuration for two sets of non-parallel growth ledges.

carbon concentration as well as the energetics of growing cementite makes the formation of the orthorhombic phase more favorable. As long as no perturbations occur, the plane defined by ABCD will be continued as illustrated in Figure 4.4a''. Thus the positions of the ferrite:cementite:austenite triple junctions will be determined by the growth ledges. If the controlling factors are idealized so that they are constant with time, the growth rate, lamellar spacing, and lamellar thickness will be constant.

Consider now a small perturbation of the conditions at the edge of the example growth ledge (such as temperature and/or composition change) so that it is no longer identical with the preceding ledge. Consider also that this perturbation has slightly increased the carbon concentration at which the designated point will begin forming cementite, thus increasing the perpendicular distance the point must travel across the FAI. In our model, the growth ledge will now grow past the geometric plane (ABCD) defined by the previous ledge, causing the FCI to be shifted over in space to A'B'C'D' (Figure 4.4a'''). It should be understood at this point that the spatial change just described will lead to the formation of a step in the FCI similar to the one at point O in the schematic. Note that if we now allow every growth ledge to form a step at the FCI in question, the ferrite:cementite boundary plane will be translated in space (shifted over) continuously as the pearlite colony grows. The resulting ferrite:cementite boundary plane morphology would give the distinct impression of lamellar curvature (Figure 4.4b). Thus the steps formed by the growth ledges provide the exact same function as the FCI direction steps discussed in results section 1.

Consider now a second set of growth ledges (not parallel to the first set) on the advancing interface with only one set of ledges forming direction steps. It should be apparent to the reader that the growth interface is moving forward while the direction steps are being formed. This is due to the simultaneous lateral movement of the two sets of non-parallel growth ledges. In this situation, both the growth ledge and the associated FCI direction step would intersect the ferrite:cementite:austenite triple junction line at an angle, as shown schematically in Figure 4.4c. This growth ledge/directional step configuration is exactly that observed experimentally (Figures 4.1-4.3), giving strong support to the proposed mechanism of directional step formation.

As a check on this model, the configuration of the FCI direction steps might be examined more closely. Since the advancement of the pearlite:austenite interface is ledge controlled, position of the interface with time is not a "continuous" function, but rather occurs by discrete steps. Thus, if the model in Figure 4.4c is correct, the presence of small jogs on the FCI interfacial steps (direction steps) is expected (Figure 4.4c). The magnitude of these jog heights would be a function of interledge spacing, ledge height, and ledge velocity. This is observed experimentally (Figure 4.5a,b). Thus the type of jog configuration observed in Figures 4.5a and b will occur if only one set of growth ledges is forming FCI directional steps while the second set of ledges acts only to advance the pearlite:austenite interface without changing the geometric plane of the FCI.

If we now allow the system to become highly perturbed with respect to microscopic variations in temperature and chemistry

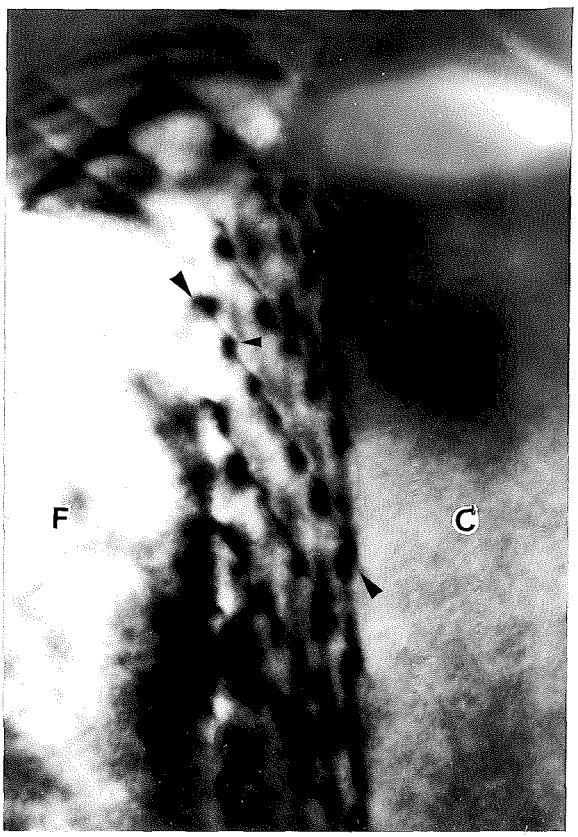

Figure 4.5 Experimental support for growth model.

a. Jogs on FCI directional steps formed as a result of non-parallel growth ledges.

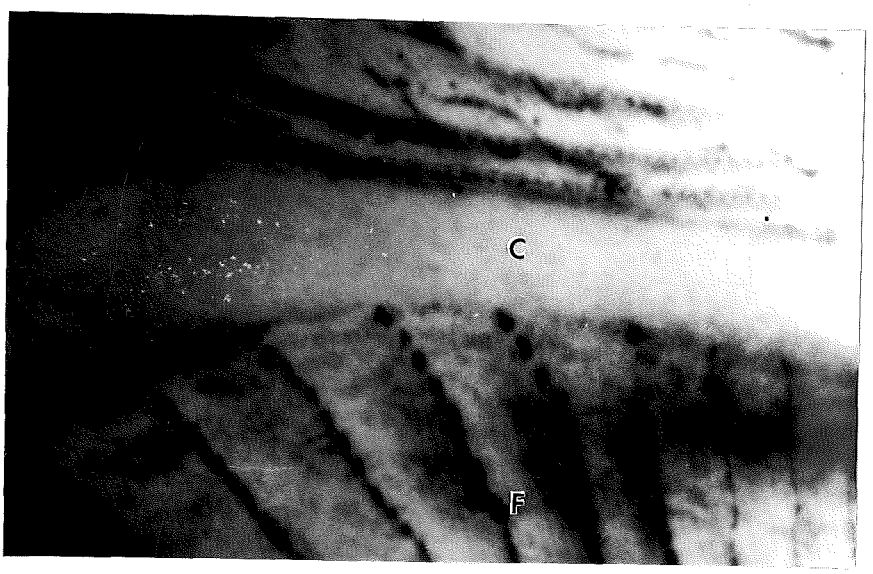

Figure 4.5 Experimental support for growth model.

b. Jogs on FCI directional steps formed as a result of non-parallel growth ledges.

0.1μm

Figure 4.5 Experimental support for growth model.

c. Jogs on FCI directional steps associated with the intersection of non-parallel FCI steps.

Figure 4.5 Experimental support for growth model.

d. Jogs on FCI directional steps associated with the intersection of non-parallel FCI steps.

during the transformations, it becomes apparent that seldom will each growth ledge be subject to the identical conditions as those preceding it. Under these conditions, it would be possible for both sets of growth ledges to form a more complex pattern of FCI direction steps. In this case, the jogs on the FCI steps will be associated with the intersection of the two sets of direction steps. This is indeed observed experimentally (Figure 4.5c,d).

Given that two (or more) non-parallel sets of growth ledges may simultaneously form FCI direction steps, it is clear that the apparent ferrite:cementite boundary plane may become parallel to a great many geometric planes without losing the atomic habit plane. In this manner, the plane rotation axis is not limited to a single geometric direction as in the one ledge model, but may have an axis corresponding to a number of geometric directions. If two (or more) sets of non-parallel FCI directional steps are present, as in Figures 4.5c,d, the boundary plane normal is dependent upon the ledge heights, spacings, and directions. If these quantities are variable, as in Figure 4.5d, the boundary plane (i.e. lamellae) not only may rotate about the FCI direction step but also has the ability to twist. The ramifications of this model on the theory of pearlite growth are substantial. In the following sections, it will be shown how the proposed growth mechanism may be extended to explain some of the more common phenomena observed during pearlite growth.

a. Lamellar Curvature and Thickness

Curvature of lamellae within a pearlite colony is a common observation with optical and electron microscopy in both high purity Fe-C steels and commercial alloys. Mehl has hypothesized that

curvature occurs during the growth process, although strain effects following the transformation have been proposed as an explanation. As discussed in results section 1 lamellar curvature occurs via FCI direction steps. This allows the "macroscopic" boundary plane to change while the "microscopic" atomic habit plane is maintained. Since it is apparent from the results section that these direction steps are formed by the lateral movement of growth ledges, a great deal of support is given to Mehl's suggestion. Further, changes in lamellar thickness may be approached using similar arguments. Once again, a deviation in the FCI plane is expected. When lamellae plate thickness changes are imaged in the TEM (Figures 1.1, 1.2) it is found that the boundary plane deviation from the atomic habit plane is accommodated by discrete steps. Thus, it would appear that adjustments of lamella thickness occur by a mechanism identical to that of lamellar curvature. In both cases, the atomic mechanism of directional step formation allows the FCI boundary plane to adjust to fluctuation in growth driving forces.

b. Maintenance of Lamellar Spacing

Jackson and Hunt (66), noting the presence of many partial lamella, proposed that spacing adjustments might occur by "lamellar faults" (Figure 4.6a). They noted that the abrupt termination or beginning of a lamella causes a rapid readjustment in the spacing of the neighboring lamella. In this manner, if the pearlite lamellar spacing becomes greater than the "optimum", the spacing may be readjusted by the creation of a new lamella. Conversely, if the spacing is too small, the growth rate may be optimized by the termination of a lamella. This type of configuration has been used successfully by Kirkaldy (40) in the theoretical perturbation

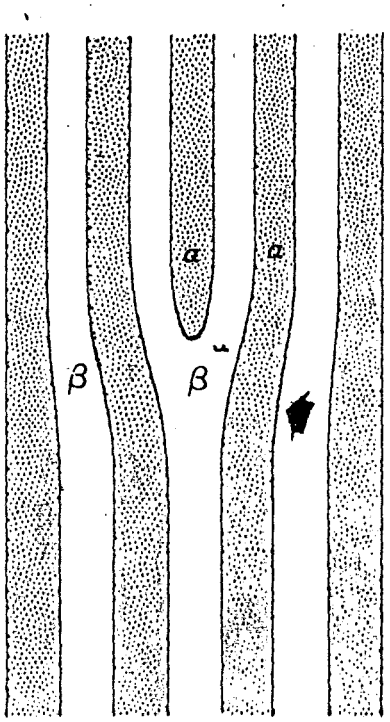

Figure 4.6 Lamellar fault mechanism.

a. Schematic showing the Jackson/Hunt lamellar fault mechanism.

Figure 4.6 Lamellar fault mechanism.

b. Lamellar faults in Fe-.8C pearlite.

Figure 4.6 Lamellar fault mechanism.

c. Lamellar faults in Fe-12Mn-.81C.

analysis of interlamellar spacing and has been observed experimentally (Figure 4.6b, c) in the present study in both Fe-.8C and Fe-12Mn-.8C. As illustrated in this figure, the lamellar fault mechanism requires a significant amount of lamellar curvature. This necessarily causes a change in the apparent habit plane in ostensible disagreement with reports of deep cusp atomic habit planes between pearlitic ferrite and cementite. In results section 1, this apparent conflict was resolved by demonstrating that lamellar curvature and thickness changes occur by discrete steps (direction steps), thus allowing the apparent habit plane to change while maintaining the low energy atomic habit plane. In Figure 1.1b, the high magnification TEM micrograph allows the examination of the "microscopic" mechanism by which the lamellar fault occurs. It is obvious that the termination of cementite lamella 1 results in the shifting over of lamella 2 by the presence of FCI steps.

In this context, the Jackson/Hunt lamellar fault may be viewed as the "macroscopic" expression of FCI directional step formation. Thus, we find strong support for the contention that lamellar spacing is determined by the energetics at the edges of the growth ledges. The argument for this point is as follows. The optimum spacing is maintained in part by the Jackson/Hunt mechanism. The Jackson/Hunt lamellar fault occurs by the creation of FCI direction steps. The FCI direction steps are in turn formed by pearlite growth ledges; therefore, the lamellar fault occurs because of the interaction between the position of the FCI and the lateral movement of growth ledges. It is therefore apparent that the lamellar spacing is determined by the energetics controlling the distance a ledge moves across a ferrite(cementite) lamella before creating

cementite(ferrite) crystal structure.

c. Branching and Holes

In 1962 Hillert (9) altered our conception of pearlite by showing that in a commercial steel each pearlite colony contained only two crystals. One ferrite and the other cementite, each intricately intertwined with the other. Based on this evidence, Hillert proposed that sidewise growth occurred by lamellar branching. The branching process is very dependent upon the ability of a pearlite constituent to form a hole through which the other constituent may grow. This mechanism would seem to require large deviations from any low energy FCI habit plane, again suggesting non-sensitivity to crystallography. However, dual sets of FCI directional steps (Figure 4.5c,d) could accommodate the complex habit plane permutations necessary for lamellar branching. An experimental example of hole formation is illustrated in the dark field micrograph in Figure 4.7. In Figure 4.7a, the hole occurs in the cementite lamella, allowing the ferrite phase to be continuous. The two sets of FCI direction steps are apparent within the hole. Such a configuration would allow branching to occur without the need of a ferrite:cementite disordered interface. In the ferrite dark field in Figure 4.7b, a highly complex branching process is imaged and may best be visualized by considering the cementite phase as growing up from "underneath" the ferrite phase, causing the FCI to be almost perpendicular to the beam direction. Note the high density of FCI steps. The bright field/dark field pair in 4.7c,d would best illustrate the application of the growth mechanism presented in this section to the Hillert mechanism of branching. The bright field in Figure 4.7c illustrates the classic "Hillert"

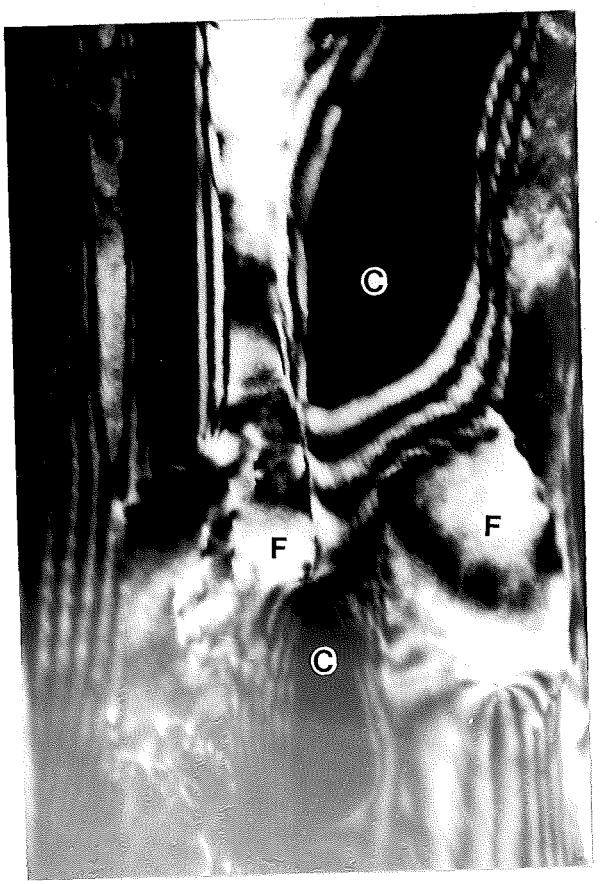

Figure 4.7 Branching via FCI direction steps.

a. Ferrite dark field showing hole formation in cementite lamella via dual FCI steps. 18h, 610C.

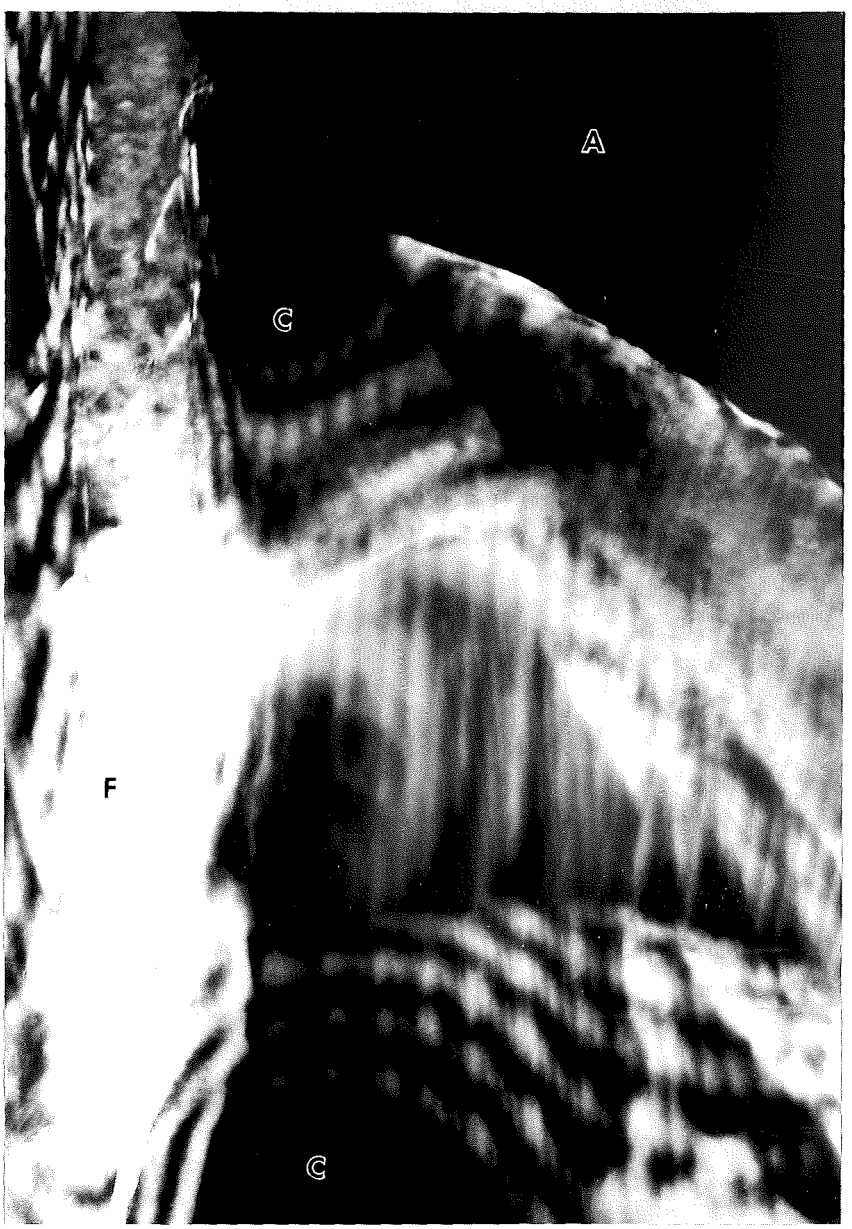

0.1μm

Figure 4.7 Branching via FCI direction steps.

b. Branching with FCI almost perpendicular to the beam direction. 7h, 600C.

Figure 4.7 Branching via FCI direction steps.

c. Bright field, dark field pair showing classic "Hillert" pearlite formed by FCI steps. 12h, 600C.

Figure 4.7 Branching via FCI direction steps.

d. Bright field, dark field pair showing classic "Hillert" pearlite formed by FCI steps. 12h, 600C.

pearlite. A continuous single crystal of grain boundary cementite is giving rise to a number of cementite lamellae by a branching process. The dark field of the arrowed region reveals that FCI direction step formation is operative even during this early stage of pearlite development. Noting that the direction steps arise from the lateral movement of growth ledges, it follows that the conditions controlling the behavior of growth ledges also determine the branching process.

d. Synchronous Growth

The interfacial structure model presented here explains this phenomena trivially. Figure 4.3 shows clearly that growth ledges sweep across both the ferrite and cementite phases, creating new bcc or orthorhombic crystal structure for each. It is the ability of these growth ledges to delay the creation of either the ferrite or cementite crystal structure (and thus form FCI direction steps) that gives the individual lamellae the necessary freedom to alter direction, branch, or change thickness quickly in response to any change in boundary conditions. The principles presented here allow all these phenomena to occur while maintaining equal growth rates for the two phases.

V. CONCLUSIONS

1) The presence of direction steps at the ferrite:cementite interface allows changes in the location of the boundary plane without changing the atomic habit plane. In this manner, lamellar curvature occurs by a mechanism deferential to the ferrite:cementite crystallography. This is the first experimental evidence that the FCI interfacial energy is truly anisotropic.

2) Ledges having heights between 10 and 90 angstroms are present on both the FAI and CAI. The imaging conditions are found to be consistent with the theory of ledge contrast. The mobility of these ledges is demonstrated by hot stage microscopy, thus, it is concluded that these interfacial defects are growth ledges. This observation is an indication that the pearlite:austenite interface is partially coherent and therefore highly dependent on the crystallography at the interphase boundary.

3) Facetting is observed at the pearlite:austenite growth interface, another indication of crystallographic dependence. It is found that there is a tendency for these facets to form on low index planes of either opposing phase, usually resulting in low index:high index planes across the interface. It was demonstrated that even this configuration can give rise to good atomic matching regions, apparently predisposing the interface to growth by the ledge mechanism.

4) Based on TEM observations, it is concluded that the FCI direction step formation occurs by the lateral movement of growth ledges on the pearlite:austenite interface. Using the proposed mechanism of the growth interface:FCI interaction, a variety of phenomena associated with the pearlite transformation are explained.

As pointed out by Hillert in 1962:

> What really matters in the development of pearlite is not one of the phases or the other but the lines (planes) of intersection between ferrite, cementite, and austenite. The formation of pearlite can be imagined as the result of the movements of those lines (planes).

The mechanism of pearlite growth that has been perceived from TEM observations would seemingly describe completely the movement of Hillert's "lines." Not only do we begin to understand the movement of these lines because of the growth ledge/direction step association, but some insight is also gained into the physical relationship that exists between each of the lines of phase intersection.

In results section 2 we showed the presence of growth ledges in association with both constituents of pearlite at the advancing pearlite interface. Section 4 extended the role of the growth ledge to show how they accounted for the directional steps at the FCI. This leads to a new explanation of a variety of pearlite phenomena. The perception that ledges with extensive deference to crystallography cannot account for intricate pattern formation

should now be dispelled. On the contrary, the presence of two or more different sets of ledges at the growth interface easily gives the necessary degrees of freedom to alter growth direction, plate thickness, or spacing quickly and efficiently.

Although the pearlite:austenite growth interface structure in binary steels cannot be observed because of the intervention of the martensite reaction, the presence of direction steps during both curvature and plate thickness adjustment (Figure 1.1) is quite obvious. Much of section 4 has dealt with the direct link between the lateral movement of growth ledges and the formation of direction steps in the high manganese steel. If the reader accepts the premise that this is the sole mechanism of directional step creation, then the generality of pearlite growth by ledges has been demonstrated.

The integrated mechanism of growth presented in this dissertation is a new concept in that it requires ledges at the pearlite:austenite growth interface which control the positions of the ferrite:cementite lamellar interfaces. The perceived behavior of the ferrite:cementite interface, however, must be viewed as the synthesis of the opposing viewpoints of Mehl and Hillert. The careful experimental observations of these two investigators are reconciled by the presence of FCI direction steps which allows for the rigid crystallographic dependence predicted by Mehl to coexist with the crystallographically unrestrained boundary plane implied by Hillert.

VI. SUGGESTIONS FOR FUTURE RESEARCH

1) A number of experimental observations have been made in this investigation which have outstripped the theoretical efforts of interphase boundary structure. For instance, the observation of facetting and growth by the ledge mechanism is not expected to occur for the random orientation relationships found between pearlite and austenite. The formation of facets on high index:low index planes was totally unexpected.

The questions which present themselves are:

1) Is the facetting crystallography observed to occur in the pearlite transformation truly a general phenomena for all non-burgers related phases?

2) Do all non-burgers related phases find a low energy interfacial configuration during the growth process, thus giving rise to growth by the ledge mechanism?

An experiment has been devised which should allow a systematic investigation of this phenomena in a system considerably easier to study than the high manganese alloy. Using a high nickel, low carbon stainless steel, the formation of ferritic grain boundary allotriomorphs should give rise to an appropriate crystallographic configuration to study non-burgers facetting. Since the allotriomorph can usually have a low index orientation relationship with only one grain, the other grain should exhibit a situation similar to that observed for pearlitic ferrite, only without the influence of the cementite phase. The investigator would be presented with a large number of interfaces in an alloy system in

which the specimen preparation is significantly easier than the high manganese alloy.

2) This dissertation has emphasized the experimental observation of the atomic mechanism of the pearlite transformation. True to the principles of reductionism, the dissection has been completed to within the limits of resolution of our instruments. The "breaking down" of the pearlite transformation now leaves the more important (and more difficult) task of putting the pieces back together.

The pearlite lamellar structure is an excellent example of ordered structures occurring in systems far from equilibrium. It is generally accepted that such structures require a positive feedback mechanism to exist. Knowing the atomic mechanism allows us to see how this feedback process manifests itself, but gives no clues as to what it might be. The identification of the controlling factors, although a noble goal, is thought to be an extremely difficult problem requiring sophisticated analysis. At this point, encouragement is the only thing that might be offered by the writer to those pursuing the underlying physical principles controlling the formation of pearlite.

REFERENCES

1. H.C. Sorby, J.I.S.I., 1, 140 (1886).

2. F.C. Hull and R.F. Mehl, Trans. ASM, 30, 381 (1942).

3. M. Hillert, Decomposition of Austenite by Diffusional Processes, p. 197, Interscience, New York, 1962.

4. M. Hillert, Decomposition of Austenite by Diffusional Processes, p. 289, Interscience, New York, 1962.

5. M.R. Plichta, J.H. Perepezko, H.I. Aaronson, and W.F. Lange, III, Acta Met., 28, 1031 (1980).

6. W.F. Lange, III, and H.I. Aaronson, submitted to Met. Trans. A.

7. T. Obara, G.J. Shiflet, and H.I. Aaronson, Met. Trans. A, in press.

8. H.I. Aaronson, Decomposition of Austenite by Diffusional Processes, p. 317, Interscience, New York.

9. H.I. Aaronson, C. Laird, and K.R. Kinsman, Phase Transformations, p. 313, ASM, Metals Park, Ohio, 1970.

10. H.I. Aaronson, J. Microsc., 102, 275 (1974).

11. Y.A. Bagaryatski, Dokl. Akad., Nauk. S.S.S.R., 73, 1161 (1950).

12. W. Pitsch, Acta Met., 10, 79 (errata p. 906) (1962).

13. N.J. Petch, Acta Crystallog., 6, 96 (1953).

14. K.W. Andrews and D.J. Dyson, Iron Steel Lond., 40, 93 (1967).

15. D.F. Lupton and D.H. Warrington, Acta Met., 20, 1325 (1972).

16. H.G. Bowden and P.M. Kelly, Acta Met., 15, 105 (1967).

17. Y. Ohmori, A.T. Davenport, and R.W.K. Honeycombe, Trans. Iron and Steel Inst. Japan, 12, 128 (1972).

18. R.J. Dippenaar and R.W.K. Honeycombe, Proc. Roy. Soc. Lond. A., 333, 455 (1973).

19. M.G. Hall, H.I. Aaronson, and K.R. Kinsman, Surface Sci., 31, 257 (1972).

20. J.M. Rigsbee and H.I. Aaronson, Acta Met., 27, 351 (1979).

21. J.M. Rigsbee and H.I. Aaronson, Acta Met., 27, 365 (1979).

22. D.A. Porter and K.E. Easterling, Phase Transformations in Metals and Alloys, Van Nostrand Reinhold (1981).

23. Pond, Scripta. Met., 12, 699 (1978).

24. H.I. Aaronson, unpublished lecture notes.

25. Howe, Gronsky, Aaronson, submitted to Acta Met.

26. G.J. Shiflet, H.I. Aaronson, and T.H. Courtney, Acta Met., 27, 377 (1979).

27. C. Benedicks, J.I.S.I., 2, 352 (1905).

28. M.E. Nicholson, Trans. TMS-AIME, 200, 1071 (1954).

29. S. Modin, Jern. Ann., 135, 169 (1951).

30. M. Hillert, Vermlandska Bergm. Foren. Ann., 29 (1958).

31. S. Modin, Jern. Ann., 142, 37 (1958).

32. A. Hultgren and H. Ohlin, Jern. Ann., 144, 356 (1960).

33. R.F. Mehl and W.C. Hagel, Prog. Mat. Sci., 6, 74 (1956).

34. C.S. Smith, Trans. ASM, 45, 533 (1953).

35. J.W. Cahn, Acta Met., 7, 18 (1959).

36. Cahn and Hagel, Decomposition of Austenite by Diffusional Processes, p. 123, Interscience, New York, 1962.

37. G.W. Rathenau and G. Baas, Acta Met., 2, 875 (1954).

38. D. Pearson and J. Verhoeven, Met. Trans., 15A, 1037 (1984).

39. H.I. Aaronson, C. Laird, and K.R. Kinsman, Scripta Met., 2, 259 (1968).

40. B.G. Koepke, R.P. Jewett, and W.T. Chandler, Trans. ASM, 58, 510 (1965).

41. L.S. Darken and R.M. Fisher, Decomposition of Austenite by Diffusional Processes, p. 249, Interscience, New York, 1962.

42. Puls and Kirkaldy, Met. Trans, 3, 2777 (1972).

43. H.O.K. Kichner, B.G. Mellor, and G.A. Chadwick, Acta Met., 26, 1023 (1978).

44. Ridley, Met. Trans., 15A, 962, (1984).

45. E.C. Bain, Trans. TMS-AIME, 100, 13 (1932).

46. E.C. Bain, E.S. Davenport, and W.S.N. Waring, Trans. TMS-AIME, 100, 228 (1932).

47. C.H. White and R.W.K. Honeycombe, J.I.S.I., 200, 457 (1962).

48. H. Brooks, Metal Interfaces, p. 20, American Society for Metals, Cleveland, Ohio, 1952.

49. J.H. van der Merwe, J. App. Phys., 34, 117 (1963).

50. J.H. van der Merwe, J. App. Phys, 34, 12 (1963).

51. J.H. van der Merwe, J. App. Phys, 34, 3420 (1963).

52. D.J.H. Cockayne, J. Microscopy, 98, 116 (1973).

53. R.W. Balluffi, G. Woodhouse, and Y. Komer, Nature and Behavior of Grain Boundaries, p. 41, Plenum Press, New York, 1972.

54. C. Laird, and H.I. Aaronson, Acta Met., 17, 505 (1969).

55. G.C. Weatherly and T.K. Mok, Surface Science, 31, 355 (1972).

56. H. Gleiter, Acta Met., 17, 565 (1969).

57. G. Garmong and C.G. Rhodes, Met. Trans., 5, 2507 (1974).

58. G. Baro and H. Gleiter, Acta Met., 22, 141 (1974).

59. S.A. Hackney and G.J. Shiflet, submittd to Acta Met.

60. N.T. Belaiew, J.I.S.I., No. 1, 201 (1922).

61. I.V. Isaichev, Zhur. Tekhn. Fiziki, 17, 835 (1947).

62. B.L. Bramfitt and A.R. Marder, Metallog., 6, 483 (1973).

63. B.L. Bramfitt and A.R. Marder, IMS Proc., 43 (1968).

64. W. Bollman, Crystal Lattices, Interfaces, Matrices, published by the author, 1982.

65. Vaughan and Silcock, unpublished research.

Appendix 1

Computer Data

Final x,y,z coordinates are given in table form. This is followed by a computer printout where:

D = distance (in angstroms) from the plane

a,b,c = crystal coordinates

l,m,n = projected cartesian coordinates

FCC (III)

0	0	0
4.671977	2.023025	-4.768372E-07
-4.671977	-2.023025	4.768372E-07
4.08798	-3.034538	-4.768372E-07
-4.08798	3.034538	4.768372E-07
-.583997	-5.057563	0
.583997	5.057563	0
2.335989	1.011513	-2.384186E-07
-2.335989	-1.011513	2.384186E-07
2.04399	-1.517269	-2.384186E-07
-2.04399	1.517269	2.384186E-07
-.2919985	-2.528782	0
.2919985	2.528782	0
-2.627987	-3.540294	2.384186E-07
2.627987	3.540294	-2.384186E-07
1.751991	-4.04605	-2.384186E-07
-1.751991	4.04605	2.384186E-07
4.379979	-.5057565	-4.768372E-07
-4.379979	.5057565	4.768372E-07
8.759958	-1.011513	-9.536743E-07
-8.759958	1.011513	9.536743E-07
6.715967	.5057567	-9.536743E-07
-6.715967	-.5057567	9.536743E-07
6.423969	-2.023026	-9.536743E-07
-6.423969	2.023026	9.536743E-07
-5.255974	-7.080588	4.768372E-07
5.255974	7.080588	-4.768372E-07
-2.919985	-6.069075	-1.192093E-07
2.919985	6.069075	1.192093E-07
-4.963975	-4.551807	2.384186E-07
4.963975	4.551807	-2.384186E-07
9.343954	4.04605	-9.536743E-07
-9.343954	-4.04605	9.536743E-07
7.007965	3.034537	-7.152558E-07
-7.007965	-3.034537	7.152558E-07
-7.299964	-5.563319	9.536743E-07
7.299964	5.563319	-9.536743E-07
9.051955	1.517269	-9.536743E-07
-9.051955	-1.517269	9.536743E-07
3.503982	-8.0921	-4.768372E-07
-3.503982	8.0921	4.768372E-07
1.459992	-6.574831	1.192093E-07
-1.459992	6.574831	-1.192093E-07
3.795982	-5.563319	-2.384186E-07
-3.795982	5.563319	2.384186E-07
8.17596	-6.069076	-9.536743E-07
-8.17596	6.069076	9.536743E-07

6.13197	-4.551807	-7.152558E-07
-6.13197	4.551807	7.152558E-07
5.839971	-7.080589	-9.536743E-07
-5.839971	7.080589	9.536743E-07
8.467959	-3.540294	-9.536743E-07
-8.467959	3.540294	9.536743E-07
-1.167994	-10.11513	0
1.167994	10.11513	0
-.8759956	-7.586344	0
.8759956	7.586344	0
-3.211984	-8.597856	0
3.211984	8.597856	0
1.167994	-9.103613	0
-1.167994	9.103613	0
13.43193	1.011513	-1.907349E-06
-13.43193	-1.011513	1.907349E-06
11.38794	2.528782	-9.536743E-07
-11.38794	-2.528782	9.536743E-07
11.09595	0	-9.536743E-07
-11.09595	0	9.536743E-07
-9.92795	-9.103613	4.768372E-07
9.92795	9.103613	-4.768372E-07
-7.591963	-8.092101	9.536743E-07
7.591963	8.092101	-9.536743E-07
-9.635953	-6.574833	9.536743E-07
9.635953	6.574833	-9.536743E-07
14.01593	6.069075	-1.430512E-06
-14.01593	-6.069075	1.430512E-06
11.67994	5.057564	-9.536743E-07
-11.67994	-5.057564	9.536743E-07
-11.97194	-7.586344	1.430512E-06
11.97194	7.586344	-1.430512E-06
13.72393	3.540294	-1.430512E-06
-13.72393	-3.540294	1.430512E-06
12.84794	-4.046052	-1.907349E-06
-12.84794	4.046052	1.907349E-06
10.80395	-2.528782	-9.536743E-07
-10.80395	2.528782	9.536743E-07
10.51195	-5.057564	-9.536743E-07
-10.51195	5.057564	9.536743E-07
13.13993	-1.517269	-1.430512E-06
-13.13993	1.517269	1.430512E-06
-5.83997	-12.13815	-2.384186E-07
5.83997	12.13815	2.384186E-07
-3.503983	-11.12664	1.192093E-07
3.503983	11.12664	-1.192093E-07
-5.547973	-9.609369	0
5.547973	9.609369	0
-7.88396	-10.62088	7.152558E-07
7.88396	10.62088	-7.152558E-07
7.591963	-11.12664	-4.768372E-07
-7.591963	11.12664	4.768372E-07
0	0	0

```
D 0
 0              0              0
 0              0              0
D 0
 0              1              1
 0              3.6            3.6
D 0
 0             -1             -1
 0             -3.6           -3.6
D 0
 1              0              1
 3.6            0              3.6
D 0
-1              0             -1
-3.6            0             -3.6
D 0
 1             -1              0
 3.6           -3.6            0
D 0
-1              1              0
-3.6            3.6            0
D 0
 0              .5             .5
 0              1.8            1.8
D 0
 0             -.5            -.5
 0             -1.8           -1.8
D 0
 .5             0              .5
 1.8            0              1.8
D 0
-.5             0             -.5
-1.8            0             -1.8
D 0
 .5            -.5             0
 1.8           -1.8            0
D 0
-.5             .5             0
-1.8            1.8            0
D 0
 .5            -1             -.5
 1.8           -3.6           -1.8
D 0
-.5             1              .5
-1.8            3.6            1.8
D 0
 1             -.5             .5
 3.6           -1.8            1.8
D 0
-1              .5            -.5
-3.6            1.8           -1.8
D 0
 .5             .5             1
 1.8            1.8            3.6
D 0
-.5            -.5            -1
-1.8           -1.8           -3.6
D 0
 1              1              2
 3.6            3.6            7.2
D 0
```

```
-1                -1                -2
-3.6              -3.6              -7.2
D 0
 .5                1                 1.5
 1.8               3.6               5.4
D 0
-.5               -1                -1.5
-1.8              -3.6              -5.4
D 0
 1                 .5                1.5
 3.6               1.8               5.4
D 0
-1                -.5               -1.5
-3.6              -1.8              -5.4
D 0
 1                -2                -1
 3.6              -7.2              -3.6
D 0
-1                 2                 1
-3.6               7.2               3.6
D 1.37651E-07
 1                -1.5              -.5
 3.6              -5.399999         -1.8
D-1.37651E-07
-1                 1.5               .5
-3.6               5.399999          1.8
D 1.37651E-07
 .5               -1.5              -1
 1.8              -5.4              -3.6
D-1.37651E-07
-.5                1.5               1
-1.8               5.4               3.6
D 0
 0                 2                 2
 0                 7.2               7.2
D 0
 0                -2                -2
 0                -7.2              -7.2
D 0
 0                 1.5               1.5
 0                 5.4               5.4
D 0
 0                -1.5              -1.5
 0                -5.4              -5.4
D 0
 .5               -2                -1.5
 1.8              -7.2              -5.4
D 0
-.5                2                 1.5
-1.8               7.2               5.4
D 0
 .5                1.5               2
 1.8               5.4               7.2
D 0
-.5               -1.5              -2
-1.8              -5.4              -7.2
D 0
 2                -1                 1
 7.2              -3.6               3.6
D 0
-2                 1                -1
-7.2               3.6              -3.6
D-1.37651E-07
 1.5              -1                 .5
 5.399999         -3.6               1.8
D 1.37651E-07
```

```
-1.5              1               -.5
-5.399999         3.6             -1.8
D-1.37651E-07
 1.5             -.5               1
 5.4             -1.8              3.6
D 1.37651E-07
-1.5              .5              -1
-5.4              1.8             -3.6
D 0
 2                0                2
 7.2              0                7.2
D 0
-2                0               -2
-7.2              0               -7.2
D 0
 1.5              0                1.5
 5.4              0                5.4
D 0
-1.5              0               -1.5
-5.4              0               -5.4
D 0
 2               -.5               1.5
 7.2             -1.8              5.4
D 0
-2                .5              -1.5
-7.2              1.8             -5.4
D 0
 1.5              .5               2
 5.4              1.8              7.2
D 0
-1.5             -.5              -2
-5.4             -1.8             -7.2
D 0
 2               -2                0
 7.2             -7.2              0
D 0
-2                2                0
-7.2              7.2              0
D 0
 1.5             -1.5              0
 5.4             -5.4              0
D 0
-1.5              1.5              0
-5.4              5.4              0
D-1.37651E-07
 1.5             -2               -.5
 5.4             -7.2             -1.8
D 1.37651E-07
-1.5              2                .5
-5.4              7.2              1.8
D 1.37651E-07
 2               -1.5              .5
 7.2             -5.4              1.8
D-1.37651E-07
-2                1.5             -.5
-7.2              5.4             -1.8
D 0
 1                2                3
 3.6              7.2              10.8
D 0
-1               -2               -3
-3.6             -7.2             -10.8
D 0
 .5               2                2.5
 1.8              7.2              9
D 0
```

```
-.5                -2                -2.5
-1.8               -7.2              -9
D 0
 1                  1.5               2.5
 3.6                5.4               9
D 0
-1                 -1.5              -2.5
-3.6               -5.4              -9
D 2.753021E-07
 1                 -3                -2
 3.6               -10.8             -7.2
D-2.753021E-07
-1                  3                 2
-3.6                10.8              7.2
D-2.753021E-07
 1                 -2.5              -1.5
 3.6               -9                -5.4
D 2.753021E-07
-1                  2.5               1.5
-3.6                9                 5.4
D 0
 .5                -2.5              -2
 1.8               -9                -7.2
D 0
-.5                 2.5               2
-1.8                9                 7.2
D 0
 0                  3                 3
 0                  10.8              10.8
D 0
 0                 -3                -3
 0                 -10.8             -10.8
D 0
 0                  2.5               2.5
 0                  9                 9
D 0
 0                 -2.5              -2.5
 0                 -9                -9
D 5.506041E-07
 .5                -3                -2.5
 1.8               -10.8             -8.999999
D-5.506041E-07
-.5                 3                 2.5
-1.8                10.8              8.999999
D 5.506041E-07
 .5                 2.5               3
 1.8                9                 10.8
D-5.506041E-07
-.5                -2.5              -3
-1.8               -9                -10.8
D 0
 2                  1                 3
 7.2                3.6               10.8
D 0
-2                 -1                -3
-7.2               -3.6              -10.8
D 0
 1.5                1                 2.5
 5.4                3.6               9
D 0
-1.5               -1                -2.5
-5.4               -3.6              -9
D 0
 2                  .5                2.5
 7.2                1.8               9
D 0
```

```
-2                -.5               -2.5
-7.2              -1.8              -9
D 0
 1.5               1.5               3
 5.4               5.4               10.8
D 0
-1.5              -1.5              -3
-5.4              -5.4              -10.8
D 2.753021E-07
 2                -3                -1
 7.2              -10.8             -3.6
D-2.753021E-07
-2                 3                 1
-7.2               10.8              3.6
D-1.37651E-07
 2                -2.5              -.5
 7.2              -9                -1.8
D 1.37651E-07
-2                 2.5               .5
-7.2               9                 1.8
D-2.753021E-07
 1.5              -2.5              -1
 5.4              -8.999999         -3.6
D 2.753021E-07
-1.5               2.5               1
-5.4               8.999999          3.6
D 0
 1.5              -3                -1.5
 5.4              -10.8             -5.4
D 0
-1.5               3                 1.5
-5.4               10.8              5.4
D-2.753021E-07
 3                -1                2
 10.8             -3.6              7.2
D 2.753021E-07
-3                 1                -2
-10.8              3.6              -7.2
```

BCC 121

2.567006	3.143928	3.576279E-07	
-2.567006	-3.143928	-3.576279E-07	
-1.925255	1.571964	-1.788139E-07	
.6417513	2.095952	1.788139E-07	
-1.925254	-1.047976	-2.384186E-07	
1.925255	-1.571964	1.788139E-07	
1.192093E-07		-2.61994	0
2.567006	.5239882	3.576279E-07	
-3.850509	3.143927	-3.576279E-07	
3.850509	-3.143927	3.576279E-07	
-1.283503	3.667915	-5.960465E-08	
-3.850509	.5239876	-4.768372E-07	
0	0	0	
5.134012	3.667916	7.152558E-07	
4.492261	1.571964	4.768372E-07	
-4.492261	-1.571964	-4.768372E-07	
4.492261	-1.047975	3.576279E-07	
-6.417515	-2.61994	-7.152558E-07	
6.417515	-2.619939	7.152558E-07	
-6.417516	-5.960465E-07		-7.152558E-07
6.417516	5.960465E-07		7.152558E-07
-5.775765	2.095951	-4.768372E-07	
-7.701019	3.667915	-1.192093E-06	
-2.567006	-5.763868	-3.576279E-07	
-.6417513	-4.715892	-1.788139E-07	
.6417513	4.715892	1.788139E-07	
1.925255	-4.191903	0	
1.283503	6.811843	2.384186E-07	
3.85051	-5.763866	7.152558E-07	
-1.283504	6.287855	0	
1.283504	-6.287855	0	
5.134012	6.287855	7.152558E-07	
-5.134012	-6.287855	-7.152558E-07	
3.208758	5.239879	4.768372E-07	
-4.492261	-4.191904	-4.768372E-07	
-3.208758	5.23988	-1.192093E-07	
-5.134013	6.811842	-3.576279E-07	
-5.775764	4.715891	-4.768372E-07	
5.775764	-4.715891	4.768372E-07	
-7.701019	6.287854	-7.152558E-07	
7.701019	-6.287854	7.152558E-07	
7.059266	2.095952	1.192093E-06	
8.984521	3.143929	9.536743E-07	
-8.984521	-3.143929	-9.536743E-07	
8.984521	.523989	9.536743E-07	
-8.342771	1.571963	-9.536743E-07	
-8.34277	-1.047977	-9.536743E-07	
8.342771	-1.571963	9.536743E-07	

-10.26803	3.143927	-9.536743E-07	
10.26803	-3.143927	9.536743E-07	
-10.26802	.5239871	-7.152558E-07	
7.701018	6.811843	9.536743E-07	
7.059267	4.715892	9.536743E-07	
-7.059267	-4.715892	-9.536743E-07	
-8.984521	-5.763868	-9.536743E-07	
8.34277	-4.191903	-7.152558E-07	
10.26802	-5.763866	1.192093E-06	
-9.626273	5.239879	-9.536743E-07	
-11.55153	6.811841	-1.192093E-06	
-.6417508	-7.335831	-1.192093E-07	
-1.283503	-9.431782	-3.576279E-07	
1.283503	9.431782	3.576279E-07	
1.283504	-8.907794	5.960465E-08	
-5.134012	-8.907794	-7.152558E-07	
-3.208757	-7.859819	-5.960465E-07	
3.208757	7.859819	5.960465E-07	
3.850508	9.955772	7.152558E-07	
7.701018	9.431784	9.536743E-07	
-7.701018	-9.431784	-9.536743E-07	
5.775763	8.383806	9.536743E-07	
-7.059266	-7.335831	-7.152558E-07	
-3.208758	7.859819	-5.960465E-08	
-.6417523	8.383806	1.192093E-07	
3.208758	-7.859819	5.960465E-08	
-5.134013	9.431782	-3.576279E-07	
5.134013	-9.431782	3.576279E-07	
-2.567007	9.955771	3.129244E-07	
5.775765	-7.33583	4.768372E-07	
7.701019	-8.907793	7.152558E-07	
-7.059268	8.383805	-2.384186E-07	
-8.984522	9.955771	-7.152558E-07	
-9.626274	7.859818	-9.536743E-07	
9.626274	-7.859818	9.536743E-07	
-11.55153	9.431782	-9.536743E-07	
11.55153	-9.431782	9.536743E-07	
11.55153	3.667916	1.430512E-06	
10.90978	1.571965	9.536743E-07	
-10.90978	-1.571965	-9.536743E-07	
10.90978	-1.047975	1.192093E-06	
-12.83503	-2.619941	-1.907349E-06	
12.83503	-2.619938	2.384186E-06	
-12.83503	-1.192093E-06		-1.430512E-06
12.83503	1.192093E-06		1.430512E-06
-12.19328	2.095951	-1.430512E-06	
-14.11853	3.667914	-1.907349E-06	
9.626272	5.239881	1.668933E-06	
11.55153	6.287855	1.430512E-06	
-11.55153	-6.287855	-1.430512E-06	
-10.90978	-4.191904	-1.430512E-06	
0	0	0	

```
D Ø
 1                Ø               -1
 2.87             Ø               -2.87
D Ø
-1                Ø                1
-2.87             Ø                2.87
D Ø
 .5               .5               .5
 1.435            1.435            1.435
D-1.171673
 .5               .5              -.5
 1.913333         .4783333        -.9566665
D-1.171673
-.5               .5               .5
-.9566665         .4783333         1.913333
D Ø
-.5              -.5              -.5
-1.435           -1.435           -1.435
D-1.171673
-1                Ø                Ø
-2.391667        -.9566666         .4783333
D-1.171673
 Ø                Ø               -1
 .4783333        -.9566666        -2.391667
D Ø
 1                1                1
 2.87             2.87             2.87
D Ø
-1               -1               -1
-2.87            -2.87            -2.87
D-1.171673
 1                1                Ø
 3.348333         1.913333         .4783333
D-1.171673
 Ø                1                1
 .4783333         1.913333         3.348333
D Ø
 Ø                Ø                Ø
 Ø                Ø                Ø
D-1.171673
 1                Ø               -2
 3.348333        -.9566666        -5.261667
D Ø
 .5              -.5              -1.5
 1.435           -1.435           -4.305
D Ø
-.5               .5               1.5
-1.435            1.435            4.305
D-1.171673
-.5              -.5              -1.5
-.9566666        -2.391667        -3.826667
D-1.171673
-1                1                2
-2.391667         1.913333         6.218333
D-1.171673
-1               -1               -2
-2.391667        -3.826666        -5.261667
D Ø
 Ø                1                2
 Ø                2.87             5.74
D Ø
```

```
 Ø               -1              -2
 Ø               -2.87           -5.74
D-1.171673
 .5              1.5             1.5
 1.913333        3.348333        4.783334
D-1.171673
 1               2               2
 3.348333        4.783334        6.218333
D-1.171673
-2               Ø               1
-5.261667       -.9566666        3.348333
D Ø
-1.5            -.5              .5
-4.305          -1.435           1.435
D Ø
 1.5             .5             -.5
 4.305           1.435          -1.435
D-1.171673
-1.5            -.5             -.5
-3.826666       -2.391667       -.9566666
D-1.171673
 2               1              -1
 6.218333        1.913333       -2.391667
D-1.171673
-2              -1              -1
-5.261666       -3.826667       -2.391667
D Ø
 2               1               Ø
 5.74            2.87            Ø
D Ø
-2              -1               Ø
-5.74           -2.87            Ø
D Ø
 2               Ø              -2
 5.74            Ø              -5.74
D Ø
-2               Ø               2
-5.74            Ø               5.74
D-1.171673
 1.5             .5             -1.5
 4.783333        .4783333       -3.826667
D-1.171673
-1.5             .5              1.5
-3.826667        .4783333        4.783334
D-1.171673
 1.5             1.5             .5
 4.783334        3.348333        1.913333
D-1.171673
 2               2               1
 6.218333        4.783333        3.348333
D Ø
 1.5             1.5             1.5
 4.305           4.305           4.305
D Ø
-1.5            -1.5            -1.5
-4.305          -4.305          -4.305
D Ø
 2               2               2
 5.74            5.74            5.74
D Ø
-2              -2              -2
-5.74           -5.74           -5.74
D-1.171673
 .5             -.5             -2.5
 1.913333       -2.391667       -6.696666
D Ø
```

```
 1                -1               -3
 2.87             -2.87            -8.609999
D 0
-1                 1                3
-2.87              2.87             8.609999
D-1.171673
 0                -1               -3
 .4783333         -3.826666        -8.131666
D 0
 .5                1.5              2.5
 1.435             4.305            7.175
D-1.171673
-.5                1.5              2.5
-.9566666         3.348333         7.653333
D 0
-.5               -1.5             -2.5
-1.435            -4.305           -7.175
D 0
 1                 2                3
 2.87              5.74             8.609999
D 0
-1                -2               -3
-2.87             -5.74            -8.609999
D-1.171673
 0                 2                3
 .4783334          4.783333         9.088333
D-1.171673
 2                 0               -3
 6.218333         -.9566666        -8.131666
D 0
 1.5              -.5              -2.5
 4.305            -1.435           -7.175
D 0
-1.5               .5               2.5
-4.305             1.435            7.175
D-1.171673
-2                 1                3
-5.261667          1.913333         9.088333
D-1.171673
-1.5              -1.5             -2.5
-3.826667         -5.261667        -6.696666
D-1.171673
-2                -2               -3
-5.261667         -6.696666        -8.131666
D-1.171673
 1.5               2.5              2.5
 4.783334          6.218333         7.653333
D-1.171673
 2                 3                3
 6.218333          7.653333         9.088333
D-1.171673
-2.5              -.5               .5
-6.696666         -2.391667        1.913333
D 0
-3                -1                1
-8.609999         -2.87             2.87
D 0
 3                 1               -1
 8.609999          2.87            -2.87
D-1.171673
-3                -1                0
-8.131666         -3.826666         .4783333
D-1.171673
-3                 0                2
-8.131666         -.9566666         6.218333
D 0
```

```
-2.5             -.5              1.5
-7.175           -1.435           4.305
D 0
 2.5              .5             -1.5
 7.175            1.435          -4.305
D-1.171673
 3                1              -2
 9.088333         1.913333       -5.261667
D 0
 3                0              -3
 8.609999         0              -8.609999
D 0
-3                0               3
-8.609999         0               8.609999
D-1.171673
 2.5              .5             -2.5
 7.653333         .4783333       -6.696666
D-1.171673
-2.5              .5              2.5
-6.696666         .4783333        7.653333
D 0
 2.5              1.5             .5
 7.175            4.305           1.435
D-1.171673
 2.5              1.5            -.5
 7.653333         3.348333       -.9566666
D 0
-2.5             -1.5            -.5
-7.175           -4.305          -1.435
D 0
 3                2               1
 8.609999         5.74            2.87
D 0
-3               -2              -1
-8.609999        -5.74           -2.87
D-1.171673
 3                2               0
 9.088333         4.783333        .4783334
D-1.171673
-2.5             -1.5            -1.5
-6.696666        -5.261667       -3.826666
D-1.171673
-3               -2              -2
-8.131666        -6.696666       -5.261667
D-1.171673
 2.5              2.5             1.5
 7.653333         6.218333        4.783334
D-1.171673
 3                3               2
 9.088333         7.653333        6.218333
D 0
 2.5              2.5             2.5
 7.175            7.175           7.175
D 0
-2.5             -2.5            -2.5
-7.175           -7.175          -7.175
D 0
 3                3               3
 8.609999         8.609999        8.609999
D 0
-3               -3              -3
-8.609999        -8.609999       -8.609999
D-1.171673
 1               -1              -4
 3.348333        -3.826667       -11.00167
D 0
```

```
 .5              -1.5            -3.5
 1.435           -4.305          -10.045
D Ø
-.5               1.5             3.5
-1.435            4.305           10.045
D-1.171673
-.5              -1.5            -3.5
-.9566665        -5.261667       -9.566666
D-1.171673
-1                2               4
-2.391667         4.783334        11.95833
D-1.171673
-1               -2              -4
-2.391667        -6.696667       -11.00167
D Ø
 Ø                2               4
 Ø                5.74            11.48
D Ø
 Ø               -2              -4
 Ø               -5.74           -11.48
D-1.171672
 .5               2.5             3.5
 1.913333         6.218333        10.52333
D-1.171673
 1                3               4
 3.348333         7.653333        11.95833
D-1.171673
 1.5             -.5             -3.5
 4.783334        -2.391667       -9.566666
D Ø
 2               -1              -4
 5.74            -2.87           -11.48
D Ø
-2                1               4
-5.74             2.87            11.48
D-1.171672
-1.5              1.5             3.5
-3.826667         3.348333        10.52333
```

FCC 221

0	0	0	
-2.398828	2.401171	-7.152557E-07	
4.799413	-1.202343	1.072884E-06	
1.197656	-4.800585	1.072884E-06	
3.601757	3.598242	0	
-3.601757	-3.598242	0	
1.202929	5.999413	-5.960464E-07	
-6.000585	-1.19707	-5.960464E-07	
2.399706	-.6011716	5.364418E-07	
.5988281	-2.400293	5.364418E-07	
1.800878	1.799121	0	
-1.800878	-1.799121	0	
4.200585	1.197949	4.768372E-07	
-1.20205	-4.199413	4.768372E-07	
-.5979493	4.200292	-7.152557E-07	
-4.199706	.6020505	-7.152557E-07	
2.998535	-3.001464	1.072884E-06	
-7.198242	3.603515	-1.907349E-06	
7.198242	-3.603515	1.907349E-06	
-3.596484	7.201757	-1.907349E-06	
3.596484	-7.201757	1.907349E-06	
-4.798535	3.002344	-1.192093E-06	
-2.997656	4.801465	-1.192093E-06	
-6.599413	1.203223	-1.192093E-06	
-1.196778	6.600585	-1.192093E-06	
-5.397363	5.402636	-1.907349E-06	
5.397363	-5.402636	1.907349E-06	
8.40117	2.395898	9.536743E-07	
6.001464	2.99707	8.34465E-07	
6.600292	.5967775	9.536743E-07	
10.8	-5.273442E-03		1.907349E-06
-10.8	5.273442E-03		-1.907349E-06
-8.400291	-.595898	-1.311302E-06	
8.999119	-1.804394	1.66893E-06	
-8.999119	1.804394	-1.66893E-06	
-2.404101	-8.398826	9.536743E-07	
-3.002929	-5.998534	8.34465E-07	
-.6032222	-6.599706	9.536743E-07	
5.272488E-03		10.8	-1.907349E-06
-5.272488E-03		-10.8	1.907349E-06
.6041004	8.399706	-1.311302E-06	
-1.795606	9.000878	-1.66893E-06	
1.795606	-9.000878	1.66893E-06	
7.203514	7.196483	0	
-7.203514	-7.196483	0	
4.804686	9.597654	-1.192093E-06	
-9.602341	-4.795312	-1.192093E-06	

5.402635	5.397362	0
-5.402635	-5.397362	0
7.802342	4.796191	5.960464E-07
-4.803807	-7.797654	5.960464E-07
3.003808	7.798534	-9.536743E-07
-7.801463	-2.996191	-9.536743E-07
-10.20117	-2.395019	-8.34465E-07
2.404979	10.19883	-8.34465E-07
-9.59707	6.004687	-2.384186E-06
-5.995312	9.602929	-2.384186E-06
8.395897	-8.404099	2.622604E-06
7.79707	-6.003807	2.384186E-06
5.996191	-7.802928	2.384186E-06
-7.796191	7.803808	-2.384186E-06
11.99765	-4.805859	2.622604E-06
-13.19883	2.406445	-2.384186E-06
9.597947	-4.204687	2.384186E-06
11.39883	-2.405566	2.622604E-06
-11.39795	4.205567	-2.145767E-06
10.19678	-6.60498	3.099441E-06
15.59941	-1.207617	2.861023E-06
13.19971	-.6064446	2.384186E-06
13.79853	-3.006738	2.861023E-06
4.794141	-12.00234	2.622604E-06
-2.393556	13.20117	-2.384186E-06
4.195312	-9.602048	2.384186E-06
2.394434	-11.40117	2.622604E-06
-4.194434	11.40205	-2.145767E-06
6.59502	-10.20322	3.099441E-06
12.00293	5.99414	1.66893E-06
9.60322	6.595311	2.980232E-07
10.20205	4.195019	1.072884E-06
14.40176	3.592968	1.907349E-06
-14.40176	-3.592968	-1.907349E-06
-12.00205	-4.19414	-3.576279E-07
12.60088	1.793848	1.66893E-06
-12.60088	-1.793848	-1.66893E-06
-16.80058	-1.191796	-2.622604E-06
15.00058	1.192676	2.384186E-06
-14.9997	.6073244	-1.66893E-06
1.192384	-15.60058	2.861023E-06
.5935551	-13.20029	2.384186E-06
2.993262	-13.80146	2.861023E-06
-6.005858	-11.99707	1.66893E-06
-6.604686	-9.596775	2.980232E-07
-4.204979	-10.19795	1.072884E-06
3.607029	14.39824	-1.907349E-06
-3.607029	-14.39824	1.907349E-06
4.205858	11.99795	-3.576279E-07
1.806151	12.59912	-1.66893E-06
-1.806151	-12.59912	1.66893E-06
1.208201	16.79941	-2.622604E-06
0	0	0

```
3700 CLOSE #2
3710 END


D 0
 0              0              0
 0              0              0
D-1.2
 0              0              1
 .8             .8             3.2
D-1.2
 0             -1             -1
 .8            -2.8           -4
D-1.2
-1              0             -1
-2.8            .8            -4
D 0
 1             -1              0
 3.6           -3.6            0
D 0
-1              1              0
-3.6            3.6            0
D-1.2
 1             -1              1
 4.4           -2.8            3.2
D-1.2
-1              1              1
-2.8            4.4            3.2
D-.6
 0             -.5            -.5
 .4            -1.4           -2
D-.6
-.5             0             -.5
-1.4            .4            -2
D 0
 .5            -.5             0
 1.8           -1.8            0
D 0
-.5             .5             0
-1.8            1.8            0
D-.6
 .5            -1             -.5
 2.2           -3.2           -2
D-.6
-1              .5            -.5
-3.2            2.2           -2
D-1.2
 .5            -.5             1
 2.6           -1              3.2
D-1.2
-.5             .5             1
-1              2.6            3.2
D-1.2
-.5            -.5            -1
-1             -1             -4
D 0
 0              1              2
 0              3.6            7.2
D 0
 0             -1             -2
 0             -3.6           -7.2
D 0
 1              0              2
 3.6            0              7.2
D 0
```

```
-1                0                -2
-3.6              0                -7.2
D-.5999999
 0                .5                1.5
 .4000001         2.2               5.200001
D-.5999999
 .5               0                 1.5
 2.2              .4000001          5.200001
D-.5999999
-.5               1                 1.5
-1.4              4                 5.200001
D-.5999999
 1               -.5                1.5
 4               -1.4               5.200001
D 0
 .5               .5                2
 1.8              1.8               7.2
D 0
-.5              -.5               -2
-1.8             -1.8              -7.2
D-1.2
 1               -2                -1
 4.4             -6.4              -4
D-.5999999
 1               -1.5              -.5
 4               -5                -2
D-1.2
 .5              -1.5              -1
 2.6             -4.6              -4
D 0
 1               -2                -2
 3.6             -7.2              -7.2
D 0
-1                2                 2
-3.6              7.2               7.2
D-.6000001
-1                1.5               1.5
-3.2              5.8               5.200001
D 1.589457E-07
 .5              -1.5              -2
 1.8             -5.4              -7.2
D-1.589457E-07
-.5               1.5               2
-1.8              5.4               7.2
D-1.2
-2                1                -1
-6.4              4.4              -4
D-.5999999
-1.5              1                -.5
-5                4                -2
D-1.2
-1.5              .5               -1
-4.6              2.6              -4
D 0
 2               -1                2
 7.2             -3.6              7.2
D 0
-2                1                -2
-7.2              3.6              -7.2
D-.6000001
 1.5             -1                1.5
 5.8             -3.2              5.200001
D-1.589457E-07
 1.5             -.5               2
 5.4             -1.8              7.2
D 1.589457E-07
```

```
-1.5            .5              -2
-5.4            1.8             -7.2
D 0
 2              -2               0
 7.2            -7.2             0
D 0
-2               2               0
-7.2             7.2             0
D-1.2
 2              -2               1
 8              -6.4             3.2
D-1.2
-2               2               1
-6.4             8               3.2
D 0
 1.5            -1.5             0
 5.4            -5.4             0
D 0
-1.5             1.5             0
-5.4             5.4             0
D-.6000001
 1.5            -2               -.5
 5.8            -6.8             -2
D-.6000001
-2               1.5             -.5
-6.8             5.8             -2
D-1.2
 1.5            -1.5             1
 6.2            -4.6             3.2
D-1.2
-1.5             1.5             1
-4.6             6.2             3.2
D-.5999998
-1.5             2               1.5
-5               7.6             5.200001
D-.5999998
 2              -1.5             1.5
 7.6            -5               5.200001
D-1.2
 0               1               3
 .8000002        4.4             10.4
D-1.2
 1               0               3
 4.4             .8000002        10.4
D-1.2
-1              -1               -3
-2.8            -2.8             -11.2
D-.5999998
-.5             -1               -2.5
-1.4            -3.2             -9.2
D-.5999998
-1              -.5              -2.5
-3.2            -1.4             -9.2
D-1.2
 .5              .5              3
 2.6             2.6             10.4
D-1.2
 0              -2               -3
 .7999997       -6.4             -11.2
D-1.2
-1               2               3
-2.8             8               10.4
D-.5999998
 0              -1.5             -2.5
 .3999999       -5               -9.2
D-.5999998
```

```
 .5              -2              -2.5
 2.2             -6.8            -9.2
D-1.2
-.5              1.5             3
-.9999998        6.2             10.4
D-1.2
-.5             -1.5            -3
-1              -4.600001       -11.2
D-1.2
 1              -3              -3
 4.4            -10             -11.2
D-.6000001
 1              -2.5            -2.5
 4              -8.600001       -9.2
D-1.2
 .5             -2.5            -3
 2.6            -8.200001       -11.2
D-1.2
-2               0              -3
-6.4             .7999997       -11.2
D-1.2
 2              -1               3
 8              -2.8             10.4
D-.5999998
-1.5             0              -2.5
-5               .3999999       -9.2
D-.5999998
-2               .5             -2.5
-6.8             2.2            -9.2
D-1.2
 1.5            -.5              3
 6.2            -.9999998        10.4
D-1.2
-1.5            -.5             -3
-4.600001       -1              -11.2
D-1.2
 2              -3              -1
 7.999999       -10             -4
D-.6000001
 2              -2.5            -.5
 7.6            -8.599999       -2
D-1.2
 1.5            -2.5            -1
 6.2            -8.2            -4
D 3.178915E-07
 2              -3              -2
 7.2            -10.8           -7.2
D-3.178915E-07
-2               3               2
-7.2             10.8            7.2
D-.5999998
-2               2.5             1.5
-6.8             9.399999        5.200001
D-3.178915E-07
 1.5            -2.5            -2
 5.4            -9              -7.2
D 3.178915E-07
-1.5             2.5             2
-5.4             9               7.2
D-1.2
-2               3               3
-6.399999        11.6            10.4
D-.5999998
 1.5            -3              -2.5
 5.8            -10.4           -9.2
D-1.2
```

```
-1.5            2.5             3
-4.6            9.799999        10.4
D-1.2
-3              1               -3
-10             4.4             -11.2
D-.6000001
-2.5            1               -2.5
-8.600001       4               -9.2
D-1.2
-2.5            .5              -3
-8.200001       2.6             -11.2
D-1.2
-3              2               -1
-10             7.999999        -4
D-.6000001
-2.5            2               -.5
-8.599999       7.6             -2
D-1.2
-2.5            1.5             -1
-8.2            6.2             -4
D-3.178915E-07
 3              -2               2
 10.8           -7.2             7.2
D 3.178915E-07
-3              2               -2
-10.8           7.2             -7.2
D-.5999998
 2.5            -2               1.5
 9.399999       -6.8             5.200001
D 3.178915E-07
 2.5            -1.5             2
 9              -5.4             7.2
D-3.178915E-07
-2.5            1.5             -2
-9              5.4             -7.2
D-1.2
 3              -2               3
 11.6           -6.399999        10.4
```

BCC(1TO)

2.485493	-3.278256E-07		7.006208E-04
-.8284976	2.343345	7.006208E-04	
.8284976	-2.343345	-7.006208E-04	
-2.485493	3.278256E-07		-7.006208E-04
1.656995	2.343345	1.401242E-03	
-1.656995	-2.343345	-1.401242E-03	
4.970986	-6.556511E-07		1.401242E-03
-1.656995	4.686691	1.401242E-03	
1.656995	-4.686691	-1.401242E-03	
-4.970986	6.556511E-07		-1.401242E-03
3.313991	-2.343346	0	
-3.313991	2.343346	0	
0	0	0	
4.142488	2.343345	2.101863E-03	
.8284979	4.68669	2.101863E-03	
-.8284979	-4.68669	-2.101863E-03	
-4.142488	-2.343345	-2.101863E-03	
3.31399	4.68669	2.802483E-03	
-3.31399	-4.68669	-2.802483E-03	
6.627981	2.343344	2.802483E-03	
0	7.030035	2.802483E-03	
0	-7.030035	-2.802483E-03	
-6.627981	-2.343344	-2.802483E-03	
5.799484	-2.343346	7.006208E-04	
-4.142488	4.686691	7.006208E-04	
4.142488	-4.686691	-7.006206E-04	
-5.799484	2.343346	-7.006208E-04	
8.284977	-2.343346	1.401242E-03	
-4.970986	7.030037	1.401242E-03	
4.970986	-7.030037	-1.401242E-03	
-8.284977	2.343346	-1.401242E-03	
6.627981	-4.686692	0	
-6.627981	4.686692	0	
7.456479	-8.344651E-07		2.101863E-03
-2.485493	7.030036	2.101863E-03	
2.485493	-7.030036	-2.101863E-03	
-7.456479	8.344651E-07		-2.101863E-03
9.941971	-1.311302E-06		2.802483E-03
-3.313991	9.373381	2.802483E-03	
3.313991	-9.373381	-2.802483E-03	
-9.941971	1.311302E-06		-2.802483E-03
5.799484	4.68669	3.503104E-03	
2.485493	7.030036	3.503104E-03	
-2.485493	-7.030036	-3.503104E-03	
-5.799484	-4.68669	-3.503104E-03	
4.970986	7.030035	4.203725E-03	
-4.970986	-7.030035	-4.203725E-03	
8.284976	4.68669	4.203725E-03	

1.656996	9.37338	4.203725E-03	
-1.656996	-9.37338	-4.203725E-03	
-8.284976	-4.68669	-4.203725E-03	
9.113474	2.343344	3.503104E-03	
-.8284975	9.373381	3.503104E-03	
.8284975	-9.373381	-3.503104E-03	
-9.113474	-2.343344	-3.503104E-03	
11.59897	2.343344	4.203725E-03	
-1.656995	11.71673	4.203725E-03	
1.656995	-11.71673	-4.203725E-03	
-11.59897	-2.343344	-4.203725E-03	
9.113473	-4.686692	7.006208E-04	
-7.456478	7.030036	7.006208E-04	
7.456478	-7.030036	-7.006208E-04	
-9.113473	4.686692	-7.006208E-04	
11.59897	-4.686692	1.401242E-03	
-8.284976	9.373381	1.401242E-03	
8.284976	-9.373381	-1.401242E-03	
-11.59897	4.686692	-1.401242E-03	
9.941972	-7.030037	0	
-9.941972	7.030037	0	
10.77047	-2.343346	2.101863E-03	
-5.799483	9.373381	2.101863E-03	
5.799483	-9.373381	-2.101863E-03	
-10.77047	2.343346	-2.101863E-03	
13.25596	-2.343347	2.802483E-03	
-6.627981	11.71673	2.802483E-03	
6.627981	-11.71673	-2.802483E-03	
-13.25596	2.343347	-2.802483E-03	
12.42747	-9.536743E-07		3.503104E-03
-4.142488	11.71673	3.503104E-03	
4.142488	-11.71673	-3.503104E-03	
-12.42747	9.536743E-07		-3.503104E-03
14.91296	-1.66893E-06	4.203725E-03	
-4.970986	14.06007	4.203725E-03	
4.970986	-14.06007	-4.203725E-03	
-14.91296	1.66893E-06	-4.203725E-03	
7.456479	7.030035	4.904346E-03	
4.142489	9.37338	4.904346E-03	
-4.142489	-9.37338	-4.904346E-03	
-7.456479	-7.030035	-4.904346E-03	
6.627981	9.373379	5.604967E-03	
-6.627981	-9.373379	-5.604967E-03	
9.941971	7.030034	5.604967E-03	
3.313991	11.71673	5.604967E-03	
-3.313991	-11.71673	-5.604967E-03	
-9.941971	-7.030034	-5.604967E-03	
10.77047	4.68669	4.904346E-03	
.8284979	11.71673	4.904346E-03	
-.8284979	-11.71673	-4.904346E-03	
-10.77047	-4.68669	-4.904346E-03	
0	0	0	

```
D Ø
 .5                .5                .5
 1.435             1.435             1.435
D Ø
-.5               -.5                .5
-1.435            -1.435             1.435
D Ø
 .5                .5               -.5
 1.435             1.435            -1.435
D Ø
-.5               -.5               -.5
-1.435            -1.435            -1.435
D Ø
 Ø                 Ø                 1
 Ø                 Ø                 2.87
D Ø
 Ø                 Ø                -1
 Ø                 Ø                -2.87
D Ø
 1                 1                 1
 2.87              2.87              2.87
D Ø
-1                -1                 1
-2.87             -2.87              2.87
D Ø
 1                 1                -1
 2.87              2.87             -2.87
D Ø
-1                -1                -1
-2.87             -2.87             -2.87
D Ø
 1                 1                 Ø
 2.87              2.87              Ø
D Ø
-1                -1                 Ø
-2.87             -2.87              Ø
D Ø
 Ø                 Ø                 Ø
 Ø                 Ø                 Ø
D Ø
 .5                .5                1.5
 1.435             1.435             4.305
D Ø
-.5               -.5                1.5
-1.435            -1.435             4.305
D Ø
 .5                .5               -1.5
 1.435             1.435            -4.305
D Ø
-.5               -.5               -1.5
-1.435            -1.435            -4.305
D Ø
 Ø                 Ø                 2
 Ø                 Ø                 5.74
D Ø
 Ø                 Ø                -2
 Ø                 Ø                -5.74
D Ø
 1                 1                 2
 2.87              2.87              5.74
D Ø
```

```
-1              -1              2
-2.87           -2.87           5.74
D 0
 1               1              -2
 2.87            2.87          -5.74
D 0
-1              -1              -2
-2.87           -2.87          -5.74
D 0
 1.5             1.5             .5
 4.305           4.305          1.435
D 0
-1.5            -1.5             .5
-4.305          -4.305         1.435
D 0
 1.5             1.5            -.5
 4.305           4.305         -1.435
D 0
-1.5            -1.5            -.5
-4.305          -4.305         -1.435
D 0
 2               2               1
 5.74            5.74           2.87
D 0
-2              -2               1
-5.74           -5.74          2.87
D 0
 2               2              -1
 5.74            5.74          -2.87
D 0
-2              -2              -1
-5.74           -5.74          -2.87
D 0
 2               2               0
 5.74            5.74           0
D 0
-2              -2               0
-5.74           -5.74           0
D 0
 1.5             1.5             1.5
 4.305           4.305          4.305
D 0
-1.5            -1.5             1.5
-4.305          -4.305          4.305
D 0
 1.5             1.5            -1.5
 4.305           4.305          -4.305
D 0
-1.5            -1.5            -1.5
-4.305          -4.305         -4.305
D 0
 2               2               2
 5.74            5.74           5.74
D 0
-2              -2               2
-5.74           -5.74          5.74
D 0
 2               2              -2
 5.74            5.74          -5.74
D 0
-2              -2              -2
-5.74           -5.74          -5.74
D 0
 .5              .5              2.5
 1.435           1.435          7.175
D 0
```

```
-.5             -.5             2.5
-1.435          -1.435          7.175
D Ø
 .5              .5             -2.5
 1.435           1.435          -7.175
D Ø
-.5             -.5             -2.5
-1.435          -1.435          -7.175
D Ø
 Ø               Ø               3
 Ø               Ø               8.609999
D Ø
 Ø               Ø              -3
 Ø               Ø              -8.609999
D Ø
 1               1               3
 2.87            2.87            8.609999
D Ø
-1              -1               3
-2.87           -2.87            8.609999
D Ø
 1               1              -3
 2.87            2.87           -8.609999
D Ø
-1              -1              -3
-2.87           -2.87           -8.609999
D Ø
 1.5             1.5             2.5
 4.305           4.305           7.175
D Ø
-1.5            -1.5             2.5
-4.305          -4.305           7.175
D Ø
 1.5             1.5            -2.5
 4.305           4.305          -7.175
D Ø
-1.5            -1.5            -2.5
-4.305          -4.305          -7.175
D Ø
 2               2               3
 5.74            5.74            8.609999
D Ø
-2              -2               3
-5.74           -5.74            8.609999
D Ø
 2               2              -3
 5.74            5.74           -8.609999
D Ø
-2              -2              -3
-5.74           -5.74           -8.609999
D Ø
 2.5             2.5             .5
 7.175           7.175           1.435
D Ø
-2.5            -2.5             .5
-7.175          -7.175           1.435
D Ø
 2.5             2.5            -.5
 7.175           7.175          -1.435
D Ø
-2.5            -2.5            -.5
-7.175          -7.175          -1.435
D Ø
 3               3               1
 8.609999        8.609999        2.87
D Ø
```

```
-3                -3                1
-8.609999         -8.609999         2.87
D 0
 3                 3                -1
 8.609999          8.609999         -2.87
D 0
-3                -3                -1
-8.609999         -8.609999         -2.87
D 0
 3                 3                 0
 8.609999          8.609999          0
D 0
-3                -3                 0
-8.609999         -8.609999          0
D 0
 2.5               2.5               1.5
 7.175             7.175             4.305
D 0
-2.5              -2.5               1.5
-7.175            -7.175             4.305
D 0
 2.5               2.5              -1.5
 7.175             7.175            -4.305
D 0
-2.5              -2.5              -1.5
-7.175            -7.175            -4.305
D 0
 3                 3                 2
 8.609999          8.609999          5.74
D 0
-3                -3                 2
-8.609999         -8.609999          5.74
D 0
 3                 3                -2
 8.609999          8.609999         -5.74
D 0
-3                -3                -2
-8.609999         -8.609999         -5.74
D 0
 2.5               2.5               2.5
 7.175             7.175             7.175
D 0
-2.5              -2.5               2.5
-7.175            -7.175             7.175
D 0
 2.5               2.5              -2.5
 7.175             7.175            -7.175
D 0
-2.5              -2.5              -2.5
-7.175            -7.175            -7.175
D 0
 3                 3                 3
 8.609999          8.609999          8.609999
D 0
-3                -3                 3
-8.609999         -8.609999          8.609999
D 0
 3                 3                -3
 8.609999          8.609999         -8.609999
D 0
-3                -3                -3
-8.609999         -8.609999         -8.609999
D 0
 .5                .5                3.5
 1.435             1.435             10.045
D 0
```

```
-.5             -.5             3.5
-1.435          -1.435          10.045
D 0
 .5              .5             -3.5
 1.435           1.435          -10.045
D 0
-.5             -.5             -3.5
-1.435          -1.435          -10.045
D 0
 0               0               4
 0               0               11.48
D 0
 0               0              -4
 0               0              -11.48
D 0
 1               1               4
 2.87            2.87            11.48
D 0
-1              -1               4
-2.87           -2.87            11.48
D 0
 1               1              -4
 2.87            2.87           -11.48
D 0
-1              -1              -4
-2.87           -2.87           -11.48
D 0
 1.5             1.5             3.5
 4.305           4.305           10.045
D 0
-1.5            -1.5             3.5
-4.305          -4.305           10.045
D 0
 1.5             1.5            -3.5
 4.305           4.305          -10.045
D 0
-1.5            -1.5            -3.5
-4.305          -4.305          -10.045
```

FCC (01T)

0	0	0	
.0012431	-3.6	0	
-.0012431	3.6	0	
5.091168	1.758009E-03		-2.384186E-07
-5.091168	-1.758009E-03		2.384186E-07
5.092411	-3.598242	-2.384186E-07	
-5.089925	-3.601758	2.384186E-07	
5.089925	3.601758	-2.384186E-07	
-5.092411	3.598242	2.384186E-07	
2.545584	8.790045E-04		-1.192093E-07
-2.545584	-8.790045E-04		1.192093E-07
2.546827	-3.599121	-1.192093E-07	
-2.544341	-3.600879	1.192093E-07	
2.544341	3.600879	-1.192093E-07	
-2.546827	3.599121	1.192093E-07	
10.18234	3.516018E-03		-4.768372E-07
-10.18234	-3.516018E-03		4.768372E-07
10.18358	-3.596484	-4.768372E-07	
-10.18109	-3.603516	4.768372E-07	
10.18109	3.603516	-4.768372E-07	
-10.18358	3.596484	4.768372E-07	
7.636752	2.637013E-03		-4.768372E-07
-7.636752	-2.637013E-03		4.768372E-07
7.637995	-3.597363	-4.768372E-07	
-7.635509	-3.602637	4.768372E-07	
7.635509	3.602637	-4.768372E-07	
-7.637995	3.597363	4.768372E-07	
.0024862	-7.2	0	
-.0024862	7.2	0	
5.093654	-7.198241	-2.384186E-07	
-5.088682	-7.201758	2.384186E-07	
5.088682	7.201758	-2.384186E-07	
-5.093654	7.198241	2.384186E-07	
2.54807	-7.199121	-1.192093E-07	
-2.543098	-7.200878	1.192093E-07	
2.543098	7.200878	-1.192093E-07	
-2.54807	7.199121	1.192093E-07	
10.18482	-7.196483	-4.768372E-07	
-10.17985	-7.203516	4.768372E-07	
10.17985	7.203516	-4.768372E-07	
-10.18482	7.196483	4.768372E-07	
7.639239	-7.197363	-4.768372E-07	
-7.634266	-7.202636	4.768372E-07	
7.634266	7.202636	-4.768372E-07	
-7.639239	7.197363	4.768372E-07	
15.2735	5.274027E-03		-9.536743E-07
-15.2735	-5.274027E-03		9.536743E-07

15.27475	-3.594726	-9.536743E-07	
-15.27226	-3.605274	9.536743E-07	
15.27226	3.605274	-9.536743E-07	
-15.27475	3.594726	9.536743E-07	
12.72792	4.395023E-03		-9.536743E-07
-12.72792	-4.395023E-03		9.536743E-07
12.72916	-3.595605	-9.536743E-07	
-12.72668	-3.604395	9.536743E-07	
12.72668	3.604395	-9.536743E-07	
-12.72916	3.595605	9.536743E-07	
15.27599	-7.194725	-9.536743E-07	
-15.27102	-7.205273	9.536743E-07	
15.27102	7.205273	-9.536743E-07	
-15.27599	7.194725	9.536743E-07	
12.73041	-7.195605	-9.536743E-07	
-12.72543	-7.204395	9.536743E-07	
12.72543	7.204395	-9.536743E-07	
-12.73041	7.195605	9.536743E-07	
.0037293	-10.8	0	
-.0037293	10.8	0	
5.094898	-10.79824	-2.384186E-07	
-5.087439	-10.80176	2.384186E-07	
5.087439	10.80176	-2.384186E-07	
-5.094898	10.79824	2.384186E-07	
2.549313	-10.79912	-1.192093E-07	
-2.541855	-10.80088	1.192093E-07	
2.541855	10.80088	-1.192093E-07	
-2.549313	10.79912	1.192093E-07	
10.18607	-10.79648	-4.768372E-07	
-10.17861	-10.80352	4.768372E-07	
10.17861	10.80352	-4.768372E-07	
-10.18607	10.79648	4.768372E-07	
7.640482	-10.79736	-4.768372E-07	
-7.633023	-10.80264	4.768372E-07	
7.633023	10.80264	-4.768372E-07	
-7.640482	10.79736	4.768372E-07	
15.27723	-10.79473	-9.536743E-07	
-15.26978	-10.80527	9.536743E-07	
15.26978	10.80527	-9.536743E-07	
-15.27723	10.79473	9.536743E-07	
12.73165	-10.7956	-9.536743E-07	
-12.72419	-10.80439	9.536743E-07	
12.72419	10.80439	-9.536743E-07	
-12.73165	10.7956	9.536743E-07	
20.36467	7.032036E-03		-9.536743E-07
-20.36467	-7.032036E-03		9.536743E-07
20.36592	-3.592968	-9.536743E-07	
-20.36343	-3.607032	9.536743E-07	
20.36343	3.607032	-9.536743E-07	
-20.36592	3.592968	9.536743E-07	
17.81909	6.153032E-03		-1.907349E-06
-17.81909	-6.153032E-03		1.907349E-06
0	0	0	

```
D Ø
 Ø              Ø              Ø
 Ø              Ø              Ø
D Ø
 1              Ø              Ø
 3.6            Ø              Ø
D Ø
-1              Ø              Ø
-3.6            Ø              Ø
D Ø
 Ø              1              1
 Ø              3.6            3.6
D Ø
 Ø             -1             -1
 Ø             -3.6           -3.6
D Ø
 1              1              1
 3.6            3.6            3.6
D Ø
 1             -1             -1
 3.6           -3.6           -3.6
D Ø
-1              1              1
-3.6            3.6            3.6
D Ø
-1             -1             -1
-3.6           -3.6           -3.6
D Ø
 Ø              .5             .5
 Ø              1.8            1.8
D Ø
 Ø             -.5            -.5
 Ø             -1.8           -1.8
D Ø
 1              .5             .5
 3.6            1.8            1.8
D Ø
 1             -.5            -.5
 3.6           -1.8           -1.8
D Ø
-1              .5             .5
-3.6            1.8            1.8
D Ø
-1             -.5            -.5
-3.6           -1.8           -1.8
D Ø
 Ø              2              2
 Ø              7.2            7.2
D Ø
 Ø             -2             -2
 Ø             -7.2           -7.2
D Ø
 1              2              2
 3.6            7.2            7.2
D Ø
 1             -2             -2
 3.6           -7.2           -7.2
D Ø
-1              2              2
-3.6            7.2            7.2
D Ø
```

```
-1              -2              -2
-3.6            -7.2            -7.2
D 0
 0               1.5             1.5
 0               5.4             5.4
D 0
 0              -1.5            -1.5
 0              -5.4            -5.4
D 0
 1               1.5             1.5
 3.6             5.4             5.4
D 0
 1              -1.5            -1.5
 3.6            -5.4            -5.4
D 0
-1               1.5             1.5
-3.6             5.4             5.4
D 0
-1              -1.5            -1.5
-3.6            -5.4            -5.4
D 0
 2               0               0
 7.2             0               0
D 0
-2               0               0
-7.2             0               0
D 0
 2               1               1
 7.2             3.6             3.6
D 0
 2              -1              -1
 7.2            -3.6            -3.6
D 0
-2               1               1
-7.2             3.6             3.6
D 0
-2              -1              -1
-7.2            -3.6            -3.6
D 0
 2               .5              .5
 7.2             1.8             1.8
D 0
 2              -.5             -.5
 7.2            -1.8            -1.8
D 0
-2               .5              .5
-7.2             1.8             1.8
D 0
-2              -.5             -.5
-7.2            -1.8            -1.8
D 0
 2               2               2
 7.2             7.2             7.2
D 0
 2              -2              -2
 7.2            -7.2            -7.2
D 0
-2               2               2
-7.2             7.2             7.2
D 0
-2              -2              -2
-7.2            -7.2            -7.2
D 0
 2               1.5             1.5
 7.2             5.4             5.4
D 0
```

```
 2               -1.5             -1.5
 7.2             -5.4             -5.4
D 0
-2                1.5              1.5
-7.2              5.4              5.4
D 0
-2               -1.5             -1.5
-7.2             -5.4             -5.4
D 0
 0                3                3
 0                10.8             10.8
D 0
 0               -3               -3
 0               -10.8            -10.8
D 0
 1                3                3
 3.6              10.8             10.8
D 0
 1               -3               -3
 3.6             -10.8            -10.8
D 0
-1                3                3
-3.6              10.8             10.8
D 0
-1               -3               -3
-3.6             -10.8            -10.8
D 0
 0                2.5              2.5
 0                9                9
D 0
 0               -2.5             -2.5
 0               -9               -9
D 0
 1                2.5              2.5
 3.6              9                9
D 0
 1               -2.5             -2.5
 3.6             -9               -9
D 0
-1                2.5              2.5
-3.6              9                9
D 0
-1               -2.5             -2.5
-3.6             -9               -9
D 0
 2                3                3
 7.2              10.8             10.8
D 0
 2               -3               -3
 7.2             -10.8            -10.8
D 0
-2                3                3
-7.2              10.8             10.8
D 0
-2               -3               -3
-7.2             -10.8            -10.8
D 0
 2                2.5              2.5
 7.2              9                9
D 0
 2               -2.5             -2.5
 7.2             -9               -9
D 0
-2                2.5              2.5
-7.2              9                9
D 0
```

```
-2              -2.5            -2.5
-7.2            -9              -9
D 0
 3               0               0
 10.8            0               0
D 0
-3               0               0
-10.8            0               0
D 0
 3               1               1
 10.8            3.6             3.6
D 0
 3              -1              -1
 10.8           -3.6            -3.6
D 0
-3               1               1
-10.8            3.6             3.6
D 0
-3              -1              -1
-10.8           -3.6            -3.6
D 0
 3               .5              .5
 10.8            1.8             1.8
D 0
 3              -.5             -.5
 10.8           -1.8            -1.8
D 0
-3               .5              .5
-10.8            1.8             1.8
D 0
-3              -.5             -.5
-10.8           -1.8            -1.8
D 0
 3               2               2
 10.8            7.2             7.2
D 0
 3              -2              -2
 10.8           -7.2            -7.2
D 0
-3               2               2
-10.8            7.2             7.2
D 0
-3              -2              -2
-10.8           -7.2            -7.2
D 0
 3               1.5             1.5
 10.8            5.4             5.4
D 0
 3              -1.5            -1.5
 10.8           -5.4            -5.4
D 0
-3               1.5             1.5
-10.8            5.4             5.4
D 0
-3              -1.5            -1.5
-10.8           -5.4            -5.4
D 0
 3               3               3
 10.8            10.8            10.8
D 0
 3              -3              -3
 10.8           -10.8           -10.8
D 0
-3               3               3
-10.8            10.8            10.8
D 0
```

```
-3              -3              -3
-10.8           -10.8           -10.8
D Ø
 3               2.5             2.5
 10.8            9               9
D Ø
 3              -2.5            -2.5
 10.8           -9              -9
D Ø
-3               2.5             2.5
-10.8            9               9
D Ø
-3              -2.5            -2.5
-10.8           -9              -9
D Ø
 Ø               4               4
 Ø               14.4            14.4
D Ø
 Ø              -4              -4
 Ø              -14.4           -14.4
D Ø
 1               4               4
 3.6             14.4            14.4
D Ø
 1              -4              -4
 3.6            -14.4           -14.4
D Ø
-1               4               4
-3.6             14.4            14.4
D Ø
-1              -4              -4
-3.6            -14.4           -14.4
D Ø
 Ø               3.5             3.5
 Ø               12.6            12.6
D Ø
 Ø              -3.5            -3.5
 Ø              -12.6           -12.6
```

BCC 5T2

-5.858363	2.567006	-2.145767E-06	
3.515018	-3.208758	1.430512E-06	
4.686691	-.6417516	1.430512E-06	
-3.515018	3.208758	-1.430512E-06	
-7.030036	0	-1.907349E-06	
7.030036	0	1.907349E-06	
-4.686691	5.134013	-2.145767E-06	
-3.515018	-3.208758	-4.768372E-07	
3.515018	3.208758	4.768372E-07	
-1.171673	-4.492262	3.874302E-07	
2.343346	5.134013	-1.043081E-07	
-5.858364	-3.850509	-1.192093E-06	
4.768372E-07		6.417516	-9.536743E-07
-4.768372E-07		-6.417516	9.536743E-07
5.858363	1.925255	1.549721E-06	
-2.343345	5.775765	-1.549721E-06	
8.201709	2.567006	1.907349E-06	
2.343345	-7.70102	1.66893E-06	
8.201708	-3.85051	3.099442E-06	
5.858363	-4.492261	2.384186E-06	
7.030035	-6.417516	2.861023E-06	
9.373381	-1.283503	2.861023E-06	
-7.030035	6.417516	-2.861023E-06	
4.68669	-7.059268	2.622604E-06	
-5.858363	8.984522	-3.099442E-06	
4.686692	5.775765	3.874302E-07	
-2.343346	-7.059268	5.662442E-07	
-7.030036	-6.417516	-9.536743E-07	
7.030036	6.417516	9.536743E-07	
-4.686692	-7.701019	-7.450581E-08	
1.171674	8.984523	-1.192093E-06	
-1.171672	8.342771	-1.66893E-06	
9.373382	5.134013	1.788139E-06	
1.171672	-10.26802	1.907349E-06	
3.515017	-9.626273	2.384186E-06	
-3.515017	9.626273	-2.384186E-06	
-4.68669	11.55153	-3.099442E-06	
-8.201709	1.925255	-2.384186E-06	
-9.373381	-.6417511	-2.622604E-06	
-11.71673	-1.283503	-3.33786E-06	
-8.201709	-4.492262	-1.549721E-06	

-10.54505	-3.208758	-2.861023E-06	
10.54505	3.208758	2.861023E-06	
-12.8884	-3.850509	-2.622604E-06	
9.373381	-7.70102	3.814697E-06	
8.201708	-10.26803	3.814697E-06	
5.858364	-10.90978	3.099442E-06	
7.030036	-12.83503	3.814697E-06	
-7.030036	12.83503	-3.814697E-06	
3.515019	9.626274	-4.172325E-07	
5.858364	8.342771	5.066395E-07	
-3.515019	-9.626274	4.172325E-07	
8.20171	8.984522	1.013279E-06	
-5.858365	-10.26803	-1.937151E-07	
2.343347	11.55153	-1.192093E-06	
-1.171674	-10.90978	1.192093E-06	
9.536743E-07		12.83503	-1.907349E-06
-9.536743E-07		-12.83503	1.907349E-06
-2.343344	12.19328	-2.861023E-06	
2.343344	-14.11854	2.622604E-06	
4.686689	-13.47679	3.576279E-06	
-5.858363	15.40204	-3.814697E-06	
-11.71673	5.134013	-4.291535E-06	
-10.54506	3.208758	-3.099442E-06	
10.54506	-3.208758	3.099442E-06	
-9.373381	5.775765	-3.814697E-06	
-12.8884	2.567007	-3.814697E-06	
11.71673	-.641752	3.576279E-06	
-8.201709	8.342771	-3.099442E-06	
-14.06007	0	-3.814697E-06	
14.06007	0	3.814697E-06	
12.8884	1.925254	2.861023E-06	
15.23175	2.567006	3.814697E-06	
-9.373382	-7.059268	-1.549721E-06	
-11.71673	-7.701019	-2.384186E-06	
11.71673	5.775764	2.622604E-06	
-14.06007	-6.417515	-2.861023E-06	
14.06007	6.417515	2.861023E-06	
16.40342	5.134013	3.814697E-06	
-15.23175	-4.492261	-3.33786E-06	
9.37338	-14.11854	5.245209E-06	
8.201709	-16.68554	4.291535E-06	
4.686692	12.19328	-2.980232E-07	
9.373382	11.55153	7.748604E-07	
-4.686692	-14.11854	1.132488E-06	
7.030037	12.83503	0	
-7.030037	-12.83503	0	
-2.343347	-13.47678	1.192093E-06	
1.171675	15.40204	-2.145767E-06	
-1.171671	14.76029	-2.622604E-06	
1.17167	-16.68554	3.099442E-06	
3.515018	-16.04379	3.099442E-06	
0	0	0	

```
D-.5239879
-.5              -.5              .5
-.9566667        -1.530667        1.626333
D-1.047976
-.5               .5              .5
-.4783334         1.243667        1.817667
D-.5239879
 Ø                1               Ø
 .4783333         2.774333        .1913333
D-1.047976
 Ø                Ø              -1
 .9566666        -.1913333       -2.487333
D-1.047976
-1               -1               1
-1.913333        -3.061333        3.252667
D-.5239879
 Ø               -1              -1
 .4783333        -2.965667       -2.678667
D Ø
 Ø                Ø               Ø
 Ø                Ø               Ø
D-.5239879
-1                Ø               2
-2.391667        -9.566671E-02                    5.931333
D Ø
 .5              -.5             -1.5
 1.435           -1.435          -4.305
D-.5239879
 .5               .5             -1.5
 1.913333         1.339333       -4.113667
D Ø
-.5               .5              1.5
-1.435            1.435           4.305
D Ø
-1               -1               2
-2.87            -2.87            5.74
D Ø
 1                1              -2
 2.87             2.87           -5.74
D-1.047976
-1                1               2
-1.913333         2.678667        6.122667
D Ø
-.5              -1.5             .5
-1.435           -4.305           1.435
D Ø
 .5               1.5            -.5
 1.435            4.305          -1.435
D-1.047976
-.5              -1.5            -.5
-.4783333        -4.496334       -1.052333
D-1.047976
 Ø                2               Ø
 .9566666         5.548667        .3826666
D-.5239879
-1               -2               1
-2.391667        -5.835667        3.061333
D Ø
 Ø                2               1
 Ø                5.74            2.87
D Ø
```

```
 Ø               -2              -1
 Ø               -5.74           -2.87
D-1.047976
 .5               1.5            -1.5
 2.391667         4.113667       -3.922333
D-.5239879
-.5               1.5             1.5
-.9566666         4.209334        4.496333
D-.5239879
 1               2               -2
 3.348333        5.644334        -5.548667
D-1.047976
 Ø               -2              -2
 .9566666        -5.931333       -5.357333
D-.5239879
 1               Ø               -3
 3.348333        -9.566662E-02                   -8.416666
D-1.047976
 .5              -.5             -2.5
 2.391667        -1.626333       -6.792333
D Ø
 1               -1              -3
 2.87            -2.87           -8.609999
D-1.047976
 1               1               -3
 3.826667        2.678667        -8.227333
D Ø
-1               1               3
-2.87            2.87            8.609999
D-.5239879
 .5              -1.5            -2.5
 1.913333        -4.400667       -6.983667
D-.5239881
-1               2               3
-2.391667        5.644333        8.801332
D-.5239879
 .5              2.5             -.5
 1.913333        7.079334        -1.243667
D-.5239879
-.5              -2.5            -.5
-.9566666        -7.270667       -1.243667
D Ø
-1               -3              1
-2.87            -8.609999       2.87
D Ø
 1               3               -1
 2.87            8.609999        -2.87
D-1.047976
-1               -3              Ø
-1.913333        -8.801333       .3826667
D-.5239879
 Ø               3               1
 .4783333        8.514334        3.061333
D-1.047976
-.5               2.5             1.5
-.4783333        6.983667        4.687667
D-1.047976
 1               3               -2
 3.826667        8.418667        -5.357333
D-.5239879
 Ø               -3              -2
 .4783334        -8.705666       -5.548667
D Ø
 .5              -2.5            -2.5
 1.435           -7.175          -7.175
D Ø
```

```
-.5             2.5             2.5
-1.435          7.175           7.175
D-1.047976
-1              3               3
-1.913333       8.418667        8.992666
D-1.047976
-1.5            -.5             2.5
-3.348333       -1.626334       7.557667
D-.5239879
-1.5            -1.5            2.5
-3.826667       -4.400666       7.366333
D-1.047976
-2              -2              3
-4.783334       -5.931333       8.992666
D-1.047976
-1.5            -2.5            1.5
-3.348333       -7.366334       4.687667
D-1.741163E-07
-1.5            -2.5            2.5
-4.305001       -7.175          7.175
D 1.741163E-07
 1.5             2.5            -2.5
 4.305001        7.175          -7.175
D-.5239881
-2              -3              3
-5.261667       -8.705666       8.801332
D-1.047976
 1              -1              -4
 3.826667       -3.061333       -11.09733
D-.5239878
 1              -2              -4
 3.348333       -5.835666       -11.28867
D-1.047976
 .5             -2.5            -3.5
 2.391667       -7.366334       -9.662334
D 0
 1              -3              -4
 2.87           -8.609999       -11.48
D 0
-1               3               4
-2.87            8.609999        11.48
D-8.705816E-08
 .5             3.5             .5
 1.435          10.045          1.435
D-1.047976
 .5             3.5             -.5
 2.391667       9.853666        -1.052333
D 8.705816E-08
-.5             -3.5            -.5
-1.435          -10.045         -1.435
D-.5239879
 1               4              -1
 3.348333        11.38433       -2.676667
D-.5239879
-1              -4               0
-2.391667       -11.57567        .1913334
D-1.047976
 0               4               1
 .9566666        11.28867        3.252667
D-1.047976
-.5             -3.5            -1.5
-.4783335       -10.23633       -3.922333
D 0
 0               4               2
 0               11.48           5.74
D 0
```

```
 0               -4              -2
 0               -11.48          -5.74
D-.5239079
-.5              3.5              2.5
-.9566667        9.949334         7.366333
D-1.047976
 0               -4              -3
 .9566666        -11.67133        -8.227333
D-.5239881
 .5              -3.5             -3.5
 1.913333        -10.14067        -9.853666
D-.5239878
-1               4                4
-2.391667        11.38433         11.67133
D-1.047976
-2               0                4
-4.783334        -.1913334        11.86267
D 0
-1.5             -.5              3.5
-4.305           -1.435           10.045
D 0
 1.5              .5             -3.5
 4.305            1.435          -10.045
D-.5239878
-1.5             .5               3.5
-3.826667        1.339333         10.23633
D-.5239878
-2               -1               4
-5.261667        -2.965667        11.67133
D-.5239881
 1.5             1.5             -3.5
 4.783334        4.209333        -9.853666
D-1.047976
-1.5             1.5              3.5
-3.348333        4.113667         10.42767
D 0
-2               -2               4
-5.74            -5.74            11.48
D 0
 2               2               -4
 5.74            5.74            -11.48
D-1.047976
 1.5             2.5             -3.5
 5.261667        6.983667        -9.662334
D-.5239878
 2               3               -4
 6.218333        8.514334        -11.28867
D-.5239879
-1.5             -3.5             1.5
-3.826667        -10.14067        4.496333
D-1.047976
-2               -4               2
-4.783334        -11.67133        6.122667
D-.5239879
 1.5             3.5             -2.5
 4.783334        9.949333        -6.983667
D 0
-2               -4               3
-5.74            -11.48           8.609999
D 0
 2               4               -3
 5.74            11.48           -8.609999
D-1.047976
 2               4               -4
 6.696667        11.28867        -11.09733
D-1.047976
```

```
-2.5            -3.5            3.5
-6.218333       -10.23633       10.42767
D-1.047976
 1              -3              -5
 3.826667       -8.801333       -13.56733
D-.5239881
 1              -4              -5
 3.348333       -11.57567       -14.15867
D-.5239879
 .5              4.5             .5
 1.913333        12.81933        1.626333
D-1.047976
 1              5               -1
 3.826667       14.15867        -2.487333
D-1.047976
-1              -5              -1
-1.913333       -14.54133       -2.487333
D 0
 1              5               0
 2.87           14.35           0
D 0
-1              -5              0
-2.87           -14.35          0
D-.523988
-.5             -4.5            -1.5
-.9566667       -13.01067       -4.113666
D-.5239879
 0              5               2
 .4783334       14.25433        5.931333
D-1.047976
-.5             4.5             2.5
-.4783335       12.72367        7.557667
D-.5239879
 0              -5              -3
 .4783333       -14.44567       -8.418666
D-3.482327E-07
 .5             -4.5            -3.5
 1.435          -12.915         -10.045
```

Appendix 2

100 KV

M = 60,000	L = 150	R = 13.5° CW
	L = 575	R = 28.5° CW
M = 80,000	L = 575	R = 24° CW
	L = 290	R = 14.5° CW
	L = 210	R = 12° CW
M = 100,000	L = 575	R = 18.5° CW
	L = 150	R = 3.5° CW
M = 130,000	L = 575	R = 18.5° cw
	L = 150	R = 3.5° CW

R is the rotation necessary to correct for the image rotation. What follows is the rotation carried out to determine the crystallography discussed in section 3 of the results.

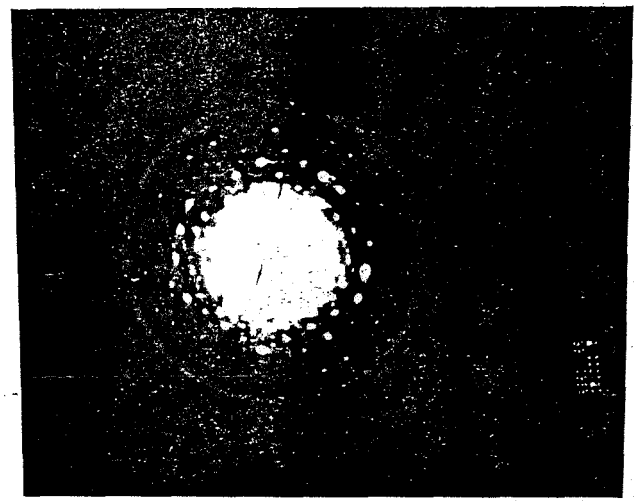


90°
LINE

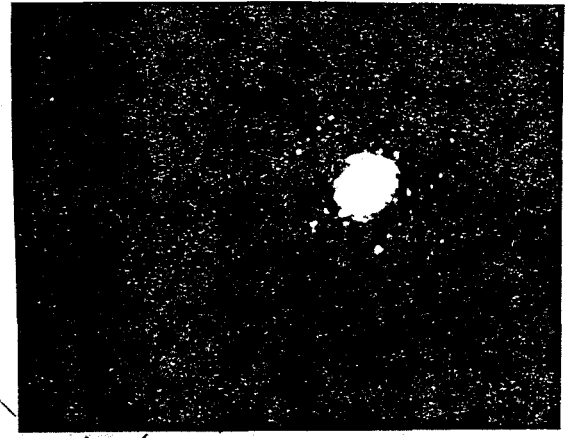

α

γ

92°

99°

[011]α

[111]γ

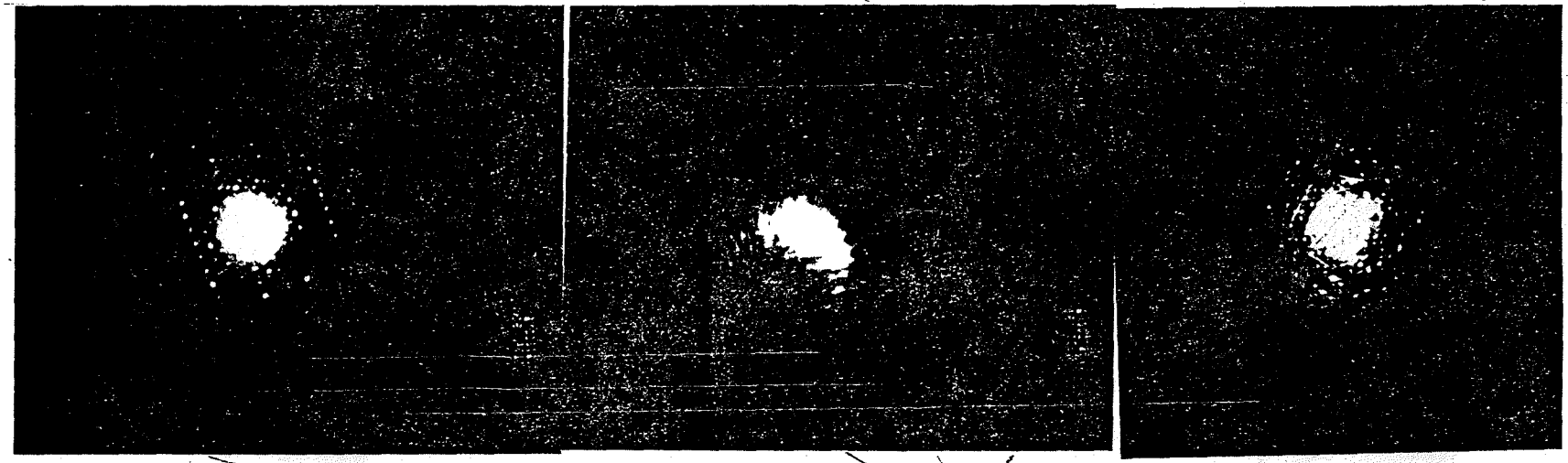


88°
89°
γ⟨220⟩
⟨411⟩c

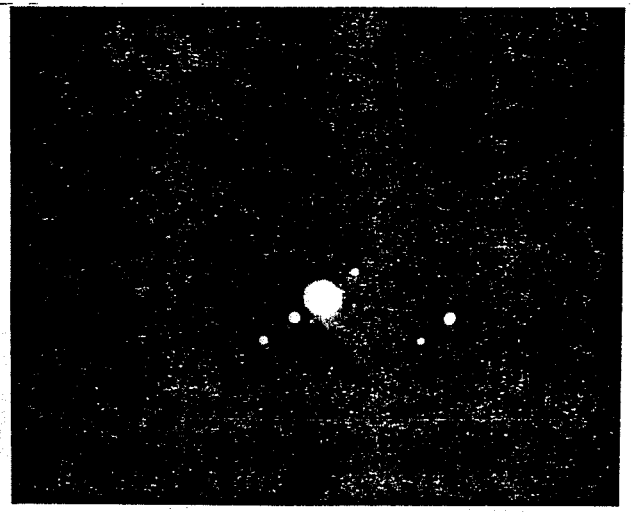

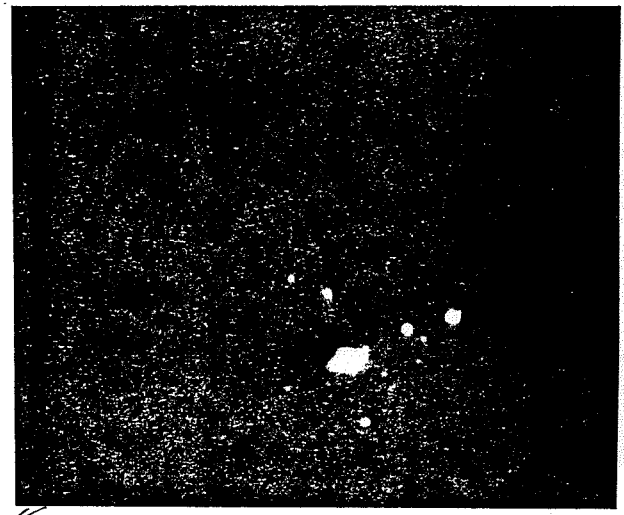

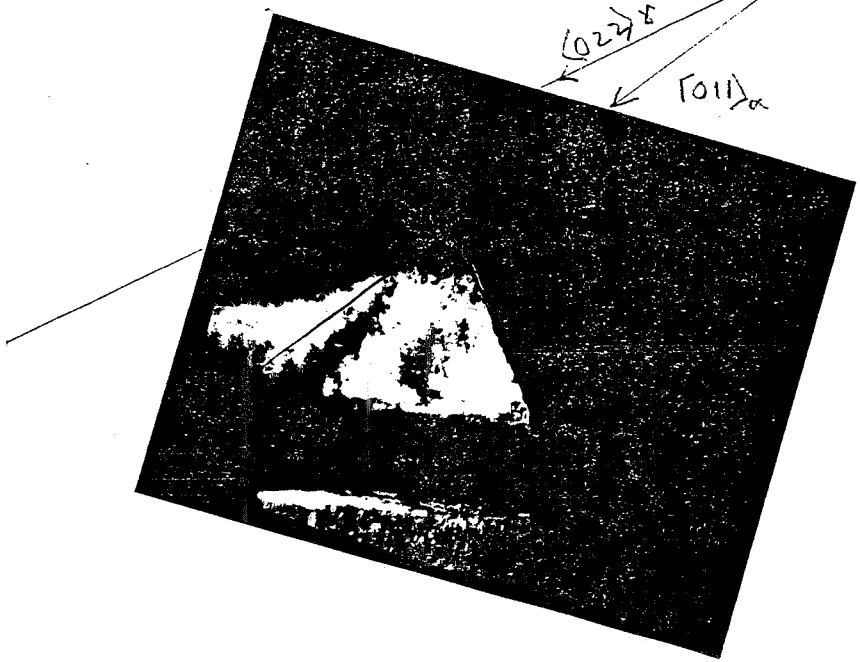
(022)γ
[011]α

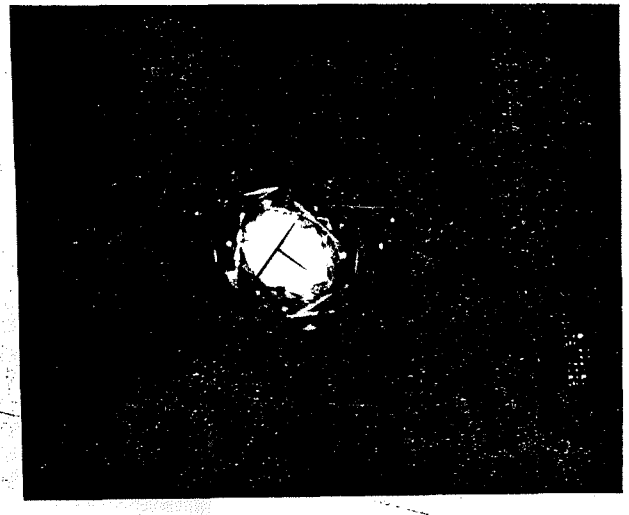

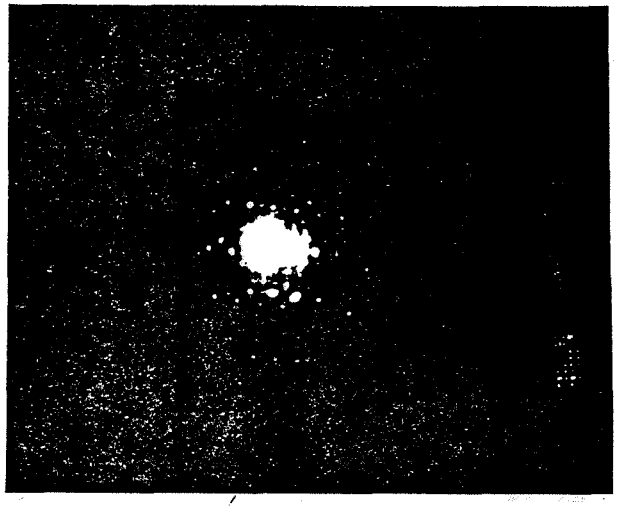


89°
<220>γ


90°
⟨200⟩γ
⟨120⟩γ

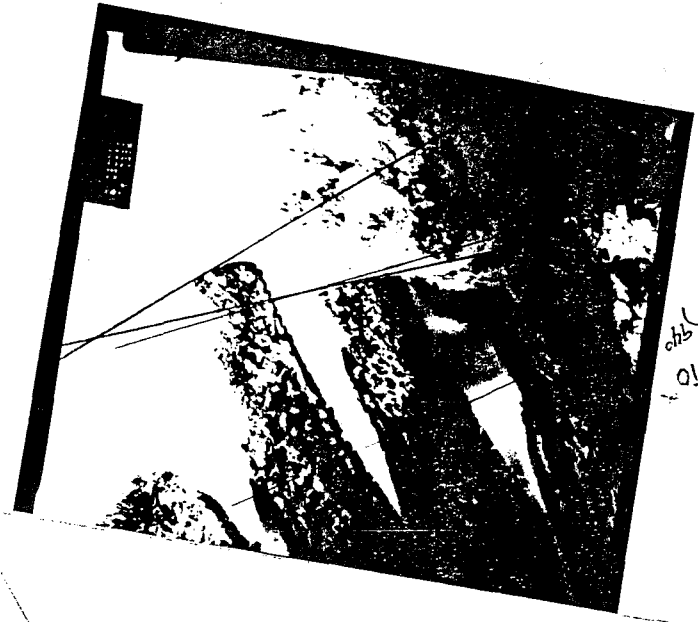

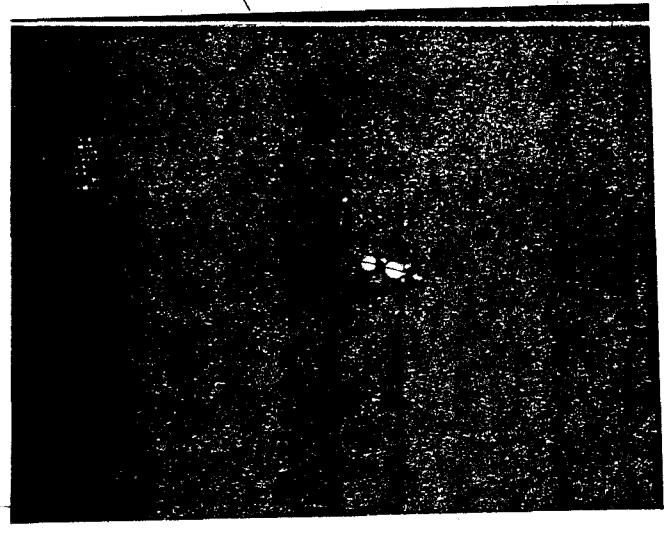

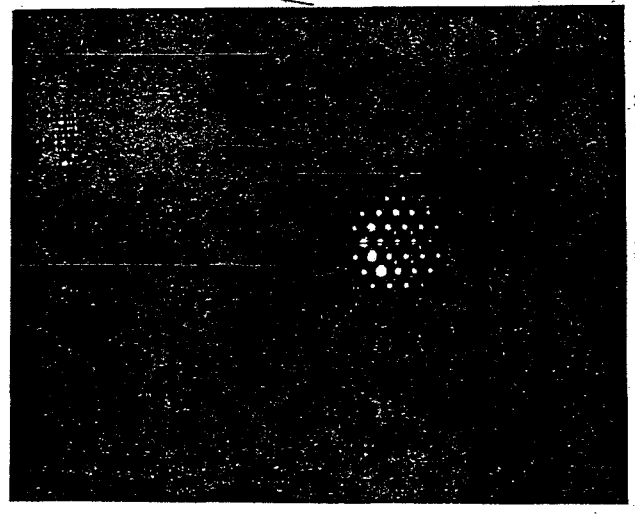

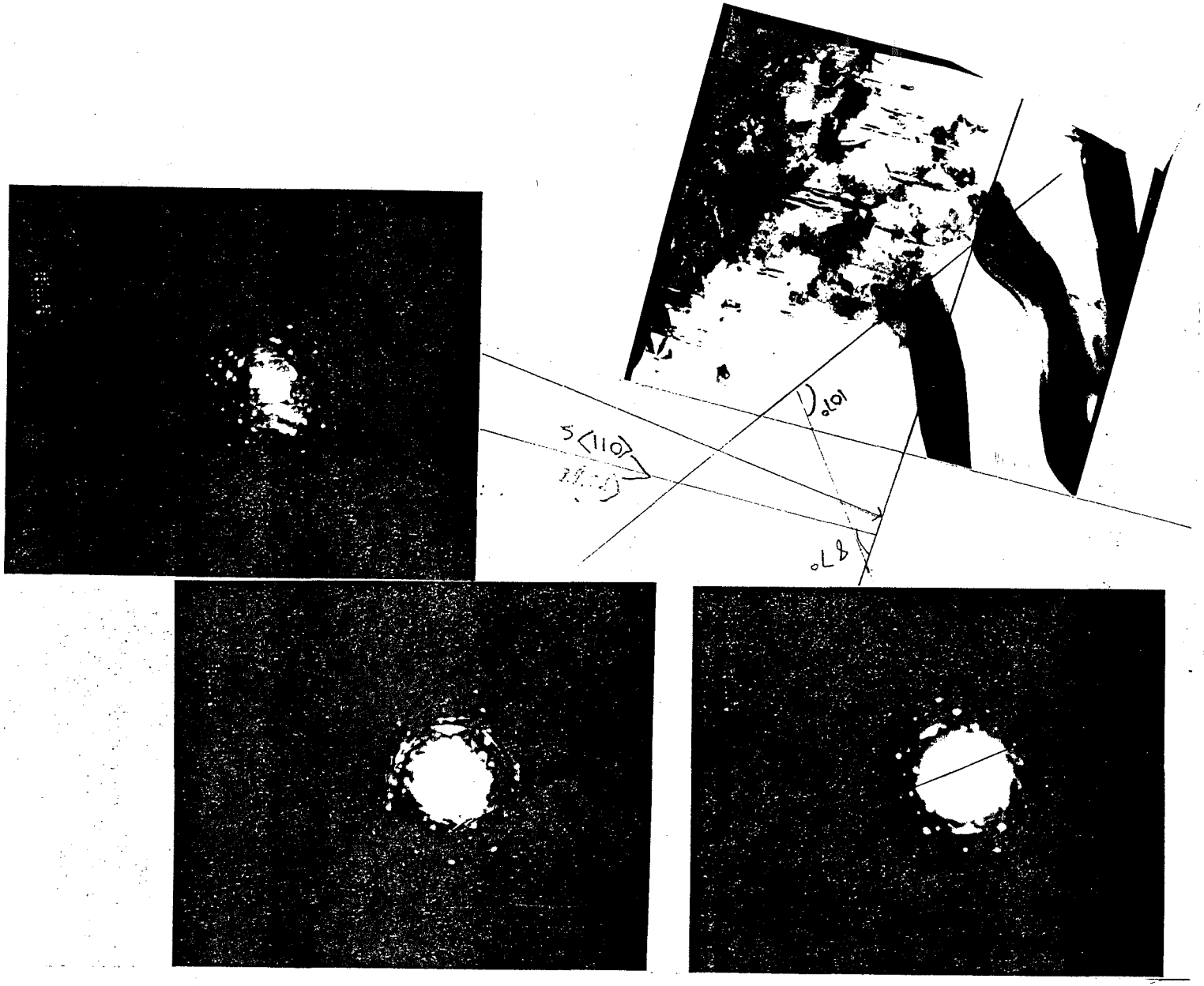
5⟨110⟩
101
87°

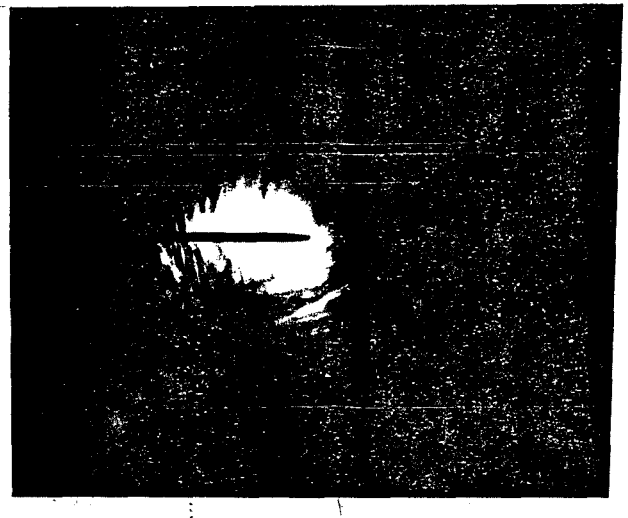

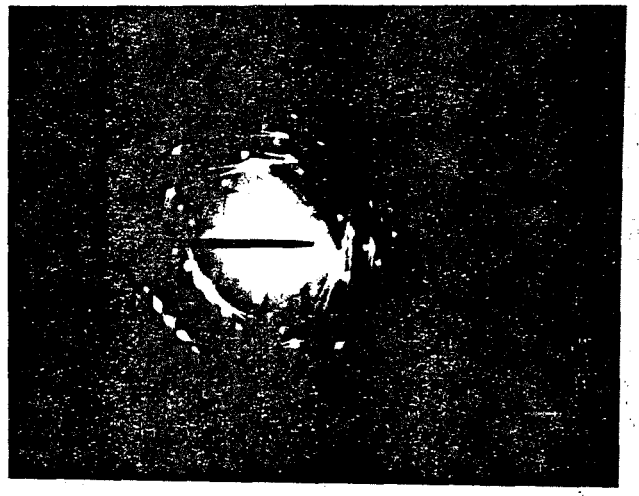

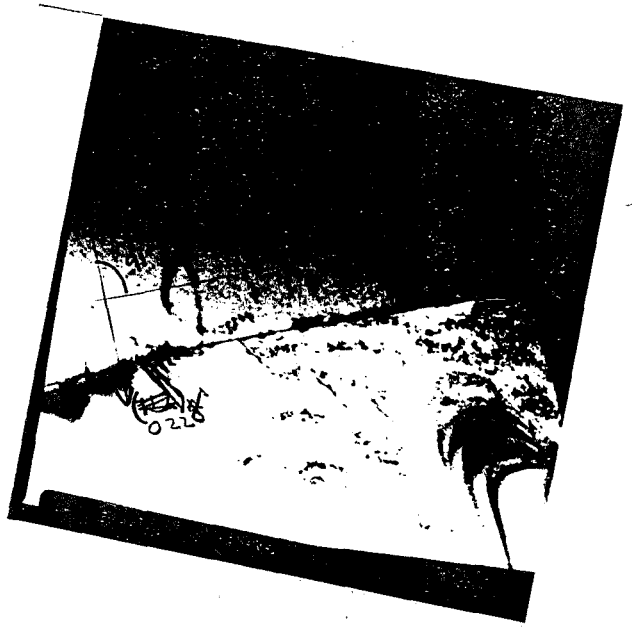

(110)α